10. SITE 756[1]

Shipboard Scientific Party[2]

HOLE 756A

Date occupied: 25 May 1988

Date departed: 26 May 1988

Time on hole: 6 hr

Position: 27°21.330'S, 87°35.805'E

Bottom felt (rig floor; m; drill-pipe measurement): 1529.0

Distance between rig floor and sea level (m): 10.87

Water depth (drill-pipe measurement; corrected m): 1518.1

Total depth (rig floor; corrected m): 1538.7

Penetration (m): 9.7

Number of cores: 1

Total length of cored section (m): 9.7 (m)

Total core recovered (m): 9.72

Core recovery (%): 100

Oldest sediment cored:
Depth sub-bottom (m): 9.7
Nature: nannofossil ooze with foraminifers
Earliest age: early Pliocene
Measured velocity (km/s): 1.5

HOLE 756B

Date occupied: 26 May 1988

Date departed: 26 May 1988

Time on hole: 8 hr, 45 min

Position: 27°21.330'S, 87°35.805'E

Bottom felt (rig floor; m; drill-pipe measurement): 1529.0

Distance between rig floor and sea level (m): 10.87

Water depth (drill-pipe measurement; corrected m): 1518.1

Total depth (rig floor; corrected m): 1633.3

Penetration (m): 104.3

Number of cores: 11

Total length of cored section (m): 104.3

Total core recovered (m): 105.70

Core recovery (%): 101

Oldest sediment cored:
Depth sub-bottom (m): 104.3
Nature: nannofossil ooze with foraminifers
Earliest age: Oligocene
Measured velocity (km/s): 1.6

HOLE 756C

Date occupied: 26 May 1988

Date departed: 27 May 1988

Time on hole: 1 day, 6 hr, 15 min

Position: 27°21.253'S, 87°35.890'E

Bottom felt (rig floor; m; drill-pipe measurement): 1526.7

Distance between rig floor and sea level (m): 10.87

Water depth (drill-pipe measurement; corrected m): 1515.8

Total depth (rig floor; corrected m): 1685.7

Penetration (m): 159.0

Number of cores: 12

Total length of cored section (m): 76.6

Total core recovered (m): 61.81

Core recovery (%): 80

Oldest sediment cored:
Depth sub-bottom (m): 150.2
Nature: foraminifer limestone
Earliest age: late Eocene
Measured velocity (km/s): 5.5

Basement:
Depth sub-bottom (m): 150.2
Nature: basalt flows
Measured velocity (km/s): 4.4–5.5

HOLE 756D

Date occupied: 27 May 1988

Date departed: 29 May 1988

Time on hole: 1 day, 15 hr, 15 min

Position: 27°21.288'S, 87°35.843'E

Bottom felt (rig floor; m; drill-pipe measurement): 1524.0

Distance between rig floor and sea level (m): 10.87

Water depth (drill-pipe measurement; corrected m): 1513.1

Total depth (rig floor; corrected m): 1685.7

Penetration (m): 221.0

Number of cores: 12

Total length of cored section (m): 101.2

Total core recovered (m): 46.04

Core recovery (%): 45

Oldest sediment cored:
Depth sub-bottom (m): 139.0
Nature: limestone
Earliest age: late Eocene
Measured velocity (km/s): 5.5

Basement:
Depth sub-bottom (m): 139.0
Nature: basalt flows
Measured velocity (km/s): 4.4–5.6

[1] Peirce, J., Weissel, J., et al., 1989. *Proc. ODP, Init. Repts.*, 121: College Station, TX (Ocean Drilling Program).
[2] Shipboard Scientific Party is as given in the list of Participants preceding the contents.

Principal results: Ocean Drilling Program (ODP) Site 756 (proposed Site NER-5A) is near the crest of the southern end of Ninetyeast Ridge. Together, the three locations drilled during Leg 121 on the Ninetyeast Ridge were designed to sample the basement through time and the sedimentary section through both time and latitude. Site 756 provides the southern and youngest end of that transect, and it is positioned midway between Deep Sea Drilling Project (DSDP) Sites 253 and 254. Specifically, the objectives were to recover a complete upper Eocene to Holocene sedimentary section for the north-south paleoceanographic transect through the eastern Indian Ocean and also to recover a significant basement section for a petrologic study of the evolution of the mantle hot spot associated with Ninetyeast Ridge and the Kerguelen Plateau.

The proposed location was picked at shotpoint 13920 on the seismic-reflection survey conducted during Cruise 2708 of the *Robert D. Conrad* (RC2708). The approach survey of Site 756 was oriented at an angle to the RC2708 survey in order to obtain seismic data along dip lines normal to a N50°E structural grain that cuts across the ridge in this area. The site location chosen is about 500 m northwest of the proposed location, thereby avoiding a small intrasedimentary fault. Site 756 is on a sedimented bench on the eastern side of Ninetyeast Ridge, in an area of rugged terrain. Numerous pinnacles near the site rise to water depths as shallow as 750 m. A fault 3 km southeast of Site 756 has a throw of about 500 m.

Hole 756A missed the mud line. Hole 756B was cored with the advanced hydraulic piston corer (APC) to 104 m below seafloor (mbsf), and then the next APC parted from excessive overpull. Hole 756C was spot cored and washed to 101 mbsf and then cored with the extended core barrel (XCB) system to 150 mbsf, where no further penetration could be made. The Navidrill (NCB) was deployed and cut three cores. Hole 756D was spot cored and washed to 139 mbsf, where hard drilling was encountered. Coring with the rotary core barrel (RCB) to a total depth of 221 mbsf recovered basaltic flows with 36% recovery.

In retrospect, the chemistry data indicate that the mud-line core at Hole 756D was too deep by about 4 m. Therefore, all depths reported in Hole 756D may be about 4 m too shallow. Detailed correlations between holes should make allowance for this possible discrepancy.

The following lithologic units are recognized (Hole 756D depths):

Unit I (0–139 mbsf): Pleistocene (Zone CN13) to upper Eocene (Zones CP15b/P16) nannofossil ooze with foraminifers. Sediment color grades from white at the top to very pale brown at the bottom. The entire unit is homogeneous in texture and heavily bioturbated. Trace amounts of altered volcanic glass occur throughout the section. A minor subunit immediately above the first volcanic unit is an upper Eocene, very hard, pale yellow limestone with planktonic foraminifers and calcareous nannofossils. Recovery in this subunit was limited to a few pieces in both Holes 756C and 756D. Although the limestone cannot be thicker than about 30 cm, the contact with the underlying basalt was not recovered intact.

Unit II (139–221 mbsf): basaltic flows with intercalated ash and soil layers. A total of 16 flow units was recovered, two from Hole 756C and 14 from Hole 756D. The flows are estimated to be 2–5 m thick, and their degree of alteration ranges from slight to high. Petrographically, the majority of the lavas are sparsely plagioclase phyric basalts and a few are aphyric, although most appear to be aphyric in hand specimen. No glassy selvages or pillowlike jointing patterns were observed. Vesicles and large cavities are common, comprising up to 20% of the rock volume. They are usually lined with saponite, and about 20% of the vesicles and cavities are infilled with calcite or goethite. Native copper was observed in one core section.

The material between the flows includes tephra, with the largest pieces 1–2 cm in size; red soil layers with montmorillonite clay and hematite; and basaltic rubble layers. Only small amounts of the interflow material were recovered, but it probably makes up more than 50% of the section.

Preliminary shipboard analysis indicates that the lavas are distinct from Indian Ocean mid-ocean ridge basalt (MORB) and that they resemble the basalts drilled previously on Ninetyeast Ridge. The lavas form a series of discrete flows with brecciated tops which apparently were erupted in a subaerial environment.

The lowermost soft sediments overlying the thin limestone layer indicate deposition in an upper bathyal environment, suggesting that initial subsidence was rapid. The oldest sediments are late Eocene (38 Ma) in age. This is some 10 m.y. younger than the basement age predicted using a hot-spot model, but it is not inconsistent with such a model if subsidence below wave base did not occur for several million years.

Very well-preserved late Eocene to Pleistocene age assemblages of calcareous nannofossils and planktonic foraminifers occur at Site 756, including a complete Eocene/Oligocene boundary sequence. Subtropical and temperate assemblages dominate the section in the middle Miocene and above, with only rare occurrences of fully tropical species, whereas in the Eocene to lower Miocene section the assemblages are mostly temperate. The temperate, austral marker species used to date the section at Broken Ridge occur in combination with known, low-latitude, subtropical marker species throughout, thereby providing a bridge between widely used low-latitude biostratigraphic zonations and the more temperate zonation schemes of the Southern Hemisphere.

The calcium ion concentration in the pore waters at Hole 756B reaches a high value of 33 mmol/L, whereas at Hole 756C, 200 m to the northeast, the high value is 13 mmol/L, which is only slightly above that of seawater. At Hole 756D, halfway between Holes 756B and 756C, the maximum calcium concentration is intermediate. These results indicate that there is a complex pattern of alteration and water transport in the basement which is reflected in the sediment column of this small bench (approximately 6 × 6 km), and large changes occur on a scale as small as 200 m.

The second deployment of the Navidrill on Leg 121 in Hole 756D was its first operational use in basaltic material. The first NCB core was a textbook case, penetrating and recovering a 4-m-thick vesicular flow before stopping its advance in the softer volcanic ash below. Four subsequent NCB runs were less successful, chiefly because of the large percentage of soft interflow material. Total NCB penetration was 8.7 m, and recovery totaled 5.7 m, of which 4.2 m was in the first core. Use of the Navidrill in these conditions proved too slow to justify continuing for scientific purposes. As it was, the U-joint in the mud motor was reduced to shrapnel during the last run. However, the experience gained in using this new technology is invaluable for engineering evaluation.

BACKGROUND AND OBJECTIVES

This section includes a brief synopsis of the overall drilling objectives of Ninetyeast Ridge and discusses in detail the goals for Site 756, the southernmost site drilled on the ridge during Leg 121. A more complete discussion of the overall objectives and their implications may be found in the "Leg 121 Background and Objectives" chapter (this volume).

Background

The Ninetyeast Ridge is a major north-south lineament in the eastern Indian Ocean. The ridge extends from about 34°S to about 10°N, a distance of almost 5000 km, where it is buried by the sediments of the Bengal Fan (Fig. 1). The relief of Ninetyeast Ridge varies from 1500 to 3000 m, and some peaks on its southern end shoal to 750 m. Its width is about 200 km, except for a 700-km-long section north of Osborne Knoll, where it is as narrow as 100 km.

Drilling results from DSDP Legs 22 (von der Borch, Sclater, et al., 1974) and 26 (Davies, Luyendyk, et al., 1974) showed that the basalts forming the basement of Ninetyeast Ridge were erupted either subaerially or in shallow water. Basement ages increase northward on the ridge and are roughly the same as the basement ages of the Indian plate to the west. Basement paleolatitudes are all near 50°S, and the basalt geochemistry is similar to that of lavas from oceanic islands, particularly Kerguelen.

The interpretation of these results is that Ninetyeast Ridge formed as the trace of the Kerguelen/Ninetyeast hot spot on the Indian plate (Luyendyk, 1977; Luyendyk and Rennick, 1977) before rifting along the incipient Southeast Indian Ridge separated Kerguelen from the Indian plate in the middle Eocene

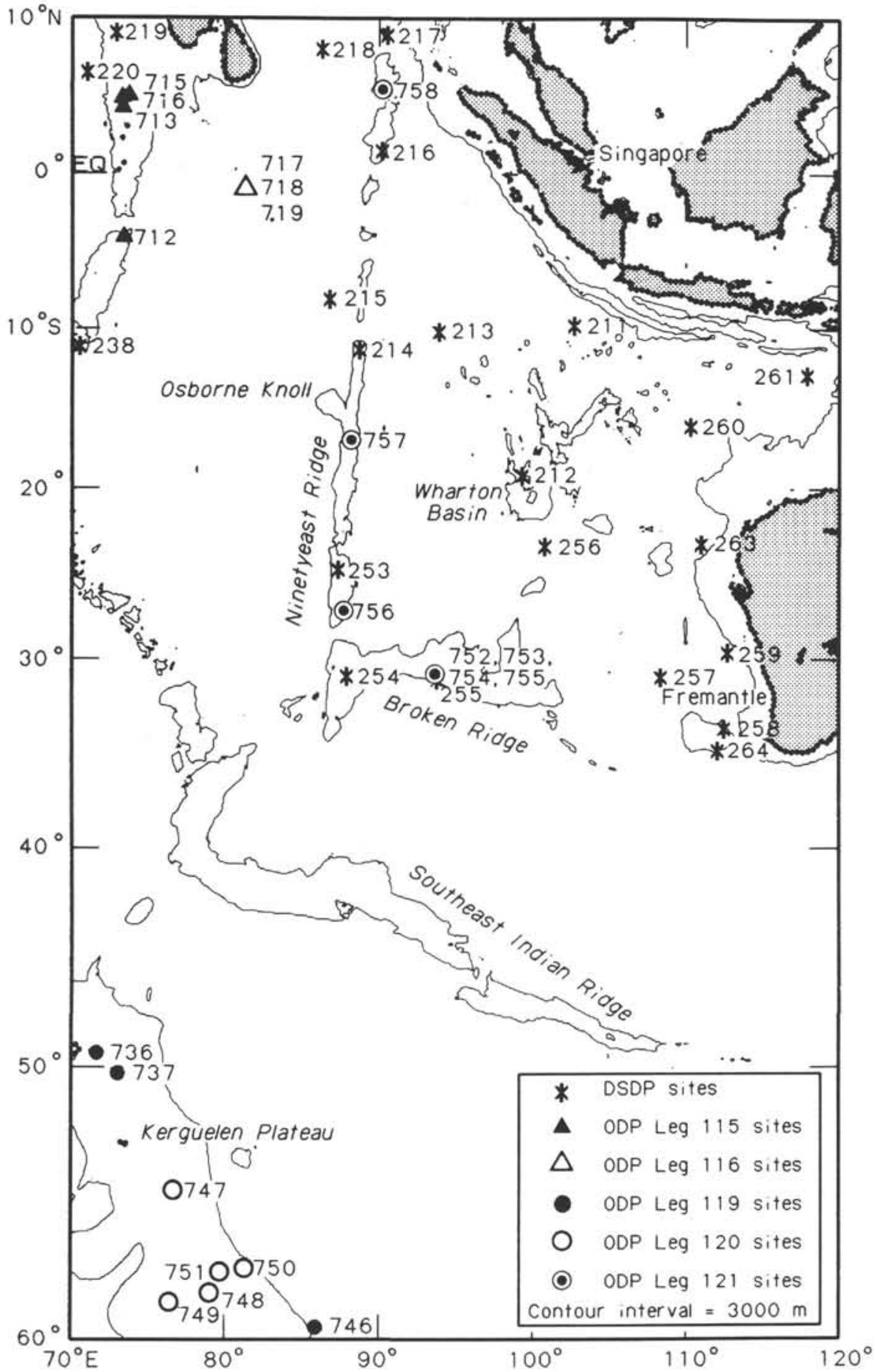

Figure 1. Bathymetric map showing the location of Site 756 at the southern end of Ninetyeast Ridge.

(Chron 18 of the geomagnetic reversal time scale). The interpretation of the origin and structure of Ninetyeast Ridge is complicated by a major left-lateral transform fault immediately east of Ninetyeast Ridge. The history of the Ninetyeast Transform Fault is poorly understood, but in Late Cretaceous to Eocene time it is presumed to have connected the Indian-Antarctic Ridge to a then-active spreading center in the Wharton Basin. This plate boundary was active until some time after Chron 20 (possibly Chron 18), when spreading in the Wharton Basin ceased and spreading on the Southeast Indian Ridge began.

Drilling was planned for three sites on Ninetyeast Ridge. Each site provides a north-south transect through time across part of the paleo-Indian Ocean. In combination with the drilling sites in Prydz Bay on the Antarctic margin and on the Kerguelen Plateau (ODP Legs 119 and 120), the Broken Ridge and Ninetyeast Ridge sites form a complete transect from south to north, spanning 75° of latitude across the present-day Indian Ocean at depths shallow enough to preserve calcareous material.

Southern Site 756

Site 756 lies midway between DSDP Sites 253 and 254 (Fig. 1). The site was positioned for recovery of a second representative sample of basement at the southern end of the ridge (hard-rock recovery at Site 253 was < 1 m). Basement age at this location is predicted to be 49 Ma according to hot-spot models of Duncan (1978) and Duncan et al. (in press). Figure 2 shows the paleogeography of the site at its predicted basement age.

Site 756 was drilled at 27°21.3′S, 87°35.8′E, in a water depth of 1519 m on a sediment-covered bench 10 km east of the crest of Ninetyeast Ridge in an area of rugged terrain. Numerous pinnacles near the site shoal abruptly to 700 m, and a fault with 500 m of vertical throw forms the southeastern edge of the bench (see Fig. 33).

Four holes on a southwest-northeast line were drilled at Site 756 (see "Operations" section, this chapter). The deepest hole penetrated 139 m of sediments and 82 m of volcanics to reach a total depth of 221 mbsf.

Objectives

In general terms, the objectives for drilling on Ninetyeast Ridge fall into three broad categories: petrology, northward motion of the Indian plate, and paleoceanography/paleoclimatology.

A basic premise of the petrologic objectives on Leg 121 was to sample the volcanism of the Kerguelen/Ninetyeast hot spot through time, by sampling along the length of the Ninetyeast Ridge to study variations on a long time scale and also by sampling vertically to study variations within individual volcanic sections on a short time scale. Site 756 provides an ideal location for a vertical section of the lava pile at the southern end of the ridge. Dredging would not be able to meet this objective for the reasons discussed in the "Leg 121 Background and Objectives" chapter.

With the unexpected discovery at Broken Ridge of an extensive ash sequence, which was produced presumably by the Kerguelen/Ninetyeast hot spot, sampling proximal ashes and basement rocks produced by the same volcanic source through the same time period (Late Cretaceous to middle Eocene) became an important objective. In particular, Site 756 provided an opportunity to sample basement of the same age (middle Eocene) as the ashes in the youngest section sampled on Broken Ridge at Site 753. Furthermore, the reverberant nature of the basement reflectors at the proposed location suggested that there was a high probability of encountering significant thicknesses of tephra between the flows, thus permitting a direct comparison to the ashes found at Broken Ridge. The drilling results confirmed the prediction of significant interflow ash material, but poor recovery of those intervals will limit the opportunity for comparison to the ashes at Broken Ridge.

The primary objective of the paleomagnetic studies of the Ninetyeast Ridge sites is to define precisely the slowing of the northward motion of the Indian plate during and after its collision with Asia. We know that it slowed by a factor of three from the rate before collision (~ 15 cm/yr, 70 to ~ 50 Ma) to the rate after collision (~ 5 cm/yr, after 40 Ma; Molnar and Tapponier, 1975; Peirce, 1978; Patriat and Achache, 1984), but the details of how it slowed are unknown. The manner in which it slowed during the middle and late Eocene may provide clues about the tectonic style of the deformation that developed between India and Asia during the early stages of collision. That style, whatever it was, controlled the pattern of faulting across southern Asia in the late Eocene and early Oligocene.

The importance of Site 756 to the northward-motion story is that it should yield a basement-determined paleolatitude for a critical time (approximately 50 Ma) within the range of current estimates of the timing of the collision (60 to 40 Ma). This should provide one firm anchor point on the northward-motion curve, as long as there is a sufficient number of flows (> 8) with reliable paleomagnetic directions to enable adequate statistical sampling of the secular variations of the Earth's field. Unfortunately, the sediments overlying the basalt are not as magnetically stable as expected. Detailed shorebased work in a magnetically clean environment will be done to try to determine reliable sedimentary paleolatitudes during the critical period when the Indian plate was slowing down.

One particular goal for a north-south paleoceanographic transect in the eastern Indian Ocean was to recover fossil records containing a mixture of species from two different climatic assemblages (e.g., temperate and subtropical). Because many of the biostratigraphic time scales are based on the fossil record from one climatic zone (usually subtropical), it is difficult to relate the fossils from one climatic assemblage to those of another with an accurate determination of relative stratigraphic ages. This confusion is further complicated by the time-transgressive nature of many critical biostratigraphic datums as the ecological limits of any particular form are approached. Sites with mixed zonal assemblages allow biostratigraphers the opportunity to work out these interzonal relationships and thus to build more robust time scales with wider applicability.

Site 756 is expected to provide a mixed assemblage fossil record that will allow bridging correlations to be made between the austral temperate assemblages common in the Southern Hemisphere, as found at Broken Ridge, and the low-latitude, subtropical assemblages that are widely used in several biostratigraphic zonation schemes (e.g., Banner and Blow, 1965; Blow, 1969; Berggren et al., 1985; Bolli et al., 1985). Initial analysis of the cores indicates that such expectations are justified.

Eolian dust recovered from pelagic sediments provides a quantitative record of both the intensity of zonal winds and the aridity of the eolian source areas (Rea et al., 1985). One important paleoclimatological goal of Leg 121 was to recover continuous stratigraphic sections of Cenozoic age in order to analyze the eolian record. Ninetyeast Ridge is ideally located for this study because it lies between the great deserts of Africa and Australia and therefore should receive an adequate supply of dust. Furthermore, locations on top of the ridge are protected from abyssal reworking and should have fewer unrecognized contributions from hemipelagic input. The backtrack history of the three sites on Ninetyeast Ridge (see Fig. 16 in the "Leg 121 Background and Objectives" chapter) will provide a paleoclimatic record that spans nearly 50° of latitude.

Site 756 was intended to provide a section in southern temperate latitudes that has a reasonably complete stratigraphic record and, therefore, a useful paleoclimatic record. In contrast, the Neogene section recovered at Broken Ridge is winnowed and may contain some minor disconformities, resulting in an incomplete paleoclimatic record.

An operational deployment of the Navidrill mud-motor coring system in basalts, originally planned for Site 757, was added to the objectives at this site because of operational considerations. The results of the NCB deployment in Hole 756C are discussed in the "Operations" section.

OPERATIONS

Site 756

With the Broken Ridge drilling operations completed, the vessel proceeded to the southernmost site to be drilled on Nine-

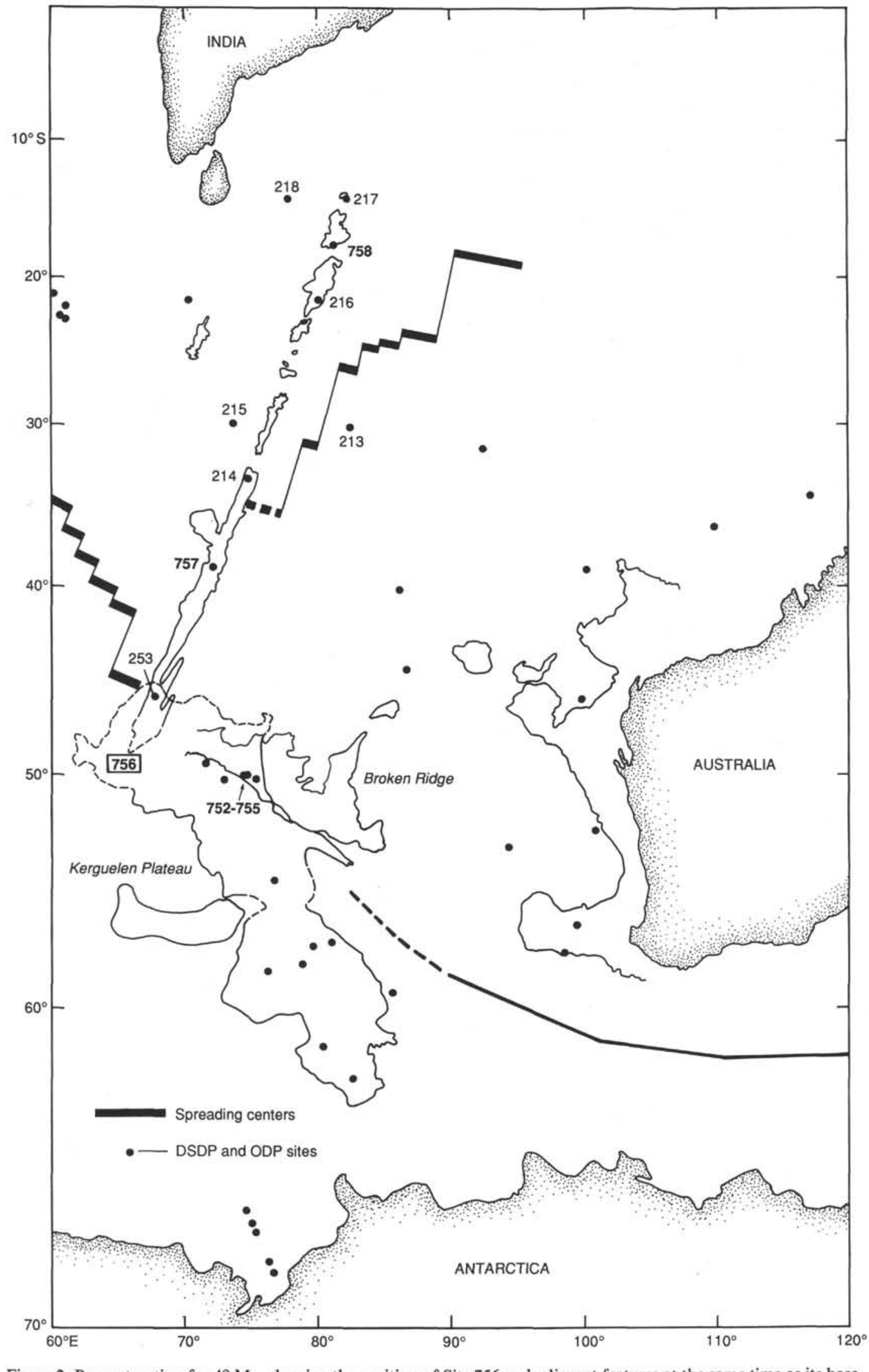

Figure 2. Reconstruction for 49 Ma, showing the position of Site 756 and adjacent features at the same time as its basement age, as predicted by Duncan et al. (in press). The northern Kerguelen Plateau is held fixed at it's present-day coordinates (model by Royer et al., in press).

tyeast Ridge. The 372-nmi transit took 32.3 hr at an average speed of 11.5 kt before the ship slowed to 6 kt and streamed the seismic gear for the site survey. The 34-nmi survey conducted at the proposed site area allowed the co-chief scientists to identify a slight fault in the sedimentary structure at the location of proposed Site NER-5. The location for the beacon drop was therefore moved about 500 m to the west-northwest.

On the second pass over the chosen location, an attempt was made to drop the beacon, but the lines fouled in the pelican hook when it was triggered and the beacon did not fall. The ship continued on to complete the site survey, which was followed by a 5-min test of the new water gun depressor fins at a speed of 10 kt. The gear was then recovered, and the ship turned and passed over the site, again guided by Global Positioning System (GPS) satellite coordinates. The next attempt to drop the beacon failed as the ship passed the site a third time. Because the GPS positioning was good, the ship was able to stop, lower thrusters, and hover over the site to begin tripping the drill string while the problems with the beacon launch technique were worked out. The beacon was finally dropped at 2150 hr on 25 May to officially begin Hole 756A.

Hole 756A

The ship was offset 100 m southwest from the beacon, drill pipe was run to the seafloor, and the mud-line APC core was shot from a depth of 1534 m, 3 m above the depth obtained by the precision depth recorder. Nevertheless, the core barrel came up overfilled with soft calcareous ooze, indicating that the bit was below the seafloor when the core was taken (Table 1).

Hole 756B

The pipe was raised to a depth of 1528 m, and Hole 756B was spudded with a successful APC core that established the water depth at 1518.1 m. The next 10 piston cores were taken without trouble in soft to firm calcareous ooze, and recovery was greater than 100% (Table 1). Core 121-756B-12H became stuck in a clay-rich zone and could not be pulled free with 120,000-lb overpull. An attempt was made to drill or wash over the stuck core barrel, and although free rotation was achieved for a few minutes, a piston rod connection failed and the bulk of the APC core was lost in the hole. The pipe was pulled clear of the seafloor at 1235 hr, 26 May.

Hole 756C

The vessel was offset 200 m northeast, 100 m past the beacon, to achieve a maximum offset from Hole 756B to allow for measurement of horizontal geochemical gradients in core samples taken at similar depths from the two holes (Fig. 3). Another mud-line APC core established the new water depth at 1526.7 m. The bit was then washed to 78.6 mbsf, where a spot piston core was taken. Washing continued to 100.9 mbsf, where coring with the XCB was begun to overlap the strata reached in Hole 756B. XCB coring continued to a depth of 150.3 mbsf, using the leg's new XCB coring system to achieve good recovery in firm chalk/limestone (Table 1). One XCB barrel became stuck in the drill pipe only 11 m below the rig floor when it was dropped to be pumped down to the bit. The problem was found and quickly remedied, and the XCB operations continued until very hard limestone, presumably overlying volcanics, was found to be impenetrable by the XCB system. The XCB tools were set aside, and the Navidrill coring system was deployed.

Three Navidrill cores were taken in five attempts. The first NCB core was cut using the high-torque, low-speed Mach 1 mud motor. The 100% recovery of a perfect section of vesicular basalt 4.2 m long demonstrated the potential of diamond coring technology in hard rock. The next two NCB runs, however, did not net any core. We assumed that the problem was motor stalling out in using the low-torque, high-speed Mach 3 mud motor in the NCB assembly. The next run recovered 1.13 m of soft weathered ash, again using the Mach 1 motor. The final core was a mere 0.4 m of basalt chunks. The NCB operations were then terminated because the rate of progress was proving to be significantly less than could be expected with the RCB system in basement material. Inspection of the Mach 1 motor while cleaning it revealed that the universal joint in the drive shaft was damaged. Later disassembly of the motor and drive shaft uncovered the problem: the knuckle-type universal joint had disintegrated completely. This was assumed to have happened during the last core attempt since some penetration into the formation was noted before the NCB was pulled. The pipe was then tripped back to

Table 1. Coring summary, Site 756.

Core no.	Date (May 1988)	Time (local)	Depth top (mbsf)	Depth bottom (mbsf)	Length cored (m)	Length recovered (m)	Recovery (%)
121-756A-							
1H	26	0350	0.0	9.7	9.7	9.72	100.0
					9.7	9.72	100.0
121-756B-							
1H	26	0435	0.0	8.5	8.5	8.45	99.4
2H	26	0510	8.5	18.1	9.6	9.39	97.8
3H	26	0545	18.1	27.7	9.6	9.56	99.6
4H	26	0620	27.7	37.3	9.6	9.72	101.0
5H	26	0655	37.3	46.9	9.6	9.53	99.3
6H	26	0730	46.9	56.2	9.3	9.73	104.0
7H	26	0810	56.2	65.6	9.4	9.86	105.0
8H	26	0845	65.6	75.2	9.6	9.60	100.0
9H	26	0920	75.2	84.9	9.7	9.96	102.0
10H	26	0950	84.9	94.6	9.7	9.92	102.0
11H	26	1025	94.6	104.3	9.7	9.98	103.0
					104.3	105.70	101.3
121-756C-							
1H	26	1400	0.0	8.8	8.8	8.77	99.6
2H	26	1525	68.9	78.6	9.7	9.24	95.2
3W	26	1625	78.6	100.9	22.3	0.05	(wash core)
4X	26	1655	100.9	110.5	9.6	9.70	101.0
5X	26	2000	110.5	120.2	9.7	8.15	84.0
6X	26	2040	120.2	129.8	9.6	7.16	74.6
7X	26	2120	129.8	139.4	9.6	8.76	91.2
8X	26	2215	139.4	144.5	5.1	3.94	77.2
9X	27	0000	144.5	150.3	5.8	0.35	6.0
10N	27	0310	150.3	154.5	4.2	4.21	100.0
11N	27	1050	154.5	156.5	2.0	1.13	56.5
12N	27	1350	156.5	159.0	2.5	0.40	16.0
	(Coring)				76.6	61.81	80.7
	(Washing)				22.3	0.05	
					98.9	61.86	
121-756D-							
1R	27	2305	0.0	9.6	9.6	9.65	100.0
2R	28	0035	70.1	79.7	9.6	9.47	98.6
3W	28	0250	79.7	139.0	59.3	1.46	(wash core)
4R	28	0430	139.0	148.6	9.6	1.75	18.2
5R	28	0615	148.6	158.3	9.7	0.69	7.1
6R	28	0850	158.3	168.0	9.7	3.14	32.4
7R	28	1210	168.0	177.7	9.7	5.25	54.1
8R	28	1625	177.7	187.4	9.7	0.80	8.3
9R	28	1850	187.4	197.0	9.6	4.31	44.9
10R	28	2115	197.0	206.6	9.6	3.50	36.4
11R	28	2350	206.6	216.2	9.6	3.30	34.4
12R	29	0440	216.2	221.0	4.8	4.18	87.1
	(Coring)				101.2	46.04	45.5
	(Washing)				59.3	1.46	
					160.5	47.50	

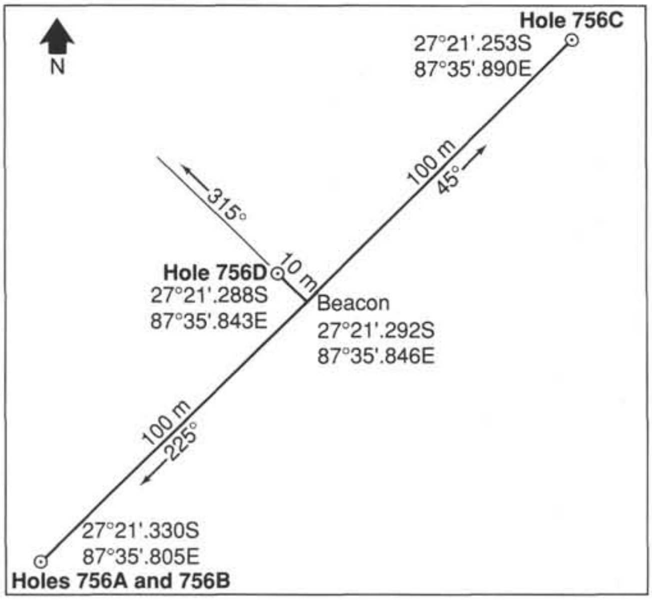

Figure 3. Beacon and relative ship positions for the four Site 756 holes.

the deck for a change over to the RCB coring system and bottom-hole assembly (BHA). The bit was on deck at 1845 hr on 27 May.

Hole 756D

An extra stand of drill collars (for more weight on the bit) and a slightly used 9⅞" C-57 hard-rock bit were made up to the BHA and tripped back to the seafloor. The vessel was offset 11 m northwest of the beacon, and Hole 756D was spudded with a mud-line punch core that established the drilling depth at 1524.0 m. Subsequent analysis of pore-water chemistry data ("Inorganic Geochemistry" section, this chapter) indicates that the recorded mud line may have been about 4 m too deep. The bit was washed to 70.1 mbsf without coring and a spot core was taken. Washing then continued to 139 mbsf, where coring resumed only inches above the contact with basalt.

Slow but acceptable progress was made into basement of vesicular basalt with typical core recovery for the RCB system, ranging from 0.69 to 5.25 m per core. Hole conditions began to deteriorate after penetrating about 30 m of basement. Regular mud sweeps were used to fight the recurring problems of excessive torque and the 1 to 2 m of fill found each time a new core was to be cut. After battling hole problems off and on for seven RCB cores, the scientific objectives were declared achieved and the hole was terminated. The depth of total penetration in this hole, and for Site 756, is 221 mbsf, with a core recovery of 36% in 82 m of penetration into the volcanic section. The drill pipe was pulled and the bit was on deck at 1020 hr, 29 May, whereupon the ship got underway for the central site on Ninetyeast Ridge, proposed Site NER-2C. Inspection of the C-57 bit found the beginnings of bearing failure on one of the four cones. The bit would have lasted for perhaps three or four more cores.

LITHOSTRATIGRAPHY AND SEDIMENTOLOGY

A 227.7-m-thick section of Pleistocene through upper Eocene sediment and basalt was recovered at Site 756 in four holes before drilling was terminated after penetrating approximately 82 m of basalt in Hole 756D (Fig. 4). Only one sedimentary unit is present at Site 756, a nannofossil ooze with foraminifer contents varying between 5% and 20%. A subunit of limestone immediately above the basaltic basement has a maximum observed thickness of 30 cm. Unit II consists of several flow units of vesicular, subaerially erupted basalt. The lithology is summarized in Table 2. Pore-water chemistry data indicate that the mud-line core at Hole 756D was too deep (overshot) by about 4 m. Therefore, all depths given for Hole 756D may be about 4 m too shallow.

Subunit IA (0–144.5 mbsf; Cores 121-756A-1H, 121-756B-1H to 121-756B-11H, 121-756C-1H to 121-756C-8X, and 121-756D-1R to 121-756D-3W) is a white (10YR 8/1 and 10YR 8/2) nannofossil ooze and nannofossil ooze with foraminifers, grading at 50 mbsf to very pale brown (10YR 8/3, 10YR 8/4, 10YR 7/3, and 10YR 7/4). Faint to moderate mottling is present in the majority of the cores, with mottles of a lighter color, usually white, in a darker matrix. Circular mottles, ringlike features of lighter color in a darker matrix, are present in Cores 121-756B-3H and 121-756B-4H (18.1–37.3 mbsf) and 121-756C-1H (0–8.5 mbsf). These are thought to be burrows with chemical reaction rims. The shell fragments in Cores 121-756A-1H and 121-756B-1H are uncharacteristic for the deep-sea nannofossil lithology. The small black flecks common throughout the sediments are identified as traces of volcanogenic glass. A single, very dark grayish brown (10YR 3/2) layer at 64–67 cm in Section 121-756C-2H-1 (9.6 mbsf) consists of highly altered volcanic glass with opaque minerals and feldspar crystals. This layer occurs only in Hole 756C.

Smear slide analyses show primarily various nannofossils (Fig. 5) and a lesser amount (5%–20%) of foraminifers in the sediments of Subunit IA. Trace amounts of radiolarians, sponge spicules, and silicoflagellates occur throughout the ooze. Micrite occurs in small amounts that never exceed 5%. Traces of volcanic glass are present in virtually every core and never exceed 2% in the dominant lithology. The ash layer at 64–67 cm in Section 121-756B-2H-1 contains 90% glass.

The mean particle diameter was determined for the bulk sediments, using the method described in the "Explanatory Notes" chapter (Fig. 6 and Table 3). The grain size has no clear linear depth relation although mean particle size notably increases between 50 and 70 mbsf. This increase corresponds stratigraphically to a decrease in the linear sedimentation rate during the Oligocene and early Miocene. Linear sedimentation rates for Site 756 average about 0.36 cm/1000 yr, varying from a low of 0.2 cm/1000 yr in the Oligocene to a high of 0.4 cm/1000 yr in the Eocene and the middle to upper Miocene. The increase in grain size and the lower sedimentation rate during the Oligocene may indicate an increase in winnowing at that time.

Subunit IB (144.5–150.3 mbsf) is a very pale brown (10YR 7/4) and dark yellowish brown (10YR 4/6) foraminifer limestone. The coarse-grained limestone is speckled with black and green flecks. These flecks are crystals of a wide variety of minerals. Plagioclase and hematite were identified by inspection. Other minerals are present, but could not be readily identified. Fragments of benthic foraminifers were also observed in the limestone.

Unit II (150.3–221.0 mbsf) is composed of vesicular basalt flows (see "Petrology" section, this chapter) that appear to have been subaerially erupted. The flows show substantial alteration. The contact between the overlying limestone and the basalt is not easily recognized, although basalt fragments are seen in the limestone and a breccia of limestone and basalt is observed in Section 121-756D-3W-CC. Shell fragments are also present in the breccia.

The basalts were erupted subaerially and then submerged in a shallow-water environment which allowed for the deposition of the limestone of Subunit IB. This interpretation is supported by the presence of shell fragments in the breccia of Core 121-756D-3W and the weathering and subsequent incorporation of basalt fragments into the limestone. Subsidence must have con-

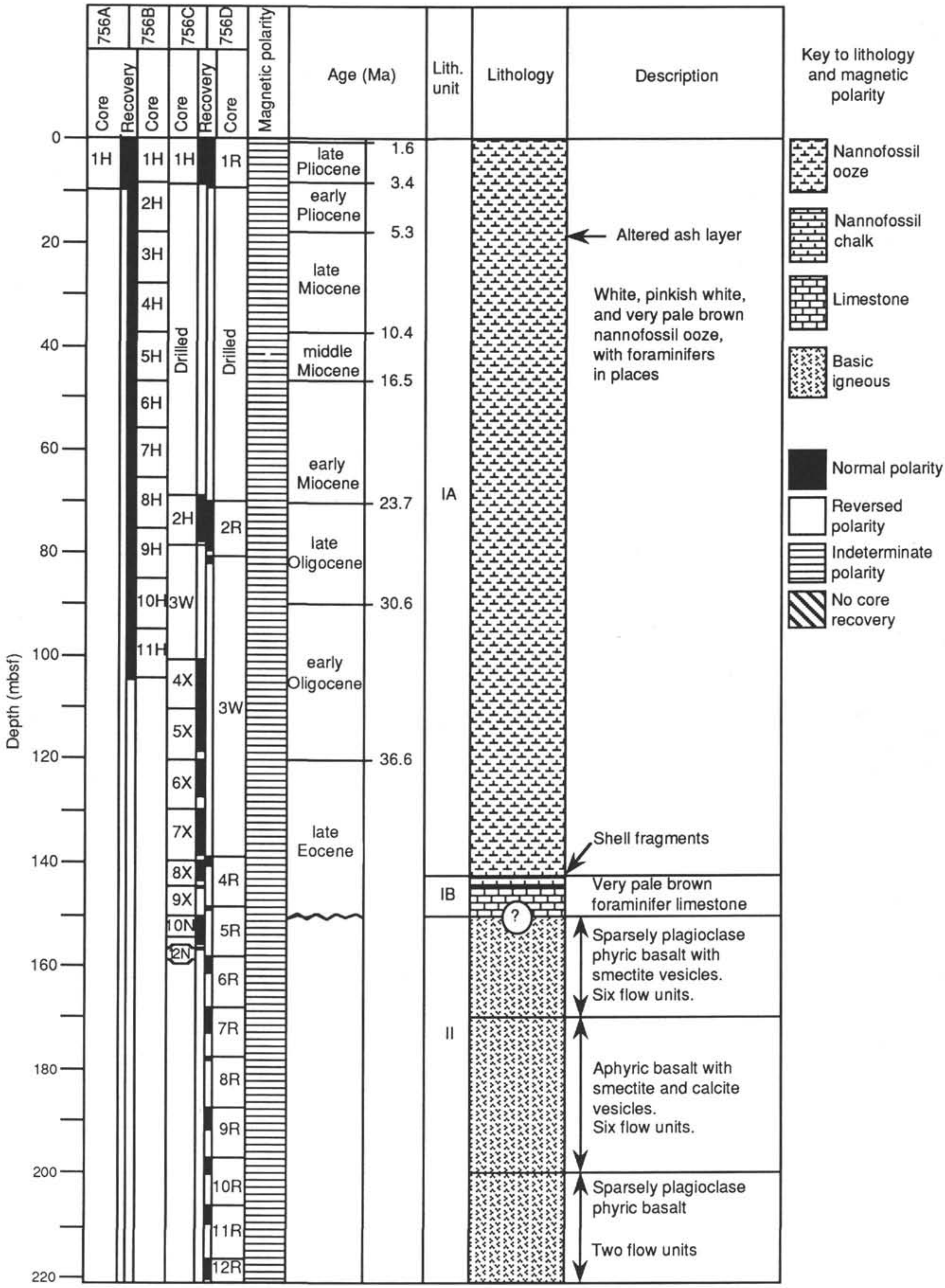

Figure 4. Site 756 summary diagram.

Table 2. Lithologic units at Site 756.

Unit	Core interval	Depth (mbsf)	Lithology	Age
IA	756A-1H	0.0–9.7	Nannofossil ooze with foraminifers and nannofossil ooze	Pleistocene to Pliocene
	756B-1H to -11H	0.0–104.3	Nannofossil ooze with foraminifers and nannofossil ooze	Pleistocene to late Oligocene
	756C-1H to -8X	0.0–144.5	Nannofossil ooze with foraminifers and nannofossil ooze	Pleistocene to late Eocene
	756D-1R to -3W	[a]0.0–139.0	Nannofossil ooze with foraminifers	Pliocene to late Eocene
IB	756C-9X	144.5–150.3	Foraminifer limestone	late Eocene
	756D-3W	[a]138.0–139.0	Foraminifer limestone	late Eocene
II	756C-9X to -12N	150.3–159.0	Basalt	
	756D-4R to -12R	[a]148.6–221.0	Basalt	

[a] Depths may be 4 m too shallow, as indicated by pore-water chemistry data.

Figure 5. SEM photomicrograph of nannofossils from Sample 121-756B-2H-1, 90 cm. Most of the fossils shown are discoasters and coccoliths.

tinued to permit the change to the lithology of Subunit IA. The high percentage of nannofossils is typical of pelagic low-productivity environments, the assumption of which is supported by the low sedimentation rates of carbonate ooze.

BIOSTRATIGRAPHY

The objectives of drilling at Site 756 were to recover a significant amount of basement section for petrologic studies of the evolution of the Kerguelen/Ninetyeast hot spot and to sample an upper Eocene to Holocene sedimentary section for paleogeographic/climatic studies of the eastern Indian Ocean.

The chemistry data indicate that the mud-line core at Hole 756D is too deep by about 4 m. Therefore, all depths in Hole 756D may be about 4 m too shallow. Detailed correlations between holes should make allowance for this discrepancy.

Upper Eocene to Pleistocene sediments from Site 756 yield well-preserved and abundant calcareous nannofossils and planktonic foraminifers that provide a relatively complete biostratigraphic zonation.

Four holes were drilled at Site 756. Hole 756A recovered just one core. About 104.3 m of a complete upper Oligocene to Pleistocene calcareous nannofossil ooze section was recovered from Hole 756B. Hole 756C was washed down to 100.9 mbsf; however, two spot cores were taken, one at the mud line and another at 68.9 mbsf. These cores were dated as late Pliocene and

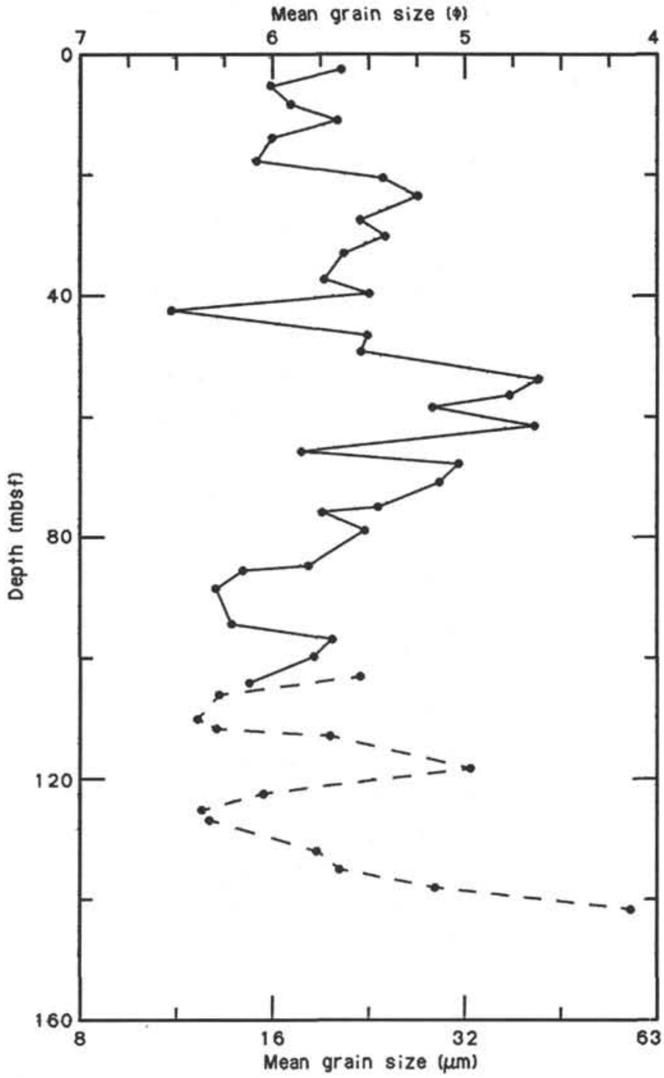

Figure 6. Grain-size analyses for Site 756. The solid line represents data from Hole 756B, and the dashed line data from Hole 756C. A grain-size maximum occurs between 50 and 70 mbsf.

early Miocene, respectively. Middle Oligocene to upper Eocene sediment was found in Samples 121-756C-4X-CC to 121-756C-9X-CC (100.9–150.3 mbsf). The oldest sediment above the basalt in Hole 756C is a pale brown foraminiferal limestone of late Eocene age (CP15b). Two spot cores from Hole 756D, one from the mud line and the other from 79.9 mbsf, show ages of latest Miocene to Pliocene and early Miocene, respectively. The brown foraminiferal limestone from a wash core just above the basalt was dated at latest Eocene (CP15b/16). Figure 7 summarizes the age-depth relationship at Site 756 using the datum levels in Table 4.

Calcareous nannofossils at Site 756 are abundant and well preserved. The Pliocene and Pleistocene calcareous nannofossil assemblages are low latitude in nature. The older assemblages are considered to be of a more high-latitude affinity.

Planktonic foraminifers are abundant and well preserved at Site 756. The upper Miocene to Holocene planktonic foraminifer assemblages are dominated by subtropical and temperate forms. This provides a good bridge for correlating the temperate planktonic foraminifer zonation schemes used on Broken Ridge with the more widely used subtropical-tropical zonation

Table 3. Grain-size analyses for Site 756.

Core, section, interval (cm)	Depth (mbsf)	Mean diameter (μm)	(ϕ)
121-756B-			
1H-2, 90	2.4	20.10	5.64
1H-4, 90	5.4	15.50	6.01
1H-CC, 1	8.5	16.70	5.90
2H-2, 90	10.9	19.80	5.66
2H-4, 90	13.9	15.60	6.00
2H-CC, 1	18.1	14.80	6.08
3H-2, 90	20.5	23.40	5.42
3H-4, 90	23.5	26.50	5.24
3H-CC, 1	27.7	21.50	5.54
4H-2, 90	30.1	23.50	5.41
4H-4, 90	33.1	20.30	5.62
4H-CC, 1	37.3	19.00	5.72
5H-2, 90	39.7	22.30	5.49
5H-4, 90	42.7	10.90	6.52
5H-CC, 1	46.9	22.10	5.50
6H-2, 90	49.3	21.60	5.53
6H-5, 90	53.8	41.00	4.61
6H-CC, 1	56.2	37.00	4.76
7H-2, 90	58.6	27.90	5.16
7H-4, 90	61.6	40.40	4.63
7H-CC, 1	65.6	17.50	5.84
8H-2, 90	69.9	30.80	5.02
8H-4, 90	72.9	28.80	5.12
8H-CC, 1	75.2	23.00	5.44
9H-1, 90	76.1	18.90	5.73
9H-3, 90	79.1	21.90	5.51
9H-CC, 1	84.9	18.00	5.80
10H-1, 90	85.8	14.20	6.14
10H-3, 90	88.8	12.90	6.28
10H-CC, 1	94.6	13.60	6.20
11H-2, 90	97.0	19.50	5.68
11H-4, 90	99.0	18.30	5.77
11H-CC, 1	104.3	14.50	6.11
121-756C-			
4X-2, 90	103.2	21.70	5.53
4X-4, 90	106.2	13.00	6.27
4X-CC, 1	110.5	12.00	6.38
5X-2, 90	112.9	12.90	6.28
5X-4, 10	115.9	19.40	5.69
5X-CC, 1	120.2	32.20	4.96
6X-2, 90	122.6	15.20	6.04
6X-4, 90	125.6	12.20	6.36
6X-CC, 1	129.8	12.50	6.32
7X-2, 90	132.2	18.40	5.76
7X-4, 90	135.2	20.00	5.64
7X-CC, 1	139.4	28.40	5.14
8X-2, 90	141.8	56.80	4.14

schemes used at this site. The middle Miocene to Eocene assemblages consist of more temperate faunas that are similar to the assemblages of the same age found on Broken Ridge. Furthermore, a complete Eocene/Oligocene boundary was recovered.

The calcareous nannofossil and planktonic foraminifer biostratigraphic subdivisions and datum marker species of Site 756 are summarized in Figures 8 and 9. Reworking is common at Site 756. A few Oligocene and early Eocene age calcareous nannofossils and planktonic foraminifers were found mixed in with the Miocene and Pliocene sediments.

Benthic foraminifers are consistently found through all the sections. The benthic foraminifer assemblages indicate that the water depth at Site 756 was lower bathyal from the late Eocene to Pleistocene. However, inner neritic, larger benthic foraminifers were found in the late Eocene age limestone (lithologic Subunit IB) overlying the basalt in Hole 756D, which indicates that rapid subsidence occurred during the late Eocene (Fig. 10).

Calcareous Nannofossils

Sediments recovered from Site 756 contain abundant calcareous nannofossils. Sample analyses resulted in a relatively complete biostratigraphic zonation, ranging from upper Eocene to Pleistocene. Calcareous nannofossil preservation is generally good throughout the section, but moderate to poor in the upper Eocene sediments.

Okada and Bukry's (1980) low-latitude calcareous nannofossil zonation scheme was successfully applied for nearly all of the sections at this site. Difficulties occurred where some marker species in the middle and lower Miocene sections are missing, in which case Martini's (1971) calcareous nannofossil zonation scheme was used to define the zones.

Pleistocene

Pleistocene sediments were found to 0.47 mbsf at Site 756. The assemblage consists of abundant *Rhabdosphaera clavigera*, *Rhabdosphaera stylifera*, few *Helicosphaera wallichii*, common *Pseudoemiliania lacunosa*, and *Crenalithus doronicoides*. This assemblage is assignable to Zone CN13. The presence of abundant *R. clavigera* and *R. stylifera* is characteristic of low-latitude assemblages.

The Pliocene/Pleistocene boundary is placed in Section 121-756B-1H-1 (0.47–1.97 mbsf), where the last occurrence of *Discoaster brouweri* is noted.

Pliocene

Pliocene calcareous nannofossil assemblages are dominated mainly by diverse and abundant discoasters, ceratoliths, and amauroliths, which characterize a warm subtropical environment. The assemblage consisting of abundant *D. brouweri*, *Discoaster tamalis*, and *Calcidiscus macintyrei* in Section 121-756B-1H-4 (4.5–6.00 mbsf) and Sample 121-756C-1H-CC (8.8 mbsf) is of late Pliocene age (CN12). Abundant *Ceratolithus rugosus*, *Ceratolithus acutus*, *Amaurolithus primus*, *Reticulofenestra pseudoumbilica*, and *D. tamalis* in Samples 121-756B-1H-CC to 121-756B-3H, 149–150 cm, are representative of Zones CN10 to CN11 of the early Pliocene. Sample 121-756D-1R-CC (9.5 mbsf) is of latest Miocene to early Pliocene age. The Miocene/Pliocene boundary should be located below Zone CN10b in Section 121-756B-2H-CC (18.1–19.6 mbsf).

Miocene

Discoasters and some ceratolith forms characterize the upper Miocene sections. Unfortunately, overgrowth and etching of the discoasters prevent quick and accurate identification.

Samples 121-756B-4H, 47–48 cm, to 121-756B-4H-CC (22.6–27.7 mbsf) contain *A. primus*, *Amaurolithus delicatus*, *D. brouweri*, *Discoaster surculus*, and *Discoaster pentaradiatus*, which are indicative of Zone CN9. The occurrence of *Discoaster neohamatus* and *R. pseudoumbilica* without *D. surculus* in Sample 121-756B-4H-4, 90–91 cm, denotes Zone CN8. Zone CN7 is indicated by the presence of *D. hamatus* in Samples 121-756B-4H-4, 47–48 cm, to 121-756B-4H-CC (34.17–37.3 mbsf). *Catinaster coalitus* was not found in this section. Zone CN6 is based on the absence of *D. hamatus* and the presence of *Discoaster exilis*, *Discoaster variabilis*, and *C. macintyrei* in Sections 121-756B-5H-1 to 121-756B-5H-3. The presence of the same assemblage plus *Cyclicargolithus floridanus* and the absence of *Sphenolithus heteromorphus* in Sections 121-756B-5H-4 to 121-756B-5H-CC indicate Zone CN5.

The occurrence of *S. heteromorphus* in Sections 121-756B-6H-3 to 121-756B-6H-6 and in Sample 121-756C-2H-CC defines Zone CN3–4 of early Miocene age. *Sphenolithus belemnos* is present in Samples 121-756B-6H-6, 100–105 cm, to 121-

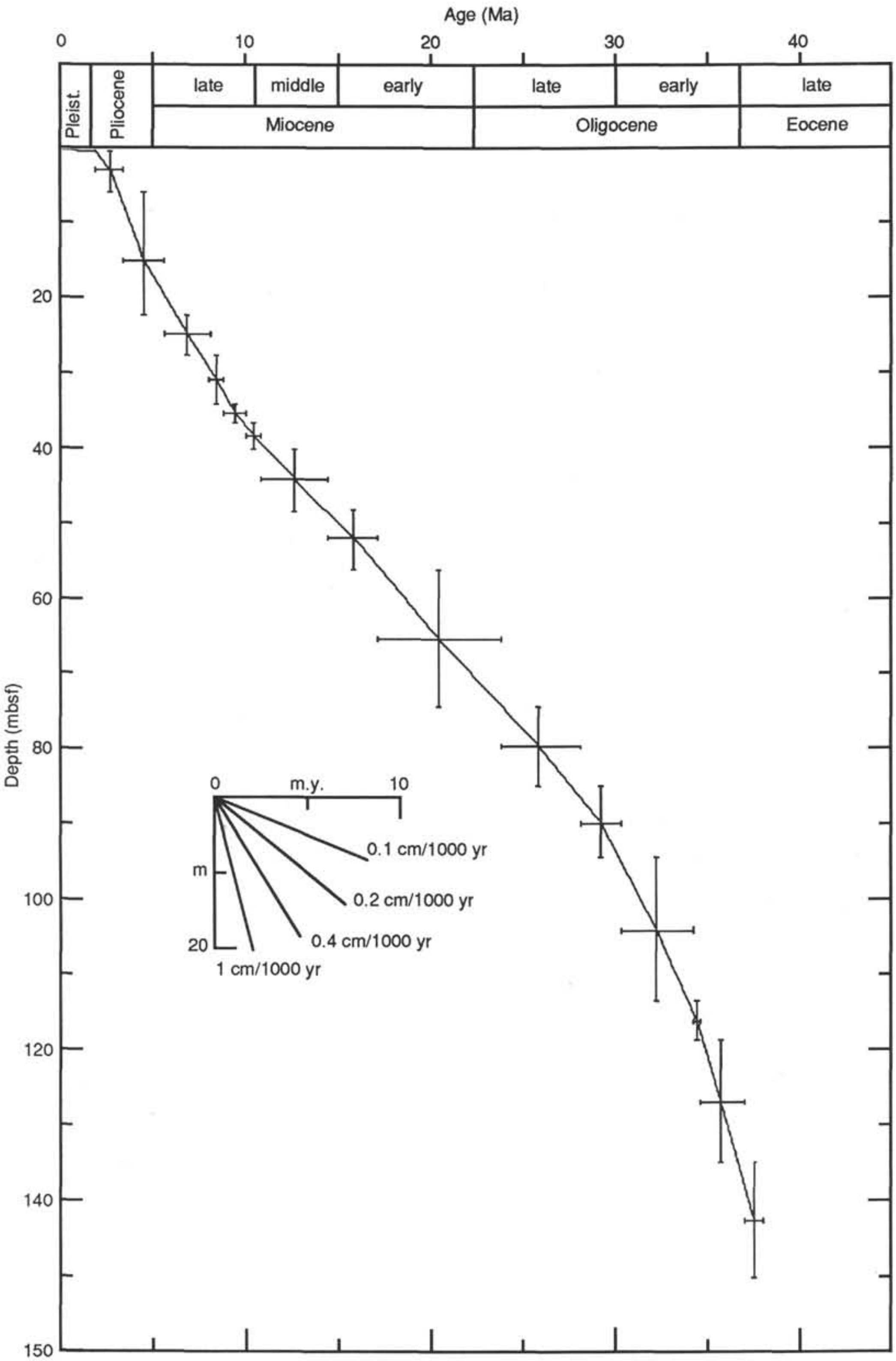

Figure 7. Age vs. depth plot for Site 756. Vertical bars represent the stratigraphic ranges and horizontal bars represent the ranges of the zones.

Table 4. Calcareous nannofossil and planktonic foraminifer datums at Site 756.

Species event[a]	Age (Ma)	Depth (mbsf)
Calcareous nannofossils		
LO *Discoaster brouweri*	1.90	0.47–1.97
LO *Reticulofenestra pseudoumbilica*	3.50	4.50–6.00
FO *Discoaster tamalis*	3.80	8.00–8.50
LO *Discoaster hamatus*	8.85	34.70–35.67
FO *Discoaster hamatus*	10.00	37.30–38.80
LO *Sphenolithus heteromorphus*	14.40	45.40–46.90
FO *Sphenolithus heteromorphus*	17.10	54.70–56.20
LO *Sphenolithus ciperoensis*	25.20	73.70–74.70
FO *Sphenolithus ciperoensis*	30.20	94.60–96.10
LO *Reticulofenestra umbilica*	34.60	117.70–119.20
LO *Discoaster saipanensis*	36.70	134.90–136.40
Planktonic foraminifers		
LO *Globorotalia multicamerata*	2.9	1.5–3.0
LO *Globoquadrina altispira*	2.9	1.5–3.0
LO *Sphaeroidinella seminulina*	3.0	3.0–8.5
FO *Globorotalia tosaensis*	3.1	3.0–8.5
LO *Globorotalia margaritae*	3.4	8.5–13.0
LO *Globigerina nepenthes*	3.9	8.5–13.0
FO *Sphaeroidinella dehiscens*	8.1	8.5–13.0
FO *Globorotalia tumida*	5.2	18.1–21.1
FO *Globigerinoides conglobatus*	5.3	18.1–21.1
LO *Globoquadrina dehiscens*	5.3	18.1–21.1
FO *Globorotalia margaritae*	5.6	18.1–21.1
FO *Globorotalia plesiotumida*	7.7	27.7–37.3
LO *Globorotalia siakensis*	10.4	38.8–41.8
FO *Globigerina nepenthes*	11.3	38.8–41.8
LO *Globorotalia peripheroacuta*	14.6	41.8–43.3
LO *Globigerinita stainforthi*	17.4	46.9–56.2
LO *Globorotalia kugleri*	21.8	56.2–65.6
FO *Globoquadrina dehiscens*	23.2	65.6–75.2
LO *Globigerina angulisuturalis*	23.2	65.6–75.2
LO *Chiloguembelina cubensis*	30.0	65.6–75.2
FO *Globigerina angulisuturalis*	31.6	84.9–94.6
LO *Pseudohastigerina*	34.0	94.6–104.3

[a] FO = first occurrence; LO = last occurrence.

756B-7H-1, 100–105 cm, which places the interval in Zone CN2.

The presence of *Zygrhablithus bijugatus*, *C. floridanus*, *Cyclicargolithus abisectus*, and *Dictyococcites bisectus* in Sections 121-756B-8H-6 to 121-756B-7H-1 and Sample 121-756D-3W-CC indicates Zone CN1.

The Oligocene/Miocene boundary at Site 756 is noted in Section 121-756B-8H-6 (75.6–74.1 mbsf), based on the last occurrence of *Sphenolithus ciperoensis*.

Reworking is common in the Miocene section at Site 756. Some Oligocene and late Eocene age species, such as *Z. bijugatus*, *D. bisectus*, *Reticulofenestra umbilica*, and *Chiasmolithus altus* were found mixed with the Miocene assemblages.

Oligocene

The relatively well-preserved Oligocene calcareous nannofossil assemblages at Site 756 are characterized by the presence of *Sphenolithus predistentus*, *Sphenolithus distentus*, and *S. ciperoensis*. The occurrence of *S. ciperoensis* together with *S. distentus* in Sections 121-756B-8H-6 to 121-756B-10H-CC indicates Zone CP19. The co-occurrence of *S. distentus* with *S. predistentus* in Sample 121-756B-11H-CC (104.3 mbsf) and in the interval from Section 121-756C-5X-2 to Sample 121-756C-4H-CC indicates Zone CP18. Zone CP17 at this site is characterized by the occurrence of *S. predistentus* and the absence of *R. umbilica* in Sections 121-756C-5X-1 to 121-756C-5X-8 (113.5–118.7 mbsf). Zone CP16 is indicated by the presence of *R. umbilica*, *Ericsonia subdisticha*, and the high-latitude marker species *Isthmolithus recurvus* in Samples 121-756C-5X-CC and 121-756C-6X-CC (118.7–134.9 mbsf). Placement of the Eocene/Oligocene boundary is based on the last occurrence of *Discoaster saipanensis* in Section 121-756C-7X-2 (134.9–136.4 mbsf).

Eocene

The lowermost sediments above the basalt are late Eocene in age. This age is indicated by the calcareous nannofossil assemblage consisting of the marker species *I. recurvus*, *Chiasmolithus omaruensis*, and *D. saipanensis* in the core-catcher samples from Cores 121-756C-7X through 121-756C-9X-CC (134.9–150.3 mbsf). This assemblage is assignable to Zone CP15b.

Planktonic Foraminifers

The primary objective at Site 756 for the planktonic foraminifer paleontologists was to determine whether the late Paleogene to Neogene age planktonic foraminifer assemblages are of a different faunal composition than those recovered at Broken Ridge.

Neogene

A well-preserved, early Miocene to Pleistocene age assemblage of planktonic foraminifers was recovered from Hole 756B. Dominating the assemblage are typical warm to subtropical faunas and other more cosmopolitan species. The presence of most, if not all, low-latitude marker species made it possible to apply the zonation schemes of Banner and Blow (1965) and Blow (1969). We found difficulties in trying recognize the low-latitude zonal boundaries of Bolli and Saunders (1985) because of the lack of their zonal taxa.

Pliocene

A complete Pliocene sequence of sediments was recovered down to 8.5 mbsf. The faunas are dominated by tropical to warm-subtropical species, such as *Globigerinoides obliquus*, *Globigerinoides extremus*, *Globigerinoides sacculifer*, and *Globigerinoides ruber pyramidalis*, and the more temperate to subtropical species *Globorotalia crassaformis*, *Globorotalia conomiozea*, and *Globigerina bulloides*. Rare throughout the Pliocene are fully tropical *Pulleniatina* sp., *Sphaeroidinella* sp., *Neogloboquadrina* sp., *Globorotalia tumida tumida*, *Globorotalia tumida flexuosa*, and *Globigerinoides fistulosus*. This assemblage contrasts with the Pliocene faunas at Broken Ridge, which have an affinity with other temperate faunas in the Southern Hemisphere.

Miocene

The upper Miocene faunas in the interval from Samples 121-756B-2H-3, 100–105 cm, to 121-756B-4H-CC are similar to those at Broken Ridge, in the abundance of the species *G. bulloides*, *Globigerina nepenthes*, *Globigerina falconensis*, and *Globoquadrina dehiscens*. However, a large proportion of the faunas is composed of warm, subtropical forms such as *Globorotalia menardii*, *Globorotalia limbata*, *Globorotalia multicamerata*, *Sphaeroidinellopsis multiloba*, *Globorotalia merotumida*, and *Globorotalia plesiotumida*.

The middle Miocene faunas in the interval from Samples 121-756B-5H-1, 100–105 cm, to 121-756B-5H-CC are similar to those at Broken Ridge. Similarly, zonation of the sediments was impossible because of the absence of some marker species from the *Globorotalia fohsi* lineage. The warm, subtropical forms *Globorotalia praefohsi* and possibly *Globorotalia fohsi* are present, but only in rare occurrences. Abundant throughout the middle Miocene is the warm, subtropical species *Globigerinoides ruber*.

The early/middle Miocene boundary based on the first appearance of *Orbulina* sp. was not recognized. Early Miocene age assemblages in Cores 121-756B-6H and 121-756B-7H con-

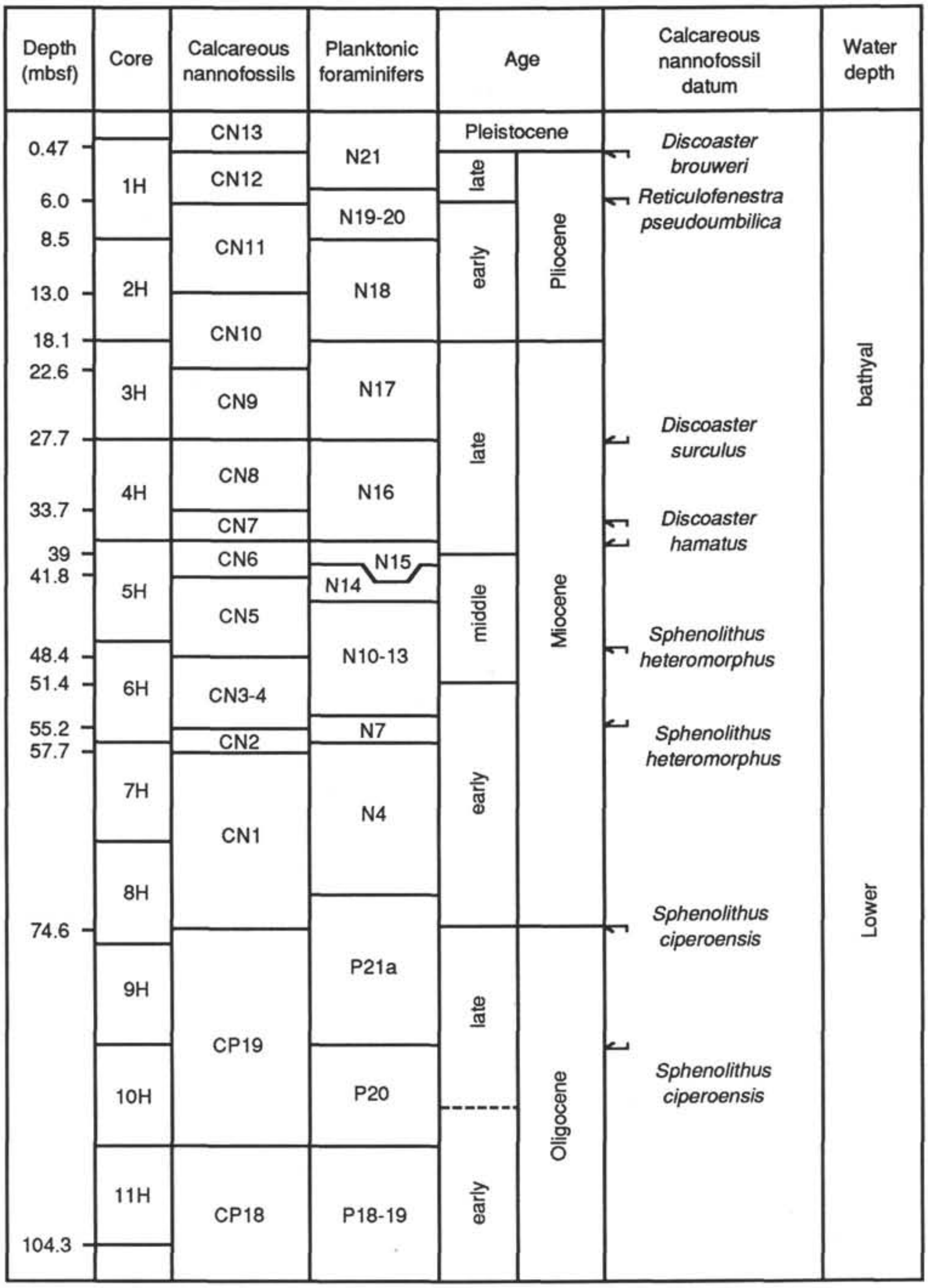

Figure 8. Biostratigraphic zonation of Hole 756B.

sist of more temperate faunas and, therefore, are similar to those from Broken Ridge.

Throughout the entire section, preservation of the planktonic foraminifer assemblages is excellent. We observed only a few reworked fossils, which presumably washed in from higher topography. The planktonic foraminifers present in the upper Miocene and Pliocene are of a subtropical nature and therefore are different from the temperate faunas of Broken Ridge. The faunas of early to middle Miocene age have a greater affinity with the more temperate assemblage of the Southern Hemisphere. The Oligocene/Miocene boundary is placed between Samples 121-756B-7H-CC and 121-756B-8H-CC at the first appearance of *G. dehiscens* and *Globorotalia kugleri*. In the Oligocene, faunas are of a temperate nature and subtropical forms are totally absent.

Paleogene

Oligocene to Eocene

Early to late Oligocene age faunas of a similar temperate nature were recovered from Cores 121-756B-8H to 121-756B-11H. Hole 756C contains principally late Paleogene faunas of late Eocene to Oligocene age. Overlap of the Oligocene from Holes 756B and 756C was obtained. Of greatest interest in Hole 756C is the good preservation of a complete Eocene/Oligocene boundary sequence with a diverse fauna. Late Eocene age faunas are

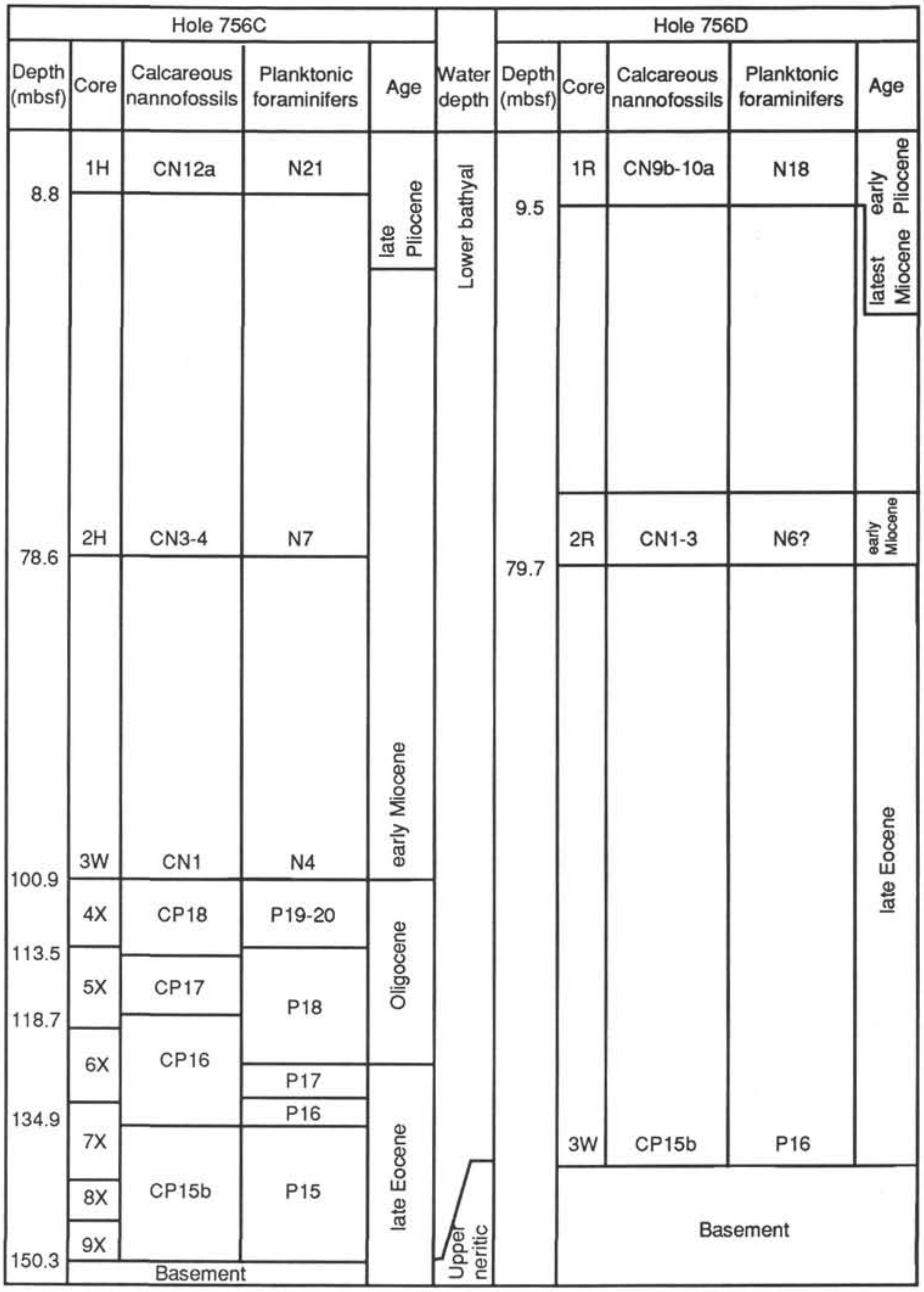

Figure 9. Biostratigraphic zonation of Holes 756C and 756D.

dominated by the temperate species *Globigerinatheka luterbacheri* and *Globigerinatheka index*.

Benthic Foraminifers

Core-catcher samples from Holes 756A through 756D were examined for >125-μm-sized foraminifers. The benthic foraminifers are well preserved, except for specimens in Samples 121-756B-6H-CC, 121-756B-9H-CC, 121-756C-3W-CC, and 121-756C-6X-CC.

Pliocene to Pleistocene

Pliocene to Pleistocene faunas were recognized in Samples 121-756A-1H-CC, 121-756B-1H-CC, 121-756B-2H-CC, 121-756C-1H-CC, and 121-756D-1R-CC. The assemblages are characterized by middle to lower bathyal taxa such as *Osangularia culter*, *Pleurostomella* spp., *Globocassidulina* cf. *crassa*, and *Stilostomella lepidula*. Other species present are *Globocassidulina subglobosa*, *Cibicidoides kullenbergi*, *Oridorsalis umbonatus*, *Planulina wuellerstorfi*, *Rectuvigerina* cf. *striata*, *Rectuvigerina multicostata*, *Laticarinina pauperata*, *Uvigerina hispida*, *Pullenia* spp., and *Nodosaria* spp. These taxa are usually found in Holocene sediments of the eastern Indian Ocean and are associated with Indian Deep Water and the Indian Bottom Water (Corliss, 1979; Peterson, 1984).

Miocene

Upper Miocene faunas were recovered in Samples 121-756B-3H-CC and 121-756B-4H-CC. The Miocene assemblages are

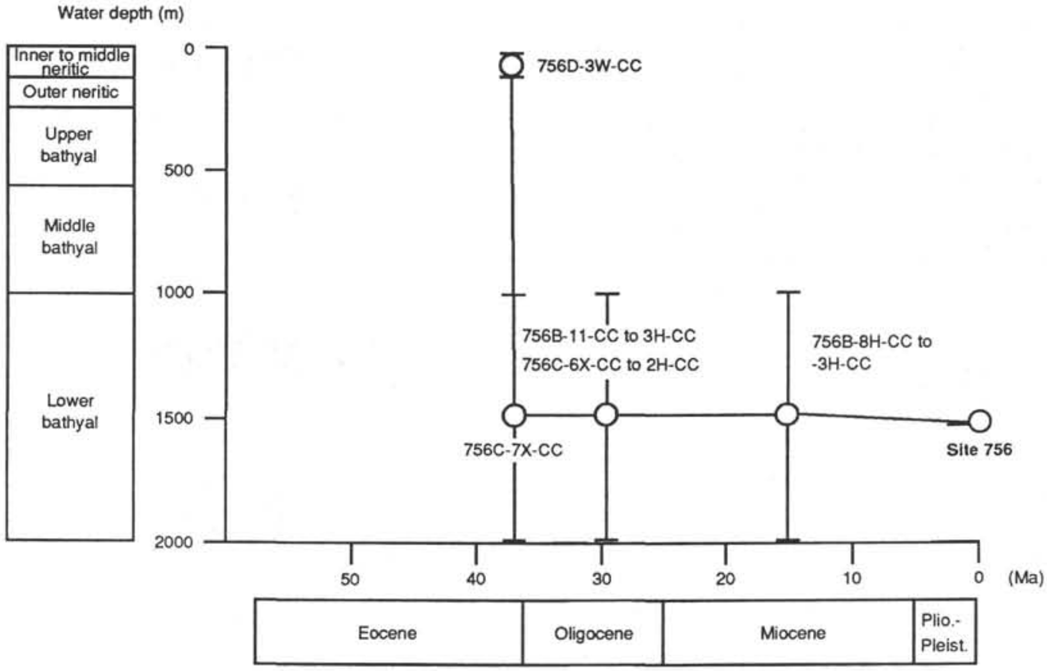

Figure 10. Water depths vs. age at Site 756 as deduced from benthic foraminifer assemblages.

characterized by *G. subglobosa*, *S. lepidula*, *Stilostomella spinulosa*, *Pleurostomella alternans*, *L. pauperata*, *Uvigerina perigrina*, *Uvigerina proboscidea*, *Gyroidina soldanii*, and *Dentalina* spp. This assemblage is similar to those recovered in the Pliocene and Pleistocene, except for *Pullenia* spp. and *Cibicidoides* spp. Middle Miocene faunas (Sample 121-756B-5H-CC) are dominated by *Globocassidulina* spp., and *Burseolina pacifica*. *C. kullenbergi* is also common, along with *S. lepidula*, *Astrononion echolsi*, *Brizalina thalmanni*, *Nonion germanicum*, *Pleurostomella acuminata*, *L. pauperata*, and *O. umbonatus*.

Lower Miocene benthic foraminiferal faunas are characterized by *Cibicidoides* spp. and *C. kullenbergi*. Associated taxa include *Planulina* spp., *O. umbonatus*, *Pullenia bulloides*, *L. pauperta*, *G. subglobosa*, and *A. echolsi*. This is indicative of a lower bathyal depth.

Oligocene

Oligocene faunas from Samples 121-756B-8H-CC to 121-756B-11H-CC, 121-756C-2H-CC to 121-756C-5X-CC, and 121-756D-2R-CC are represented by *Cibicidoides* spp., including the larger forms *Cibicidoides mexicana* and *Cibicidoides havanensis*. *Globocassidulina* spp. are common, particularly *Globocassidulina globosa*. Other species identified include *P. bulloides*, *Pullenia quinqueloba*, *O. umbonatus*, *Nonion affine*, *S. lepidula*, *Textularia flinti*, *Orthomorphina* spp., and *G. soldanii*. These taxa indicate that deposition occurred at lower bathyal depths during the Oligocene.

Eocene

Eocene faunas found in Samples 121-756C-6X-CC, 121-756C-7X-CC, and 121-756D-3W-CC include *Uvigerina* spp., *O. umbonatus*, *Globocassidulina* spp., *G. soldanii*, *Osangularia truncanus*, *Anomalinoides pseudogrosserugosa*, *C. havanensis*, *P. quinqueloba*, and *Bulimina trinitatensis*. In addition, deep-water taxa such as *Bulimina impendens*, *Alabamina* cf. *dissonata*, *Stilostomella* spp., *Rectuvigerina*, and agglutinated forms *Martinottiella scabra* and *Vulvulina* spp. are present. These are indicative of a lower bathyal depth.

Sample 121-756D-3W-CC contains *C. havanensis*, *Bulimina tuxpomensis*, *O. umbonatus*, *P. quinqueloba*, and *A. pseudogrosserugosa*. This fauna is similar to those recovered above. Limestone fragments (lithologic Subunit IB) were found associated with Sample 121-756D-3W-CC. These fragments contain marine pelecypods, corals, echinoids, and miliolids. Some larger benthic foraminifers (*Lepidocyclina*) indicate a neritic environment. This suggests that rapid subsidence must have happened in the late Eocene.

Diatoms

No diatoms or other siliceous microfossils were found in the core-catcher samples at Site 756.

IGNEOUS PETROLOGY

Basaltic basement was drilled in Holes 756C (150.3 mbsf) and 756D (139.0 mbsf). In Hole 756C, 8.7 m of basalt underlying calcareous sediments of late Eocene age was drilled to a total depth of 159.0 mbsf. A total of 5.99 m of basalt and basaltic tephra was recovered in Cores 121-756C-9X through 121-756C-12N, for a recovery rate of 66%. The actual sediment/basalt contact was not recovered, but only a small part of the core is missing.

In Hole 756D, 82.0 m of basalt underlying sediments of late Eocene age was drilled to a total depth of 221.0 mbsf. A total of 26.92 m of basalt was recovered in Cores 121-756D-4R through 121-756D-12R, for a recovery rate of 33%. Again, the actual sediment/basalt contact was not recovered from the small missing part of the core.

The basalts form a series of discrete lava flows, distinguished on the basis of macroscopic features such as brecciated flow tops and degree of alteration. There are only slight variations in modal mineralogy between the different units. The lavas appear to have been erupted in a subaerial environment.

Macroscopic Core Descriptions

Hole 756C

The 5.99 m of recovered material includes two basalt flow units (756C-F1 and 756C-F2) and an intercalation of basaltic tephra (Unit 756C-S1) (see the Hole 756C barrel sheets). Flow Units 756C-F1 and 756C-F2 are 4.35 and 0.57 m thick, respectively. The basalts are microcrystalline to fine grained, sparsely plagioclase-phyric to aphyric, and moderately to highly altered. Both units are vesicular, especially Unit 756C-F1, and several vesicles are cavities over 10 mm across. Many of the vesicles are filled with a varying assemblage of the iron-bearing minerals limonite and goethite, saponitic smectite, and calcite. No glassy selvages or flow contacts were recovered.

The tephra horizon is a basaltic agglomerate, with millimeter-scale ash bands. It is completely weathered to a dark red-brown clay and is hematite-rich in places (Section 121-756C-11N-CC; confirmed by X-ray diffraction (XRD); Table 5).

Hole 756D

We recognize 14 lithologic units within the recovery of 26.92 m of basalt (Fig. 11). Recognition of flow units is based on (1) color change (e.g., Sections 121-756D-7R-4 to 121-756D-8R-1), (2) presence of brecciated horizons (Section 121-756D-7R-1), and (3) proportion of vesicles (Section 121-756D-9R-4). Correlation with Units 756C-F1 and 756C-F2 is not possible at this stage.

A rotary core bit was used to drill the basement section of this hole; less-coherent interflow lithologies, such as ashes, breccias, and agglomerates, were probably lost. The curated thickness of the flow units varies considerably. Of the 14 units recognized in the core from Hole 756B, seven are over 2 m thick; of these, four have recovered thicknesses of over 4 m.

All of the basalts have a microcrystalline to fine-grained groundmass and are aphyric to sparsely plagioclase-phyric. They are macroscopically indistinguishable from the basalts of Hole 756C. Most of the units are vesicular; rarely does the vesicle content exceed 20%, but the proportion of large vesicles or cavities is high.

Alteration varies from slight to high. Many units are pervasively oxidized, but the central parts of several units (e.g., Unit 756D-F6 in Core 121-756D-7R-3) preserve evidence of an earlier alteration during a much lower oxidation state; they have a dark gray color. Nevertheless, the proportion of secondary minerals in these nonoxidized zones is as high as in the oxidized zones, and they cannot be considered unaltered.

Table 5. Mineral determinations from XRD analyses of Site 756 basalts.

Core, section, interval (cm)	Location	XRD identification
121-756C-		
10N-1, 42–44	Vein	Calcite, smectite
10N-1, 144–145	Cavity lining	Goethite
10N-2, 7–8	Vesicle and vein	Smectite (saponite?), plagioclase
10N-3, 85–86	Vein	Unknown phase: 2.98, 2.46, 2.07, 2.03, 1.89, and 1.86 Å
11N-CC	Clay	Smectite (montmorillonite?) and hematite
121-756D-		
4R-1, 125–126	Vesicle	Goethite, smectite
5R-1, 24–25	Vesicle	Smectite
6R-1, 107–108	Vesicle	Calcite
6R-2, 44–45	Vesicle	Smectite
7R-2, 67–68	Vesicle	Calcite
8R-1, 33–34	Cavity lining	Goethite, smectite
8R-1, 51–52	Vesicle	Calcite
9R-3, 25–26	Vein	Calcite
10R-2, 138–139	Vesicle	Smectite
11R-1, 36–37	Vesicle	Calcite
11R-1, 40–41	Vesicle	Smectite (saponite)
12R-3, 134–135	Vesicle	Smectite (saponite), calcite

Note: The 17 samples were selected from both fracture fillings and filled vesicles in the basalt units. The diffraction patterns indicate that smectites and calcite are the dominant secondary minerals present in these flows.

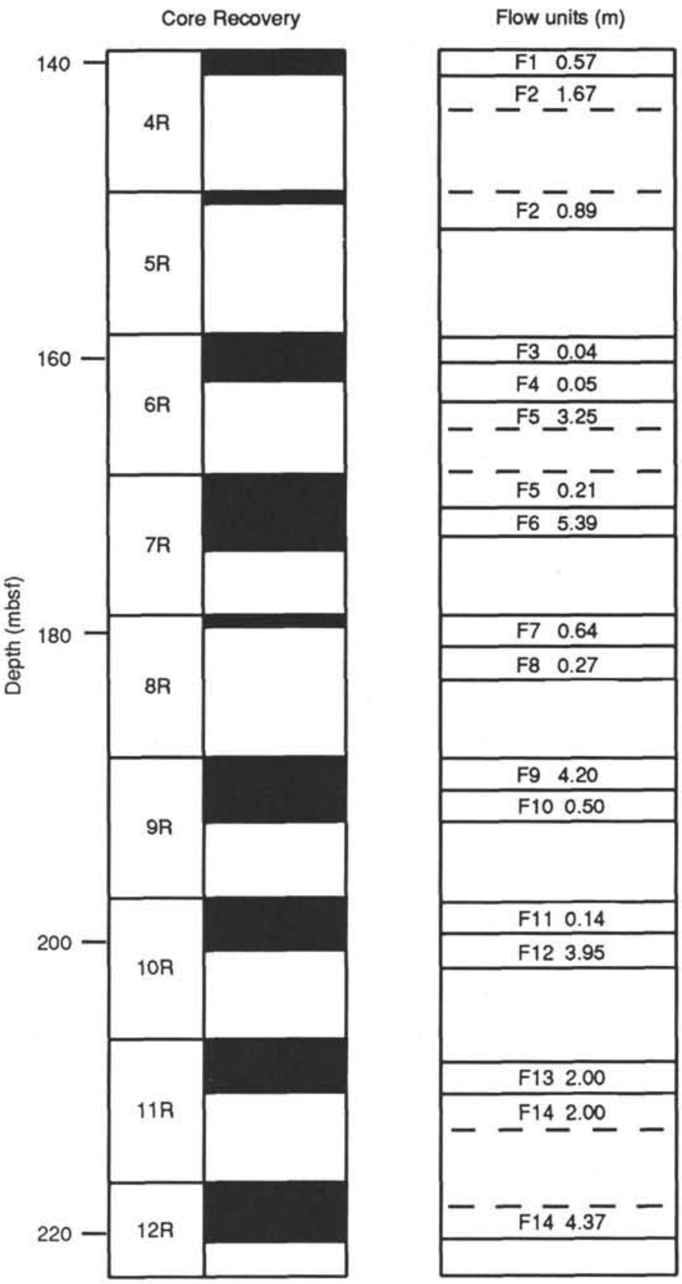

Figure 11. Summary lithologic log of the basaltic units recovered from Hole 756D. Thicknesses of units are based on curated core lengths.

The alteration of the basalt is intrinsically associated with ubiquitous fracture, vesicle, and cavity fillings. Fillings of limonite (and other iron oxides and hydroxides), brown smectite, and calcite are associated with oxidized areas, and blue-green saponite is associated with the nonoxidized parts. Where the paragenetic sequence can be determined, calcite development has postdated other secondary mineral growth, and the oxidative alteration postdates the nonoxidative alteration.

We believe that these units represent subaerial lava flows, based on the high frequency of large vesicles and cavities; the absence of glassy selvages, quench textures, and pillow forms;

and the sporadic occurrence of oxidized basaltic breccia and agglomerate. Furthermore, the exsolution textures observed in the opaque mineralogy are consistent with a slowly cooled, nonquenched eruption environment (see "Paleomagnetics" section, this chapter). An accurate assessment of the true thickness of each flow is not possible, but from the distribution of the units in the recovered section, we estimate that flow thicknesses may be on the order of 2 to 6 m.

Petrography

Twenty-one thin sections from the lithologic units defined by macroscopic observation were described.

Because Holes 756C (Units 756C-F1 and 756C-F2) and 756D (Units 757D-F1 to 756D-F14) do not differ significantly, they are described together. Detailed descriptions of the thin sections are published in this volume. Table 6 lists the different mineral proportions and distributions plotted in Figure 12 for Hole 756D.

Primary Mineralogy

Phenocrysts

The majority of the basalts studied are aphyric or sparsely plagioclase-phyric. Only Sample 121-756D-6R-2, 49–52 cm (Piece 1B), contains 5% plagioclase phenocrysts; the other samples contain less than 2%. The plagioclase phenocrysts commonly occur as glomerophyric clots, and in Unit 756D-F12 they are intergrown with clinopyroxene phenocrysts. The phenocrysts are less than 1.5 mm in diameter. They are commonly slightly altered to a pale green clay mineral.

Olivine, now completely replaced by green smectite-vermiculite or red iddingsite, is a rare phenocryst phase, occurring in trace amounts in Units 756D-F2, 756D-F6, and 756D-F9. Clinopyroxene phenocrysts occur in Unit 756D-F12 in typically small amounts—generally less than 3%. No spinel phenocrysts were seen.

Groundmass

Plagioclase occurs as small microlites (from 100 to 500 μm), usually euhedral to subhedral and showing simple binary twinning. They appear to be primarily labradorite. Their proportion varies between 30% and 50%. Clinopyroxene is always present in the groundmass as relatively small anhedral crystals (50 to 200 μm) and constitutes 15% to 30% of the rock. Opaques occur as small anhedral to subhedral crystals (50 to 100 μm), commonly with a cubic form and always in association with clinopyroxene, smectite, iddingsite, and olivine (where present) in the groundmass. The shape and internal reflections indicate that magnetite is dominant. Ilmenite is much rarer. The opaques are homogeneously distributed, and their proportion is relatively high, varying between 5% and 15%. In the very fine-grained samples, the opaques are disseminated throughout the mesostasis.

Unaltered olivine is rare and may not occur. Olivine is altered to iddingsite, smectite, and vermiculite. These alteration minerals are usually less than 10% of the rock. There is some ambiguity as to whether the original olivine represented a true groundmass phase or microphenocrysts. Certainly, the aforementioned larger crystals were without a doubt phenocrystal, but the smaller pseudomorphs have a more equivocal origin.

Altered and recrystallized volcanic glass occurs in almost all of the samples. No fresh volcanic glass was observed, but recrystallized material is ubiquitous in the groundmass in varying proportions between 10% and 40%. The principal groundmass mineral observed is a secondary green smectite (saponite; Table 5) with associated iron oxides and hydroxides.

Secondary Mineralogy

All of the basalts studied from Site 756 have undergone some degree of alteration, although the intensity of the alteration varies considerably throughout the core. The alteration ranges from 20% to 40% (i.e., moderate), except in Samples 121-756D-4R-1, 22–26 cm (Piece 4), 121-756D-11R-2, 47–50 cm (Piece 9), 121-756D-11R-3, 49–51 cm (Piece 3A), and 121-756D-12R-2, 128–131 cm (Piece 1E), where it is up to 70%. The higher intensity alteration zones are closely related to the presence of vesicles and veins. A clear correlation exists between the color of the basalt and the alteration mineral association: brownish to orange gray for calcite, iron hydroxides or oxides and brown smectites constitute the principal secondary mineral association, and bluish to greenish-dark gray where blue-green saponitic smectites are the dominant secondary mineral phase. None of the basalts recovered at Site 756 can be considered unaltered.

Secondary mineral species determined by XRD are presented in Table 5. Samples were selected from veins and vesicles, as indicated. The main secondary minerals are calcite, which usually precipitated late in the paragenetic sequence, brown smectite, green smectite (saponite), and goethite. No zeolite minerals were detected.

The alteration led to a pervasive replacement of the mesostasis and olivines by clay minerals and the infilling of many of the vesicles. The majority of the units are vesicular, although the size (2 to 15 mm) and concentration (5% to 20%) varies considerably. About 50% are filled, most commonly (>90%) with a green (saponitic) smectite and brown smectite. Some iron oxides or hydroxides (goethite and/or limonite) also occur as fillings, especially where calcite is also present as a filling (5% to 10%) or in veins (1 mm to 3 cm thick). The alteration mineral paragenesis is similar to that reported at DSDP Site 257 (Kempe, 1974). Only two vesicular basalts, Samples 121-756D-10R-3, 63–67 cm (Piece 4), and 121-756D-11R-2, 47–50 cm (Piece 9), show a regular distribution of vesicles constituting more than 30% of the rock. In the former sample, vesicles are filled by smectites with rare plagioclase microlites; in the latter, vesicles are lined by smectites and filled with calcite. The smectite and plagioclase assemblage may be derived from vesicle-filling mesostasis.

Flow orientation was observed in some thin sections from flow units at the bottom of the core, starting at Unit 756D-F12. Flow orientation is evidenced mainly by orientation of the plagioclase microlites and by smectite-filled planar vesicles and small subhorizontal fractures and laminae.

Texturally, the rocks are aphyric or sparsely plagioclase-phyric basalt. They are all microcrystalline and holocrystalline, with a hypidiomorphic texture. Some have a subophitic texture tending to subtrachytic where there is a flow orientation, but most have a microcrystalline, or even cryptocrystalline, groundmass dominated by altered mesostasis; in these rocks, accurate identification of the proportion of groundmass mineral phases is extremely difficult.

Petrographic observations agree with the macroscopic descriptions and geochemistry in showing that the basalts from Holes 756C and 756D are similar and vary little downhole, except in color and extent and type of alteration. They appear to be petrographically distinct from the basalts recovered at DSDP Sites 214 and 216, which have a higher proportion of clinopyroxene than plagioclase (Hekinian, 1974) and quartz infillings in vesicles.

Geochemistry

Thirteen samples from nine flow units were analyzed for major and trace element abundances by shipboard X-ray fluorescence (XRF) (Table 7). Based on SiO_2 vs. Na_2O + K_2O (not

Table 6. Modal analyses of basalt thin sections, Site 756.

	756C-10N-1, 130–132 cm (Piece 2H)	756C-10N-3, 48–49 cm (Piece 1E)	756C-12N-1, 29–30 cm (Piece 4)	756D-4R-1, 22–26 cm (Piece 4)	756D-4R-1, 113–116 cm (Piece 15)	756D-5R-1, 45–46 cm (Piece 7)	756D-6R-2, 17–18 cm (Piece 1A)	756D-6R-2, 49–52 cm (Piece 1B)	756D-7R-1, 66–67 cm (Piece 11A)	756D-7R-2, 38–40 cm (Piece 1C)	756D-7R-2, 67–68 cm (Piece 1E)	756D-8R-1, 44–46 cm (Piece 9)	756D-9R-3, 137–140 cm (Piece 4E)	756D-10R-2, 108–111 cm (Piece 9A)	756D-10R-3, 63–67 cm (Piece 4)	756D-11R-2, 47–50 cm (Piece 9)	756D-11R-3, 49–51 cm (Piece 3A)	756D 12R-2, 128–131 cm (Piece 1E)
Flow unit	756C-F1	756C-F1	756C-F2	756D-F1	756D-F2	756D-F2	756D-F5	756D-F5	756D-F6	756D-F6	756D-F6	756D-F7	756D-F9	756D-F12	756D-F12	756D-F13	756D-F14	756D-F14
Phenocrysts																		
Plagioclase (%)	0	0	1–2	1–2	1–2	1–2	2–3	5	1–2	1	0	0	Tr	Tr	Tr	1–2	Tr	Tr
diameter (mm)	—	—	1–2	0.5–2	1–2	0.5–2	2	0.5–2	0.5–2	1	—	—	1	1	1	2–3	2	1
[a]Olivine	0	0	0	0	Tr	0	0	0	Tr	0	0	0	2	0	0	0	0	0
Groundmass																		
Plagioclase (%)	45	45	30	30	30	40	30	40	32	40	30	32	34	35	35	15	35	25
Microlite (length in mm)	0.1–0.4	0.1–0.4	0.1–0.2	0.1–0.2	0.1–0.3	0.1–0.3	0.2	0.1–0.5	0.05–0.1	0.1–0.2	<0.1	0.1–0.2	0.1	0.1	0.1–0.5	0.1	0.2–0.5	0.1–0.2
Clinopyroxene (%)	25	30	25	30	25	28	30	25	23	20	25	20	23	25	23	15	35	25
diameter (mm)	0.1–0.2	0.1–0.2	0.1–0.2	<0.1	<0.1	0.1–0.2	0.05–0.1	0.1–0.2	0.1–0.2	0.05–0.1	0.1–0.2	0.05–0.1	0.1	[d]0.05–0.2	[d]0.05–0.2	<0.1	0.05	0.05
Opaques (%)	10	10	10	10	9	10	7	8	7	12	10	8	12	15	12	10	8	15
[b]Altered olivine	<5	<5	5	5	5	5	0	5	5	0	10	5	0	0	0	10	0	0
Mesostasis	13	15	25	10	15	15	20	15	15	27	25	35	25	24	29	18	21	30
Vesicles	0	0	0	5	15	0	5	5	15	0	1	0	5	0	0	30	0	0
Vesicle fillings	—	—	—	s, c	s, c	—	s	s	s, c	—	s	—	s	—	—	s	—	—
Alteration (%)	20–30	10–20	20	>50	30–50	20–40	20–40	20–30	40–60	10–20	>70	20–40	20–30	30–40	30–40	>80	>50	60–70
[c]Sample number	—	—	—	1	2	3	4	5	6	7	8	9	10	11	12	13	14	15

Note: Modal analysis performed by visual estimation. Tr = trace (<1%); s = smectite; c = calcite.
[a] Smectite or iddingsite pseudomorphs after olivine.
[b] Includes microphenocrystal olivine.
[c] Refers to samples plotted in Figure 12.
[d] Includes 1%–3% microphenocrysts of clinopyroxene.

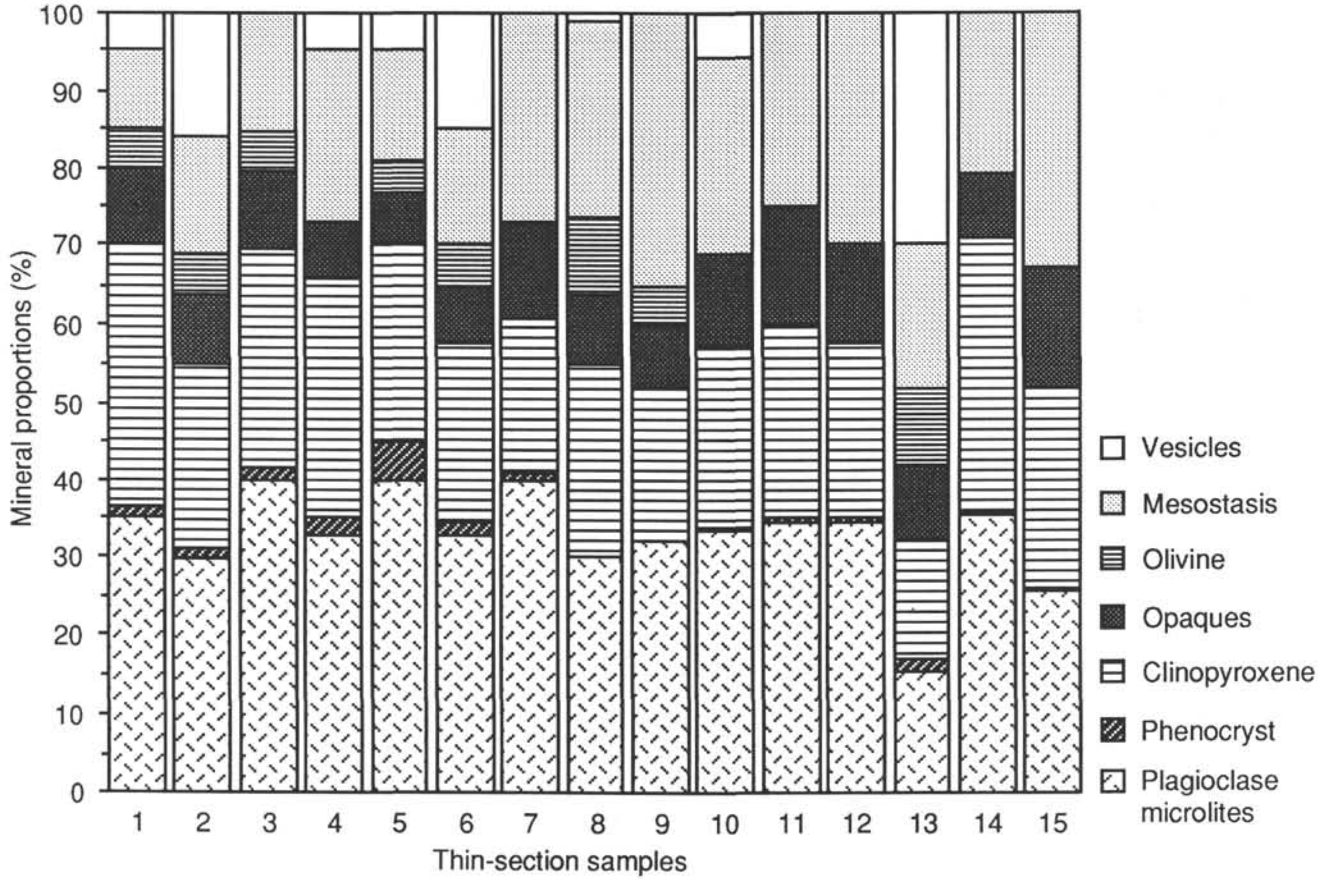

Figure 12. Estimated modal mineral proportions for a downhole succession of basalt thin sections, Hole 756D. Sample numbers refer to intervals in Table 6.

shown) and SiO_2 vs. FeO/MgO trends (Fig. 13), Site 756 lavas are tholeiitic basalts. This is consistent with the normative mineralogy (Table 7), which shows that the basalts are, with one exception, all hypersthene normative. Their low phenocryst content (<2%) means that the bulk-rock compositions approximate basaltic liquids, although the rocks have undergone variable degrees of posteruptive alteration.

The basalts have low MgO contents (<8%) and high FeO/MgO ratios (>1.35); consequently, they are probably not primary magmas. The two most evolved lavas, which are lowest in MgO and highest in incompatible element content, are the uppermost flows in Holes 756C and 756D (Table 7) (e.g., note the relatively high Zr, Y, and V contents in the uppermost sample from Hole 756D; Fig. 14).

These compositional data can be used to evaluate several important problems that differ in scale:

1. What is the relationship of these lavas to each other? Can they be related to a common parental magma composition or do they require complex petrogenetic processes or different mantle source compositions.

2. How do Site 756 lavas compare with southern Ninetyeast Ridge lavas recovered 400 km south at DSDP Site 254 and with lavas from the central Ninetyeast Ridge at DSDP Sites 214 and 216, which are more than 1600 km north.

3. Where do Site 756 basalts fit in the wide spectrum of basaltic compositions that range from incompatible element-depleted tholeiitic basalts formed at spreading-ridge axes (N-type MORB) to incompatible element-enriched alkali basalts on Kerguelen and Heard islands?

Our discussion focuses on the following points:

1. Most of the basalts from Holes 756C and 756D form coherent geochemical trends consistent with derivation from a common parental magma by fractional crystallization. For example, abundances of the relatively incompatible elements (i.e., elements with mineral/melt partition coefficients less than unity: Ti, P, Ba, Y, Zr, Nb, and Ce) are positively correlated (e.g., Fig. 15). In contrast, the abundances of K, Rb, and, to a lesser extent, Sr, elements known to be mobile during the deuteric or hydrothermal alteration of basaltic rocks, vary erratically. Abundances of K_2O and Rb are correlated. Low K and Rb contents are characteristic of Site 756 basalts with a blue-gray color (see macroscopic and petrographic descriptions). Despite this mobility of K and Rb, evidence from petrographic and loss-on-ignition data (Table 7) indicates that the Site 756 samples are less altered than previously recovered Ninetyeast Ridge lavas (Frey et al., 1977).

Two samples were selected from Section 121-757D-11R-2 to evaluate compositional differences between oxidized and nonoxidized parts of the core (Samples 121-756D-11R-2, 123–130 cm). The lower MgO, CaO, and Zn and the higher Fe_2O_3, K_2O, and Rb in the oxidized part of core are readily apparent. Macroscopically, the oxidative alteration appears to be superimposed on the more pervasive nonoxidative alteration of basalt, and the former is invariably associated with calcite-filled veins.

The alteration history of these rocks is therefore complex. The earliest preserved alteration event appears to have produced the blue-gray mineralogy dominated by saponitic smectite. This may be a low-temperature event. Subsequently, the basalt was

Table 7. XRF analyses and normative mineralogy of basalts from Holes 756C and 756D.

	756C-10N-3, 49–52 cm (Piece 1E)	756C-12N-1, 30–33 cm (Piece 4)	756D-4R-1, 22–26 cm (Piece 4)	756D-6R-2, 49–52 cm (Piece 1B)	756D-6R-3, 0–8 cm (Piece 1A)	756D-7R-2 38–40 cm (Piece 1C)	756D-8R-1, 12–15 cm (Piece 2)	756D-9R-3, 137–140 cm (Piece 4E)	756D-10R-2, 108–111 cm (Piece 9A)	756D-11R-2, 123–130 cm (Piece 13A)		756D-12R-2, 28–32 cm (Piece 1A)	756D-12R-2, 90–92 cm (Piece 1C)
										Brown, oxidized	Blue, nonoxidized		
Flow unit	756C-F1	756C-F2	756D-F1	756D-F5	756D-F5	756D-F6	756D-F7	756D-F9	756D-F12	756D-F14	756D-F14	756D-F14	756D-F14
Major elements (wt%)													
SiO_2	47.45	48.18	46.99	48.03	48.58	48.81	48.94	47.80	48.48	47.33	49.02	48.94	48.44
TiO_2	2.75	2.20	2.57	2.05	2.08	2.33	2.00	1.94	1.96	2.21	2.29	2.01	1.97
Al_2O_3	15.13	15.66	15.47	15.14	15.48	15.12	15.00	14.42	14.44	15.21	15.90	14.66	14.50
[a]Fe_2O_3	13.01	13.77	14.87	12.46	12.36	11.99	12.64	12.13	12.54	15.29	12.68	12.19	12.01
MnO	0.17	0.16	0.15	0.19	0.18	0.15	0.14	0.18	0.17	0.16	0.15	0.15	0.18
MgO	6.60	7.12	4.70	7.42	7.24	6.74	7.14	7.88	7.70	6.12	6.64	7.58	7.92
CaO	10.60	9.41	10.50	10.50	10.94	11.06	10.72	11.52	11.18	9.56	10.23	10.67	11.10
Na_2O	3.07	2.72	3.47	2.69	2.56	2.94	2.48	2.53	2.42	2.54	2.97	2.73	2.69
K_2O	0.55	0.64	0.61	0.22	0.30	0.37	0.54	0.20	0.22	0.82	0.40	0.55	0.19
P_2O_5	0.26	0.18	0.25	0.17	0.17	0.20	0.19	0.16	0.16	0.17	0.17	0.16	0.16
	99.60	100.06	99.58	98.88	99.89	99.70	99.80	98.77	99.27	99.40	100.45	99.65	99.14
Loss on ignition	1.26	2.40	0.75	0.78	0.82	1.22	2.17	0.96	0.85	1.76	1.07	1.20	0.68
[b]FeO/MgO	1.77	1.74	2.85	1.51	1.54	1.60	1.59	1.38	1.47	2.25	1.72	1.45	1.36
[c]CIPW norms													
Nepheline	0.0	0.0	2.0	0.0	0.0	0.0	0.0	0.0	0.0	0.0	0.0	0.0	0.0
Orthoclase	3.3	3.8	3.7	1.3	1.8	2.2	3.2	1.2	1.3	4.9	2.4	3.3	1.2
Albite	26.4	23.3	26.2	23.3	21.9	25.3	21.2	21.9	620.8	621.9	625.3	623.4	623.2
Anorthite	26.2	28.9	25.2	29.2	30.2	27.4	28.5	628.0	628.4	628.9	629.0	626.5	627.4
Diopside	21.0	14.2	22.0	18.9	19.4	22.3	19.9	24.1	22.2	15.9	17.3	21.5	22.6
Hypersthene	1.2	12.8	0.0	12.7	13.8	6.8	15.6	8.7	15.4	11.8	11.5	10.1	10.5
Olivine	13.4	9.6	12.5	7.8	6.0	8.6	4.7	9.5	5.2	9.6	7.3	8.6	8.5
Apatite	0.58	0.40	0.56	0.38	0.38	0.44	0.42	0.36	0.36	0.38	0.37	0.35	0.36
Ilmenite	5.31	4.23	4.97	3.98	4.00	4.50	3.85	3.77	3.79	4.28	4.38	3.87	3.81
Magnetite	2.63	2.77	3.01	2.53	2.49	2.43	2.55	2.47	2.54	3.10	2.54	2.46	2.43
Trace elements (ppm)													
Rb	14	22	8	<1	1	6	18	2	2	28	4	43	2
Sr	185	145	194	171	177	199	152	166	165	171	180	171	165
Ba	62	42	51	36	47	74	50	42	39	37	43	47	39
V	384	305	428	324	343	335	294	316	312	351	352	313	323
Cr	187	221	144	232	253	191	244	229	226	191	199	184	182
Ni	82	104	95	80	82	86	111	89	88	86	85	92	88
Cu	193	132	98	132	101	160	103	97	100	121	117	70	53
Zn	116	119	110	100	103	102	105	100	102	95	114	98	100
Y	35	27	37	28	29	31	27	28	28	26	26	26	27
Zr	165	121	155	117	119	139	115	108	110	127	133	114	112
Nb	12.4	8.8	11.1	8.5	9.0	9.2	10.8	8.6	7.9	9.8	9.7	8.0	7.9
Ce	29	16	27	17	20	21	23	17	17	21	16	16	20

[a] Total iron reported as Fe_2O_3.
[b] Total iron as FeO.
[c] Calculated using $Fe_2O_3/(Fe_2O_3 + FeO) = 0.15$.

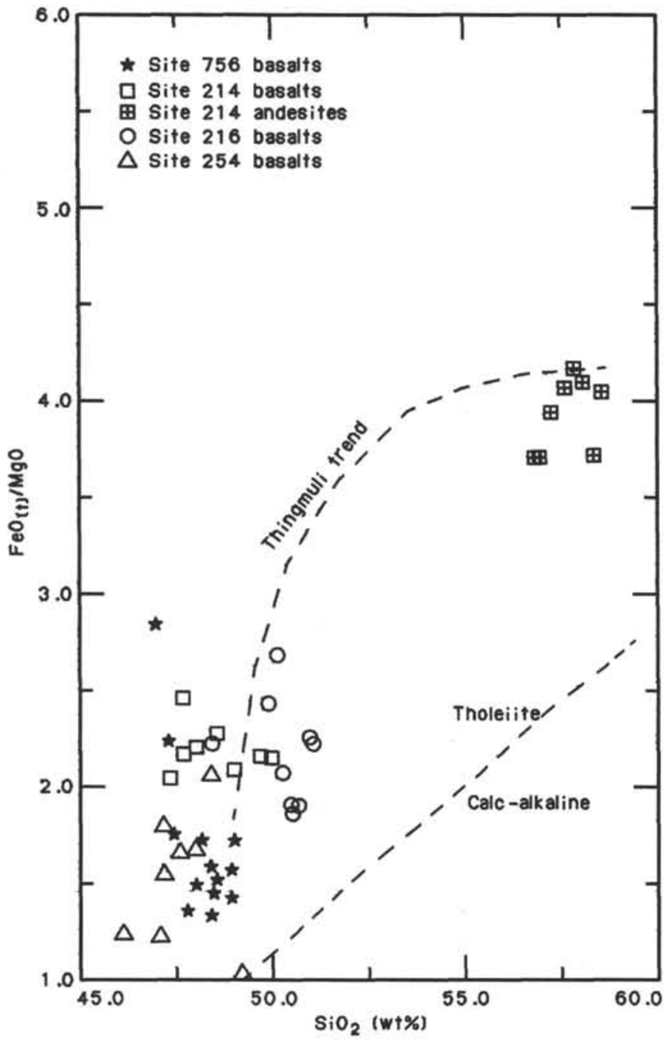

Figure 13. Plot of FeO (total Fe)/MgO vs. SiO_2 content shows that the Ninetyeast Ridge lavas (Frey et al., 1977) lie in the tholeiitic field defined by Miyashiro (1974). The Site 756 basalts overlap with the Site 254 basalts. The trend from basalts, 45% to 50% SiO_2, to more silicic lavas with a higher FeO/MgO is a typical tholeiitic differentiation trend (e.g., Thingmuli, an Icelandic volcanic center; Carmichael, 1964).

locally penetrated by oxidizing fluids which resulted in element exchange in the vicinity of the veins and produced the characteristic oxidative halos.

2. Considered as a whole, the lavas from Ninetyeast Ridge Sites 214, 216, and 254 define a fractionation path from tholeiitic basalt to ferrobasalt to oceanic andesite (icelandite) (Frey et al., 1977; Ludden et al., 1980); this compositional trend is typical of volcanic centers in Iceland (Figs. 13 and 16). In major element composition, Site 756 lavas are at the basaltic end of this crystal fractionation path and overlap with basalts from Site 254 (Figs. 13 and 16). However, trace element abundance trends require significant petrogenetic differences between lavas from the southern Ninetyeast Ridge Sites 254 and 756; for example, the offset V-Y trends (Fig. 17) reflect either distinct parental magmas or different petrogenetic processes, such as varying degrees of melting or different crystallization paths. Although the data are sparse, abundance ratios of incompatible elements may also differ among the Ninetyeast Ridge sites (Fig. 18). The distinct fields may be related to a changing source composition or varying mixing proportions between depleted (in this example, high Zr/Nb and Y/Nb ratios) and enriched (low Zr/Nb and Y/Nb ratios) sources. If these geochemical differences between sites are confirmed by shorebased trace element and isotopic studies, they will provide important constraints on the evolution of Ninetyeast Ridge volcanism over a 50-Ma time scale.

3. Site 756 basalts are compositionally distinct from the tholeiitic basalts erupted at the Indian Ocean spreading-ridge axes and Kerguelen Island (Figs. 15 and 19). However, basalts from Ninetyeast Ridge, Indian Ocean spreading-ridge axes, and Kerguelen Island form linear geochemical trends (Fig. 19) that may reflect mixing of depleted (MORB-related) and enriched (plume-related) components. The trace element signature of the Ninetyeast Ridge basalts is dominated by enriched components similar to those represented in the transitional plateau lavas of Kerguelen Island (Fig. 19; Weis et al., 1988).

Conclusions

1. Basalts of at least late Eocene age were recovered at Site 756. Two flow units are recognized in the core from Hole 756C, and 14 flow units are recognized in Hole 756D. The available data preclude any direct correlation between the flow units of the two holes.

2. The basalts were probably erupted in a subaerial environment as thin flows.

3. There are slight variations in mineralogy from unit to unit, but the basalts are either sparsely plagioclase-phyric or aphyric. Many of the flow units are vesicular; large vesicles or cavities are common.

4. All of the basalts have undergone moderate or high degrees of alteration. Two stages of alteration are apparent: an earlier, nonoxidative alteration associated with the development of blue-green saponitic smectites, and a later oxidative alteration. The latter is commonly associated with calcite-filled fractures, around which it forms alteration halos.

5. The basalts are commonly fractured; the fractures (and many of the vesicles) are filled by clay minerals and (later) calcite; no zeolites were observed.

6. Most of the Site 756 lavas are tholeiitic basalts; however, the uppermost flow units in Holes 756C and 756D have the highest abundances of incompatible trace elements and are transitional to alkali basalts on a normative basis.

7. There are significant geochemical differences between basalts from Ninetyeast Ridge Sites 756 and 254 (400 km south). Nevertheless, as a group all Ninetyeast Ridge lavas define coherent geochemical trends that do not overlap with the basalts produced at the Indian Ocean Ridge spreading centers. Based on shipboard data, basalts from Site 756 originated via a mixture of components related to depleted MORB and ocean island (Kerguelen?) mantle sources.

PALEOMAGNETICS

Susceptibility

Susceptibility values for lithologic Unit I of Hole 756B (0–104 mbsf) (Fig. 20) are relatively high for the first 2 m (1×10^{-6} to 2×10^{-6} cgs units). The origin of these unexpectedly high values is unclear. They may be the result of rust contamination, but a similar short, moderately positive zone also exists in the mud-line core at the top of Hole 756C (Core 121-756C-1R, not shown in Fig. 20), suggesting that the susceptibilities may reflect actual sediment characteristics. Below 2 mbsf, the data are fairly featureless to about 47 mbsf, with values in the range of 10^{-7} cgs units, both positive and negative. There is a broad peak in the data extending from 47 to 65 mbsf. Base levels are around 10^{-5} cgs units, with a maximum of 1.2×10^{-4} cgs units at 53.2 mbsf. The general rise in susceptibility parallels a change in color from white to pale brown and presumably records an in-

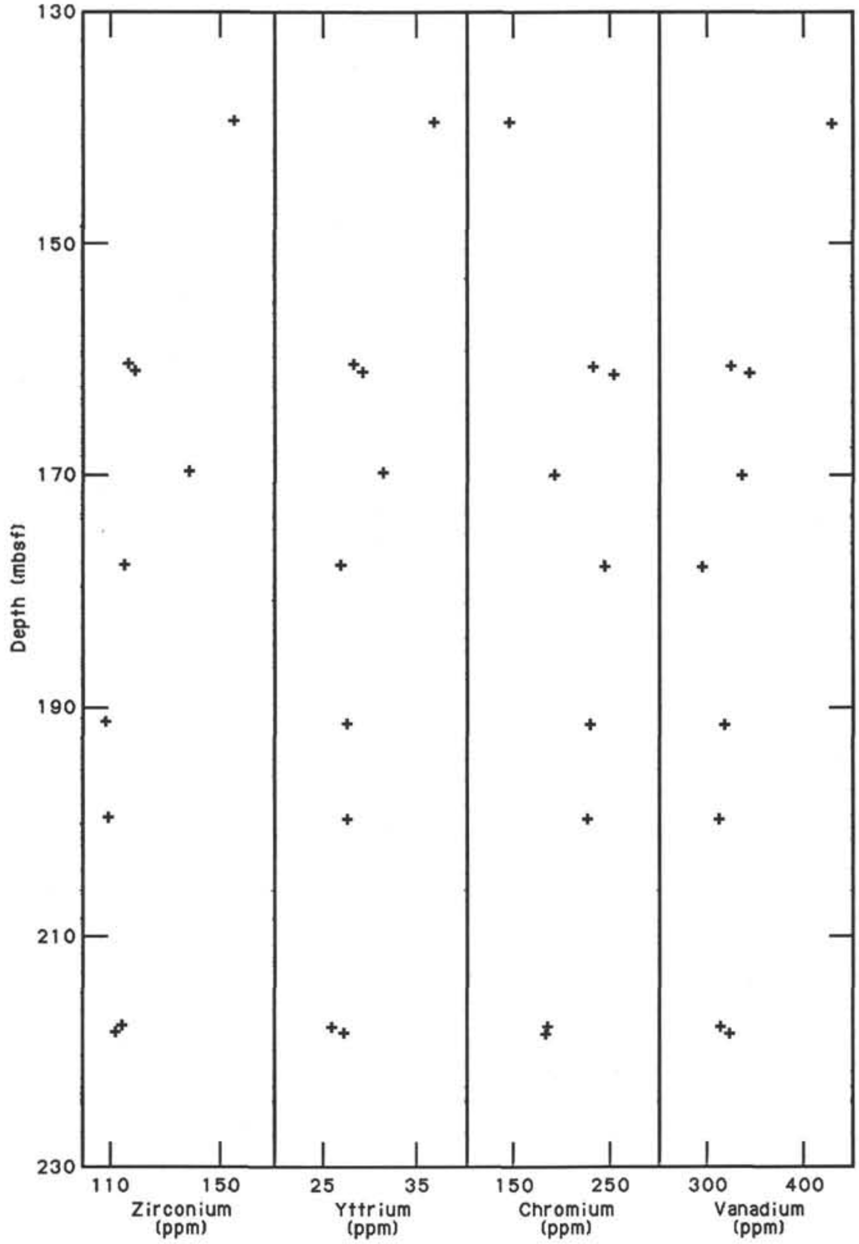

Figure 14. Abundances of Zr, Y, Cr, and V as a function of depth in the Hole 756D basalts. The uppermost sample has the highest abundance of the incompatible elements V, Y, and Zr and correlates with the uppermost of the two units drilled in Hole 756C.

crease in iron oxide content. There is also a great deal of short-wavelength structure in the record. No corresponding changes are visible in the cores, however, and the origin of these short-wavelength susceptibility variations is unclear. Below 65 mbsf, susceptibilities are in the range of 2×10^{-6} cgs units, and they gradually rise to about 2×10^{-5} cgs units at the bottom of Hole 756B (104 mbsf). Some fine-scale structure below 65 mbsf also has no obvious origin.

With the exception of the mud-line and one spot core (not shown in Fig. 20), the data from Hole 756C start at 101 mbsf (based on drilling data), overlapping Hole 756B by a few meters. The correlation of the susceptibility records of Holes 756B and 756C is not clear. There are peaks of similar magnitude at 101 and 104 mbsf in Hole 756C and at 102.5 and 103.8 mbsf in Hole 756B, but their structure is not sufficiently distinctive for confident correlation. Susceptibility values for lithologic Unit I in Hole 756C (101–143 mbsf) are moderate at the top (5×10^{-6} cgs units) and gradually increase to 2×10^{-5} to 3×10^{-5} cgs units by 143 mbsf. Not shown on Figure 20 is an unrecovered section (143–150 mbsf) followed by basalt (150–155.5 mbsf). The small amount of basalt recovered from this hole has susceptibility values typically around 5×10^{-4} to 10^{-3} cgs units, with some measurements as high as 4×10^{-3}.

Hole 756D cored the top of the basalts at 148.6 mbsf (lithologic Unit II). As there is no reason to expect lateral continuity of basalt susceptibilities, because the possibly limited area/extent of a given flow, we did not attempt to correlate the holes. Susceptibilities of Hole 756D (Fig. 20) are similar to those of the basalts recovered from Hole 756C. Typical values are around 5×10^{-4} cgs units, with peaks above 10^{-3} cgs units. The recov-

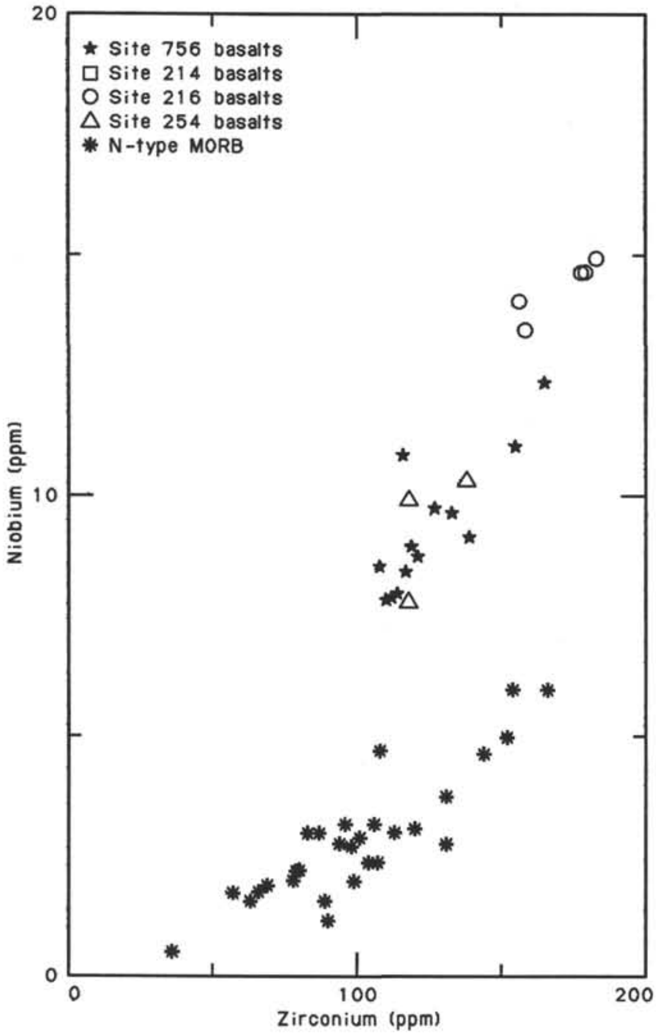

Figure 15. Abundances of incompatible elements Zr and Nb in the Ninetyeast Ridge basalts. The Site 756 basalts have a coherent trend, and the Ninetyeast Ridge basalts (M. A. Storey and A. D. Saunders, unpubl. data) are displaced from the N-type MORB field (Price et al., 1986; Bougault et al., 1979; Saunders, 1983).

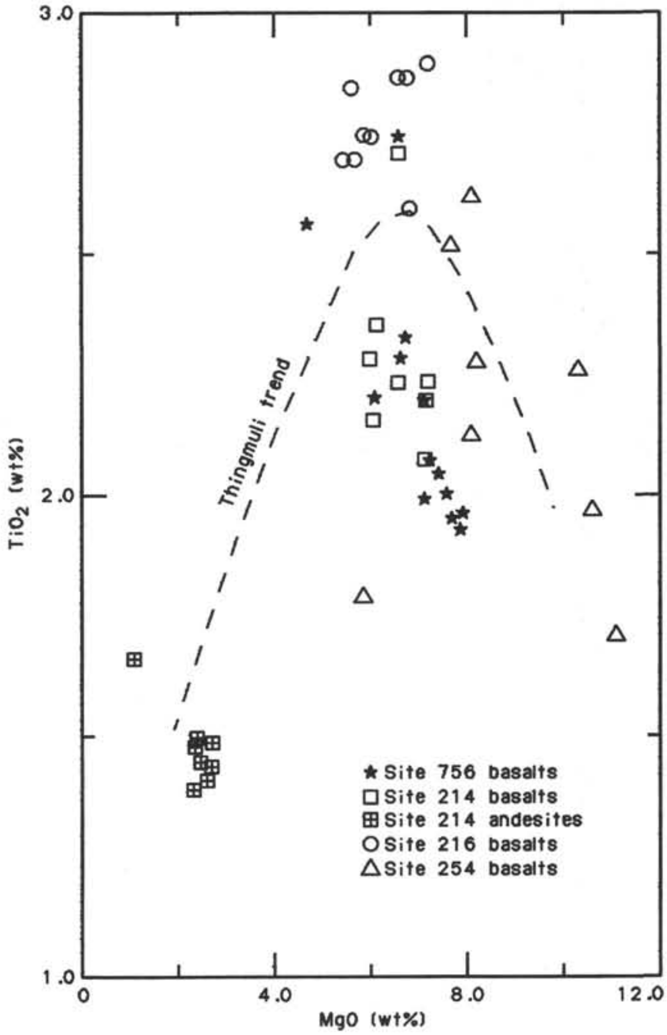

Figure 16. Plot of TiO_2 vs. MgO content shows that lavas from Ninetyeast Ridge follow a tholeiitic differentiation trend similar to that of Thingmuli (Carmichael, 1964). With initial segregation of olivine and pyroxenes, MgO decreases and TiO_2 increases; however, Fe-Ti oxides segregate from melts with 5%–6% MgO, and then TiO_2 contents decrease with decreasing MgO content. Data for Sites 214, 216, and 254 from Frey et al. (1977).

ered basalts show considerable small-scale variation in their susceptibilities. These variations presumably reflect changes in lithology, but a detailed comparison of lithology and susceptibility awaits shorebased studies.

Remanence

The natural remanent magnetization (NRM) of the sediments of Hole 756B is moderate, with whole-core measurements of about 1 mA/m at the top of the hole, increasing to 1–10 mA/m at 104 mbsf. After 9-mT alternating field (AF) demagnetization, however, the remanence generally decreases by about one order of magnitude (Fig. 21). The whole-core results for the sediments from Hole 756C are similar to those for Hole 756B (Fig. 21). Generally, the material from lithologic Unit I from both Holes 756B and 756C is too weak to be readily measured using discrete samples. We found only four suitable samples for shipboard study (spaced evenly between about 120 and 140 mbsf in Hole 756C). All four samples gave positive (reversed) inclinations and had normal overprints, some of which are sufficient to mask the reversed primary remanence (Fig. 22). These samples do not provide enough information to be of much use now in interpreting the reversal stratigraphy. Viscous remanence acquisition experiments performed on discrete samples from Site 756 and on similar sediments from Hole 757C (see "Paleomagnetics" section, "Site 757" chapter, this volume) suggest that much of the sediment NRM for both holes may be of viscous origin and acquired after recovery. We can possibly recover a stable primary remanence from these cores in a low-field environment.

The basalts are readily measurable, with NRM values in the 0.1–1.0 A/m range (Fig. 23). To the extent possible, six samples were taken from each flow unit. In most cases, one or two samples per flow unit were also taken for the study of rock magnetics. Samples were taken at evenly spaced intervals throughout the flow unit, while avoiding badly altered zones as much as possible. The fracturing of the cores into short sections made it difficult to take samples with a common horizontal orientation. Accordingly, with one exception, sample declinations are uncorrelated. No AF demagnetization was attempted because of concerns about the DC bias of the demagnetizer (see "Paleomagnetics" section of the "Explanatory Notes" chapter). The NRM directional data (Fig. 24) are generally consistent, with a sub-

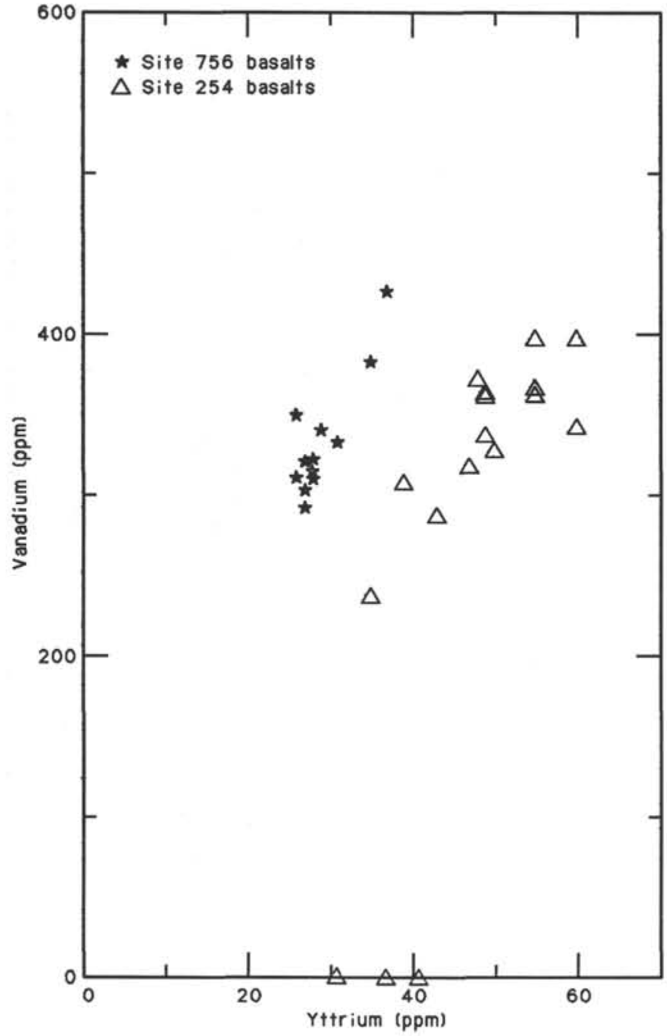

Figure 17. Plot of V vs. Y abundances shows the compositional distinction of the basalts from the two southern Ninetyeast Ridge sites. Data for Site 254 from Frey et al. (1977).

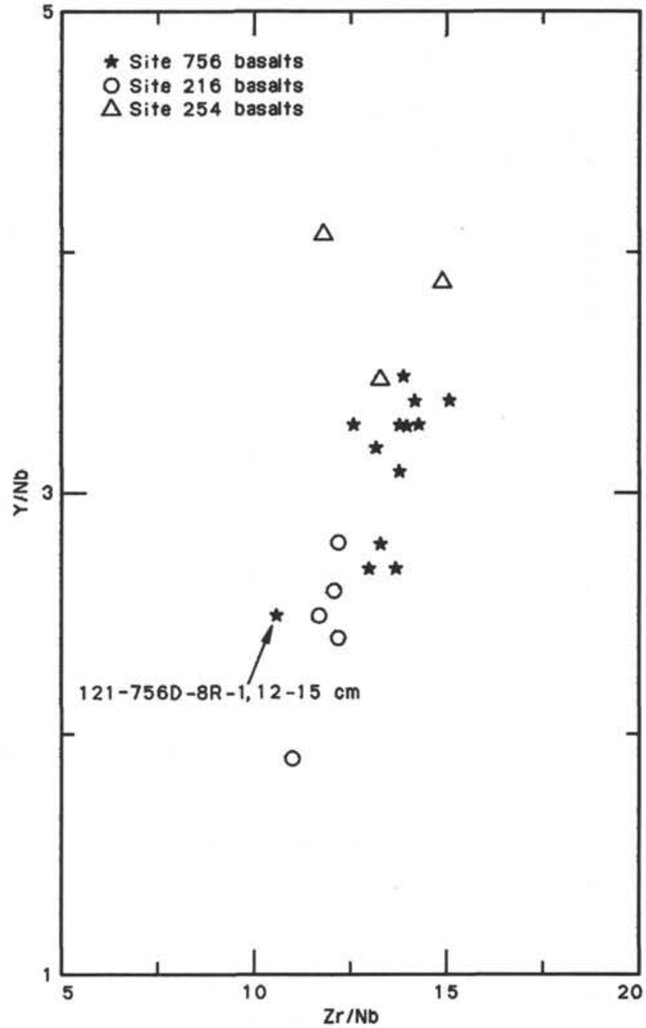

Figure 18. Ninetyeast Ridge sites are characterized by different abundance ratios Y/Nb and Zr/Nb of incompatible elements. The labeled Site 756 basalt sample is compositionally distinct from other Site 756 basalts. Data for Sites 216 and 254 courtesy of M. Storey and A. D. Saunders.

stantial majority of the samples having positive (reversed) inclinations around 60°. Preliminary shorebased studies indicate inclinations of 55° to 70° for the high-stability component of magnetization. This is somewhat lower than the expected inclination for basalts generated by the Kerguelen hot spot (about 50°S; e.g., Peirce, 1978), but more careful demagnetization studies are needed before any firm conclusions can be drawn.

Magnetostratigraphy

While the whole-core data from Hole 756C show what appear to be polarity zones, we are presently unable to confirm the zones with discrete sample measurements. Given the possibility that they may be viscous artifacts, no attempt has been made to interpret the data in terms of the geomagnetic reversal time scale (Berggren et al., 1985).

Magnetic Mineralogy of the Basalts

A complete analysis of magnetic mineralogy awaits shorebased studies with instruments not available aboard ship. Some preliminary work was done using polished thin sections prepared for core descriptions.

The primary magnetic mineral is titanomagnetite of uncertain composition. This identification is based primarily on the observation of "trellis pattern" ilmenite lamellae in some samples (Haggerty, 1976). These lamellae are the result of the subsolidus segregation of primary titanomagnetite into Fe-rich and Ti-rich regions that cannot occur in pure magnetite. This pattern commonly occurs in titanomagnetites that were oxidized at temperatures above 500°–600°C. Evidence for high-temperature alteration is not uniform, however, as some samples are dominated by optically homogeneous grains (presumably of titanomagnetite, although this identification has not been confirmed). In some cases these grains are also cracked to varying degrees, which is a typical result of low-temperature alteration (below approximately 200°C) of single-phase titanomagnetite (e.g., O'Reilly, 1984). Thermomagnetic analysis should help to determine if these grains are truly single phase or simply exsolved on too fine a scale to be observed optically. The habit of the oxides is usually anhedral with scattered subhedral grains. The lack of skeletal habits commonly seen in submarine basalts suggests subaerial deposition. Ilmenite is also common, as well as small amounts of hematite, probably of secondary origin.

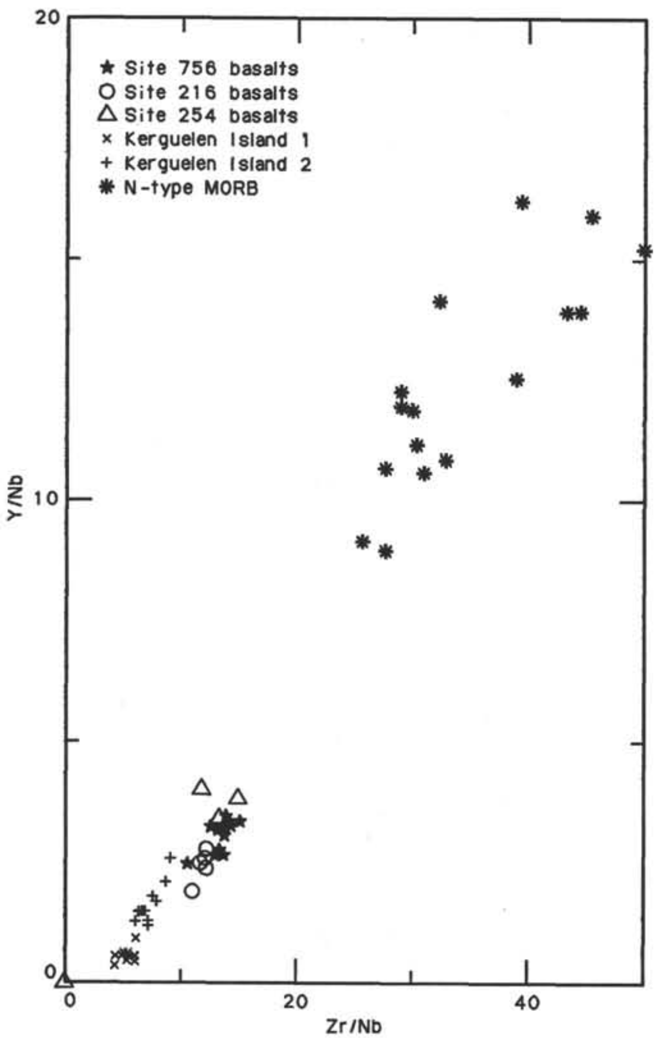

Figure 19. Large-scale plot of Y/Nb vs. Zr/Nb from Figure 18. The field for the Ninetyeast Ridge basalts is distinct from the N-type MORB and two Kerguelen Island fields. However, Kerguelen Island groups 1 (late Tertiary alkali basalts) and 2 (mid-Tertiary transitional basalts), the Ninetyeast Ridge basalts, and the N-type MORB trend form a line that may reflect mixing of depleted (high Zr/Nb ratio) and enriched (low Zr/Nb ratio) components. Data sources are the same as for Figure 15; Kerguelen Island data from Storey et al. (1988).

INORGANIC GEOCHEMISTRY

Objectives

A major objective of the Leg 121 chemical measurements of pore waters was to determine how uniform the chemical gradients in the pore fluids are in a horizontal sense. Traditionally, DSDP and ODP sites have been drilled great distances from one another, or, if drilled close together, chemical measurements were made in only one hole. The question of how uniform these chemical gradients are laterally on a scale of hundreds of meters was not addressed.

On DSDP Legs 69, 70, and 83 a series of holes was drilled only hundreds of meters apart near the Costa Rica Rift. The vertical chemical gradients showed large differences from hole to hole in Ca^{2+}, Mg^{2+}, and $^{18}O/^{16}O$ ratios (Mottl et al., 1983) that are attributable to the alteration of basaltic basement (Gieskes, 1975, 1983; Lawrence and Gieskes, 1981). The differences from hole to hole were attributed to lateral chemical changes in the pore fluids in the basement caused by convection of fluids in the basement (Mottl et al., 1983, 1987). Slow upward and downward advection of fluids through the sediments was also detected.

The question is whether these spatial changes are limited to environments like the Costa Rica Rift area where the sediment cover is currently sealing the oceanic crust. In such an environment advection of pore waters through the sediments is still occurring. Gradients are absent in most of the sediment column, where advection of fluid through the sediments is rapid and unidirectional for sufficiently long periods of time. Sharp gradients occur in the uppermost sediments in upwelling zones and in the lowermost sediments in downwelling zones. Where no or very low rates of advection occur, such as in regions between upward and downward flow regimes, gradients are present. If convection cells are not steady state and migration of cells occurs, complex patterns of chemical gradients develop in the sediments.

At the Ninetyeast Ridge sites large increases in calcium and decreases in magnesium ion concentrations of the pore waters with depth were anticipated because of the rough topography of the ridge and the possibility that large amounts of ash might be present in the sediments (see Lawrence and Gieskes, 1981). In areas where the topography is rough, faulting breaks up the basement, increasing the exposure of basalt to seawater. The high topographic relief of the basement relative to the surrounding oceanic crust causes thermal differences that help generate fluid flow. We also anticipated that horizontal changes in porewater chemistry might be caused by changes in basement structure or by the abundance of ash in the basal sediments. Thus, Ninetyeast Ridge represents an excellent location to look for lateral variations in water chemistry on a scale of hundreds of meters. Comparisons could then be made with the area in the vicinity of the Costa Rica Rift. In contrast to the Costa Rica Rift area, Ninetyeast Ridge has much older basement and therefore much lower heat flow to drive chemical reactions and induce water flow in the basement and through the sediments.

Results

Site 756 is at the southern end of Ninetyeast Ridge in a 6-km-wide sediment pond situated in very rough topography. A prominent fault is about 3 km southeast. The sediments in the pond are about 150 m thick at the site location. Four holes were drilled at Site 756: Holes 756A and 756B were drilled at the same location, Hole 756C was drilled 200 m northeast, and Hole 756D was drilled midway between Holes 756B and 756C (Fig. 3).

The chemical compositions of the pore fluids from Site 756 are given in Table 8. Increases in calcium ion concentration with depth are accompanied by decreases in magnesium ion concentration for the holes. The magnitude of these changes, however, is radically different from hole to hole. The changes with depth are large in Hole 756B, small in Hole 756C, and intermediate in Hole 756D. Figure 25 is a comparison of the changes in calcium ion concentration with depth for the three holes. In general, the decreases exhibited by both alkalinity and sulfate ion concentrations with increasing depth are matched by corresponding increases in the calcium ion concentration and decreases in the magnesium ion concentration. Salinity, chlorinity, and pH do not show any systematic changes with depth.

Discussion

Changes in the calcium and magnesium ion concentrations with depth in deep-ocean sediments reflect alteration of volcanic material in the sediments or basaltic basement below (Lawrence and Gieskes, 1981; Gieskes, 1983). Because ash abundances in the sediments at Site 756 are relatively low and little variation in ash content occurs over such short horizontal distances, the

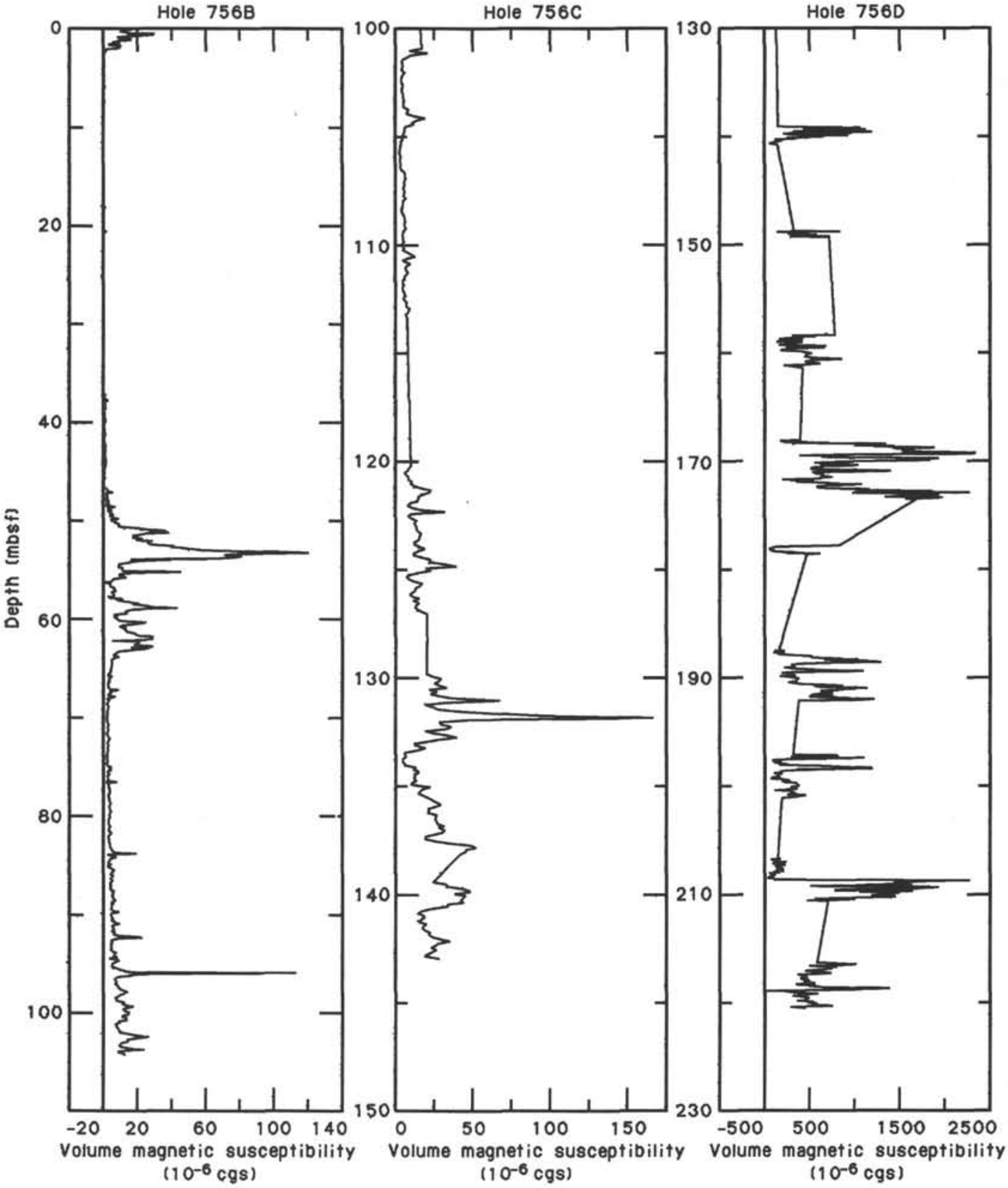

Figure 20. Volume magnetic susceptibility plots for Holes 756B, 756C, and 756D.

increases in calcium seen in Figure 25 cannot be the result of alteration of ash in the sediments. Rather, they must be caused by alteration of the basaltic basement.

The main question is what causes the calcium gradients to be so different from one hole to the next. Several explanations seem possible. One is that the basalts below Hole 756B are altering at a much greater rate than those below Hole 756C. Another is that alteration is uniform in the basalts but that waters are advecting up through the sediments at Hole 756B and downward through the sediments at Hole 756C. A third possibility is that the basalts below Hole 756B are isolated from communication with open seawater whereas those below Hole 756C are not. The first explanation seems to be the least likely. There are probably not big differences in lithology or temperature over short distances. Reaction rates should be similar over the distance covered by the three sites.

The second explanation seems possible, but a convection pattern of simple advection of water upward at Hole 756B and downward at Hole 756C can be ruled out. At vertical advection rates greater than 0.5 mm/yr, uniform chemistry is seen in the pore waters of most of the sediment column, with rapid changes occurring just below the sediment/water interface or just above the basalt/sediment interface for upward and downward advection, respectively (see Mottl et al., 1987). In the region between upward and downward flow regimes, however, gradients can be observed in the entire sediment column because the net advection rate is very low and both diffusion and slow advection control the pattern of chemical gradients. If the water circulation pattern is episodic rather than steady state, very complex patterns of chemical gradients can develop in the sediment column, with large changes both vertically and horizontally. Three-dimensional modeling may be required to fully appreciate just

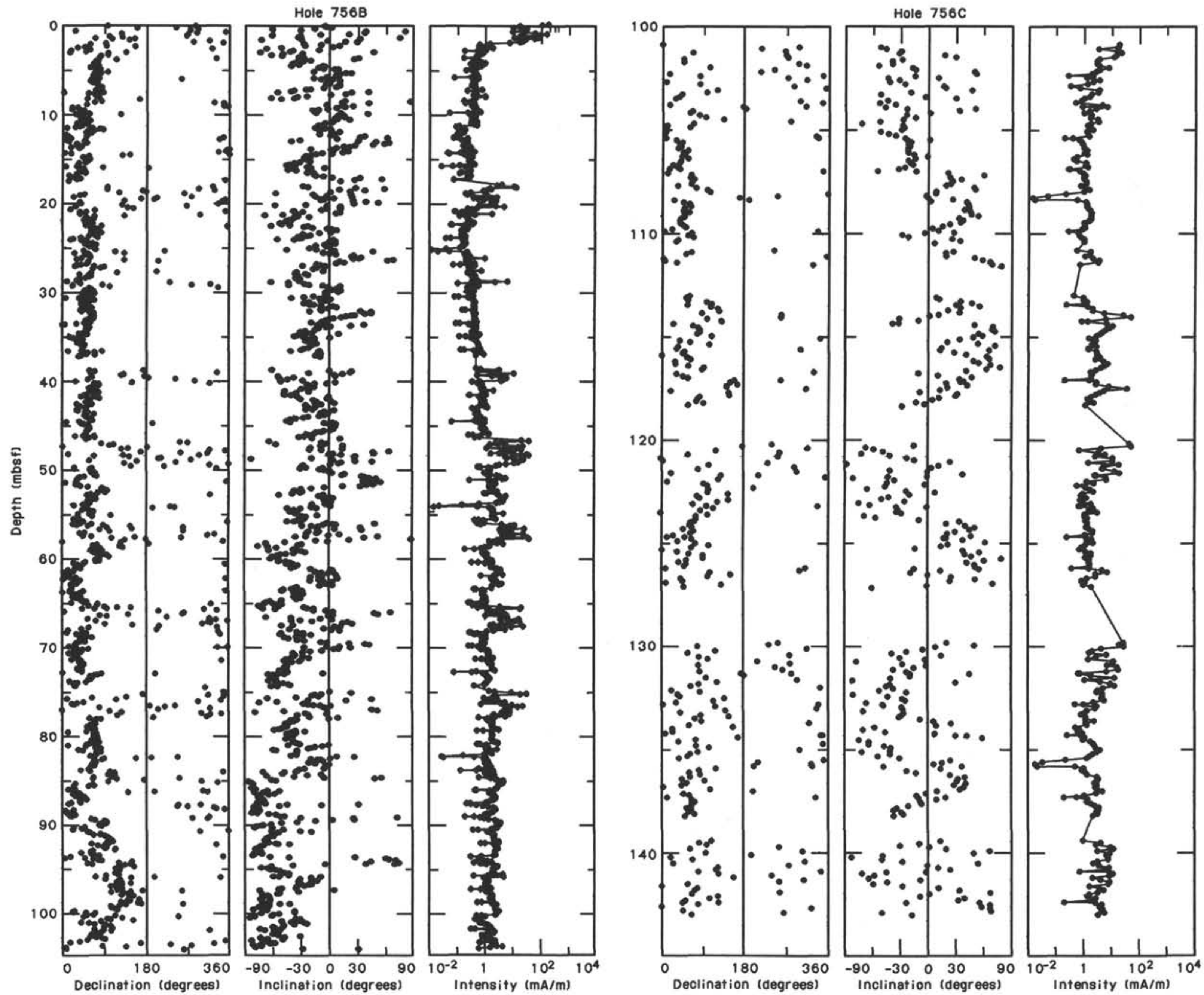

Figure 21. Remanence data after 9-mT demagnetization for Holes 756B and 756C.

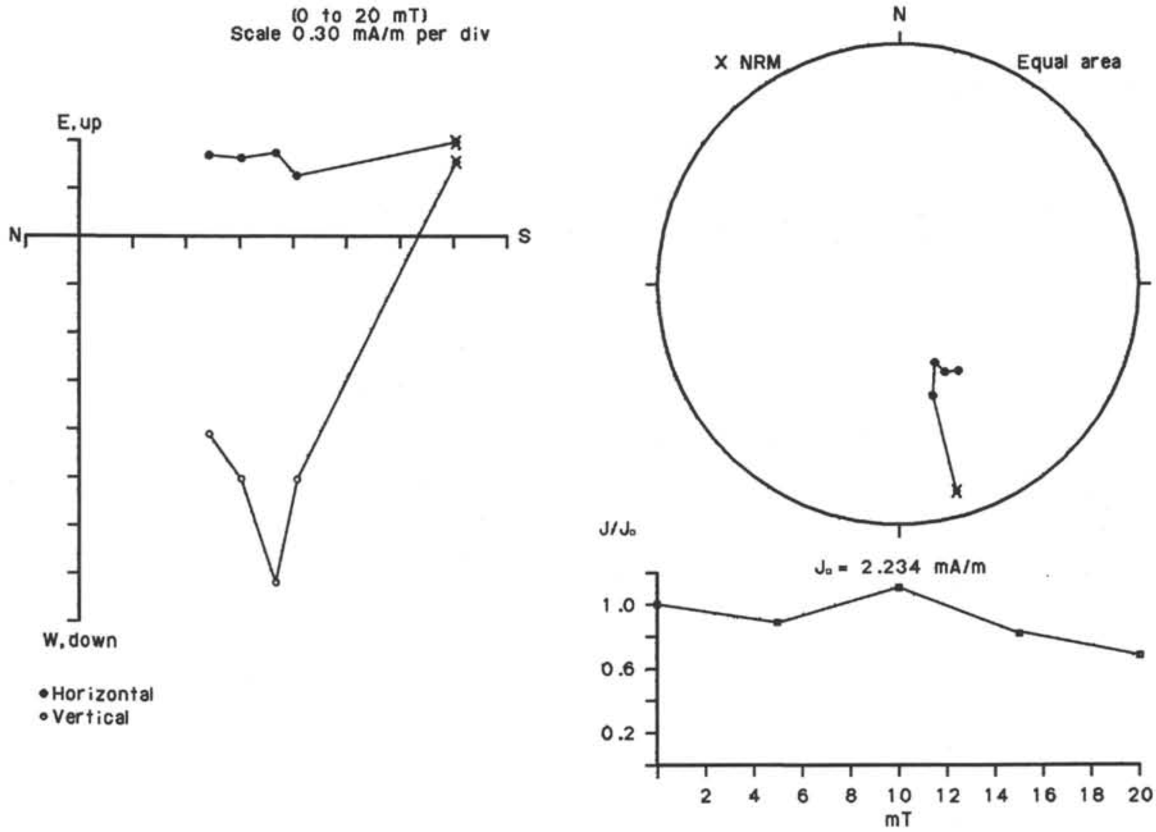

Figure 22. Zijderveld, equal area, and intensity decay plots showing removal of a normal (up) overprint (Sample 121-756C-7X-2, 18–20 cm).

what is happening. At Site 756 a pattern of complex advection of fluids through the sediment column cannot be ruled out.

The third explanation for the observed differences in the profiles seems to be the most likely. In the rough topography at this location along the Ninetyeast Ridge, faulting in the basement possibly could provide localized avenues for the advection of water from the open ocean to some areas of basement. A fault with a vertical throw of about 500 m is only 3 km southeast of Site 756 (see Fig. 33). Alteration below Hole 756C may be as extensive as that below Hole 756B. The only difference may be that chemical changes introduced into the pore waters at Hole 756C are lost more quickly because of greater communication through permeable zones with the open ocean.

A diagram to scale shows the variation of calcium ion concentrations in the sediments at the Site 756 area (Fig. 26). The contours show the changes in calcium ion concentration in a spatial sense. Although the data are more limited at Holes 756C and 756D, the vertical changes in chemistry are comparable to horizontal changes in chemistry. The chemical signal seems to be propagating from southwest to northeast, which corresponds to a general increase in the elevation of basement in that direction. Whether the chemical change seen at Site 756 is a local one controlled by localized basement structure or a chemical boundary in the pore waters of the pond as a whole is not known.

Sufficient pore-water sampling was done in Hole 756B that structure can be observed in the chemical profiles, particularly the changes in calcium ion concentration with depth (see Fig. 25). The most noticeable feature is the downward leveling off of the calcium gradient at about 60 mbsf. On the seismic profile (see Fig. 37) this break in slope corresponds to a prominent reflector. This depth also corresponds to a distinct increase with depth in the formation factor in the sediments (see Fig. 29). In addition, grain size, water content, and bulk density peak in the interval from 50 to 55 mbsf, below which they return to normal levels (see "Physical Properties" section, this chapter). These correlations suggest that there is a distinct change in the diffusion coefficient through the interval at 60 mbsf. The interpretation for a barrier to diffusion at this depth requires modeling studies for verification. Other changes in slope in the calcium ion profile are too small to be trusted as significant.

The changes in magnesium ion, sulfate ion, and alkalinity (see Table 8) appear to be directly related to the change in calcium ion. When volcanic material reacts with seawater, calcium is lost to the solution phase while magnesium is taken up from the solution (Gieskes, 1983). Sulfate would also be taken up if ferrous iron was oxidized in the preceding reaction. The decrease in alkalinity is probably a reflection of supersaturation of the solution with respect to calcium carbonate because calcium ion concentration increases with depth.

ORGANIC GEOCHEMISTRY

Concentrations of hydrocarbon gases in headspace samples and percentages of inorganic and total carbon were determined on samples from Holes 756A and 756B. No Rock-Eval pyrolyses were performed because of the low organic matter content in the sediments. A more detailed description of analytical methods is available in the "Explanatory Notes" chapter.

Gas Analyses

Concentrations of methane did not exceed the 3 ppm of laboratory air. Ethane and propane were not detected.

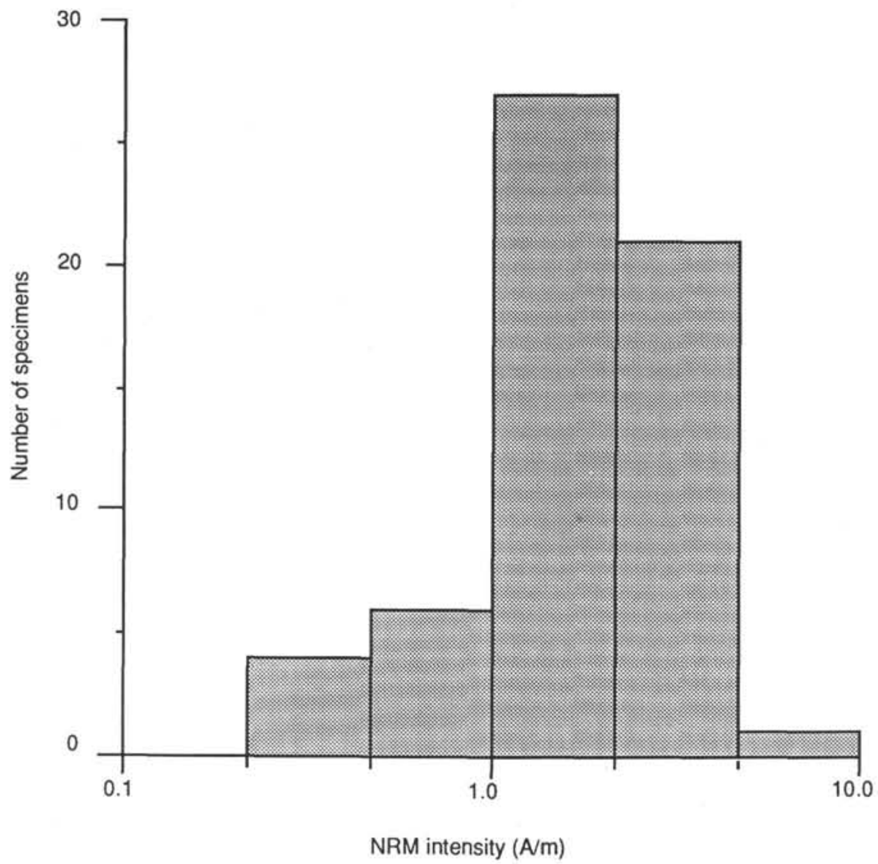

Figure 23. Histogram of NRM intensities of basalts from Site 756.

Organic Carbon

Most of the samples contain no organic carbon, and no values above 0.2% were measured (Table 9 and Fig. 27). The entire Pleistocene to upper Eocene sequence is extremely poor in organic carbon and, in this respect, is similar to its stratigraphic equivalents at Sites 752 through 755 on Broken Ridge.

Carbonate Carbon

Carbonate percentages are high in the Neogene to upper Eocene sequence drilled in Holes 756B and 756C (Table 9 and Fig. 27). There is, however, a short interval within the middle to lower Miocene sediments (51-54 mbsf) where carbonate percentages are slightly lower than in the overlying and underlying units. The lower boundary of this unit corresponds to a marked seismic reflector (see "Seismic Stratigraphy" section, this chapter). Paleontology results reveal a change from subtropical to temperate biota at the upper boundary of this interval (see "Biostratigraphy" section, this chapter). No decrease of carbonate contents was detected in this stratigraphic unit on Broken Ridge. Carbonate values drop slightly from 96% to about 90% from the base of the Miocene (74 mbsf) to the upper Eocene.

Sample 121-756C-11N-1, 90-92 cm, taken between basement basalt layers, is extremely poor in carbonate. The excursion of carbonate content at 139 mbsf is due to the fact that basalts were reached at slightly different depths in Holes 756C and 756D.

PHYSICAL PROPERTIES

Hole 756A was not used for the study of physical properties because it consists of a single core. Hole 756B was APC cored to 104 mbsf. Hole 756C was washed to 101 mbsf and XCB cored to 150 mbsf. Hole 756D was washed to 139 mbsf and RCB cored to 221 mbsf. In retrospect, the chemistry data suggest that the mud-line core at Hole 756D was too deep by about 4 m. Therefore, all depths in Hole 756D may be about 4 m too shallow. Detailed correlations between the holes should make allowance for this possible discrepancy.

The lithology of Site 756 changes from soft sediments composed of Pleistocene to upper Eocene ooze (Unit I) to basaltic flows with intercalated ash and soil layers (Unit II) (see "Lithostratigraphy and Sedimentology" section, this chapter).

Methods

Samples from this site were measured for index properties, compressional-wave velocity, vane shear strength, electric resistivity, and thermal conductivity. Descriptions of the methods used are found in the "Explanatory Notes" chapter.

Results

Index Properties

Porosity, bulk density, water content (expressed as water weight relative to wet sample weight), grain (or matrix) density, and dry-bulk density of the samples from Holes 756B, 756C, and 756D are listed in Table 10 and plotted in Figure 28. GRAPE bulk densities are in good agreement with the wet-bulk densities measured from the laboratory samples.

Two units are identified in terms of physical properties: units A (0-139 mbsf) and B (139-221 mbsf). The boundary of units A and B coincides with that of lithologic Units I and II, corresponding to the sediment/basalt contact. As expected from the change in lithology, a drastic change of bulk density, water content, porosity, and dry-bulk density occurs across this boundary

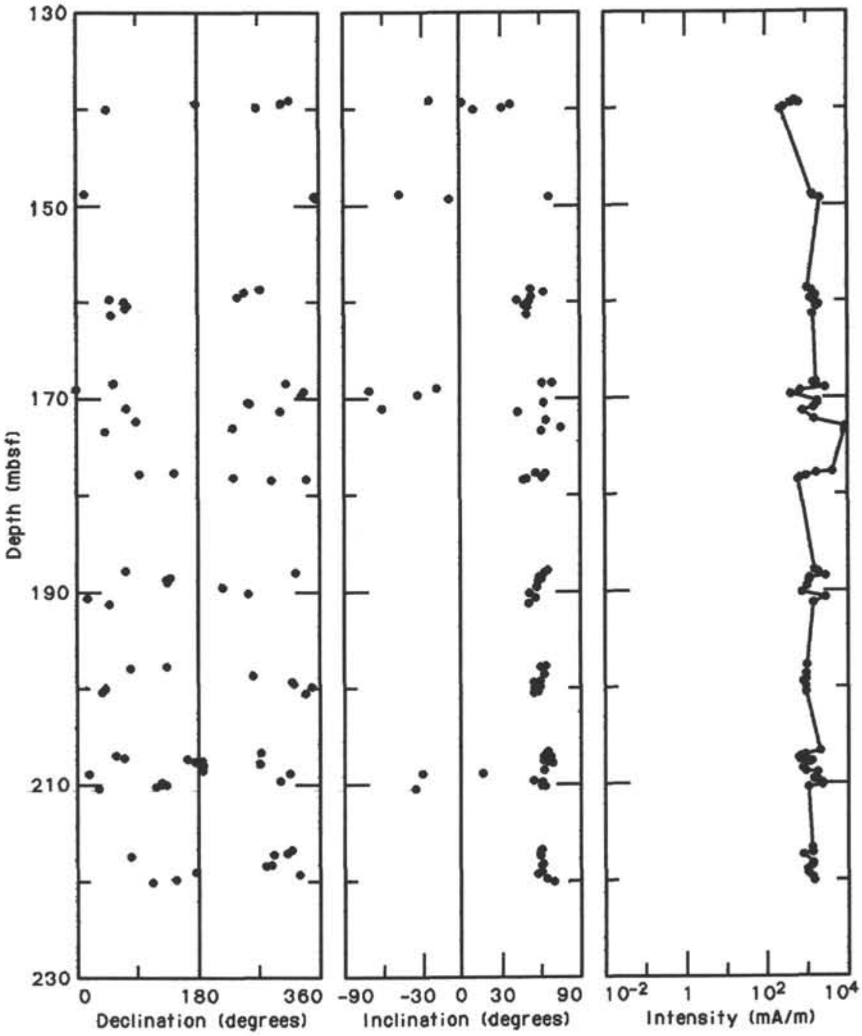

Figure 24. Remanence data for basalts from Hole 756D.

at 139 mbsf. Bulk density increases from 1.7–1.9 to 2.6–2.9 g/cm^3, and water content decreases from 30%–35% to less than 5%. Grain density also shows a slight increase at this boundary, from about 2.7 to 2.8 g/cm^3.

The index properties vary slightly in unit A. A distinct decrease in density occurs at 50–55 mbsf for both the GRAPE densities and sample bulk densities (Fig. 28), although the exact depths of the decrease do not coincide. The nannofossil ooze changes color from white to pale brown and the mean particle size of the bulk sediments notably increases at this boundary (see "Lithostratigraphy and Sedimentology" section). Above this interval, the index properties of unit A have fairly constant values and the mean bulk density is 1.72 $\pm$ 0.02 g/cm^3. Below this interval to 95 mbsf, the index properties of unit A increase as the bulk density increases from 1.6 to 1.9 g/cm^3. From 95 to 139 mbsf the bulk densities of unit A decrease with depth from 1.9 to 1.7 g/cm^3. Water content and porosity also vary correspondingly through unit A.

The bulk density of unit B is generally greater than 2.6 g/cm^3, except for two data points (Fig. 28). The shallower point represents the ooze of Core 121-756C-8X and is attributed to the depth mismatch between Holes 756C and 756D. This point should be at the bottom of unit A. The second point of low density represents agglomerate ash layers intercalated in basaltic lava flows in Core 121-756C-11N. This measurement represents the poorly recovered ash constituent of unit B. Few interflow volcaniclastics were recovered, but they may make up more than 50% of lithologic Unit II. The low density of about 2.0 g/cm^3 probably occurs repeatedly within the high-density basalts of unit B. The mean value of the bulk densities of the basalt is 2.74 $\pm$ 0.11 g/cm^3.

Vane Shear Strength

Records of torque vs. vane rotation were obtained from the APC-recovered sections in Holes 756B and 756C. The silty nature of the noncohesive calcareous sediments results in extremely low strength values (Table 11 and Fig. 29).

The wide variation of vane shear strength from 11.9 to 5.1 kPa in the uppermost 10-m section represents a boundary layer between the water column and the underlying sediments. The sediments between 10 and 50 mbsf have constant strength values, with a mean of 4.3 $\pm$ 1.3 kPa. The sediments between 50 and 115 mbsf show more variation, with a mean value of 7.4 $\pm$ 4.1 kPa. Vane shear strength increases with a steeper gradient below 115 mbsf to values greater than 40.0 kPa at the base of unit A.

Formation Factor

Formation factor was obtained by comparing the electrical resistance of a probe in soft sediment against resistance of the

Table 8. Interstitial-water geochemistry data, Site 756.

Sample (interval in cm)	Depth (mbsf)	Volume (mL)	pH	Alkalinity (mmol/L)	Salinity (g/kg)	Magnesium (mmol/L)	Calcium (mmol/L)	Chloride (mmol/L)	Sulfate (mmol/L)	Mg^{2+}/Ca^{2+}
756D-1R-1, 0-1	0.00	10			36.0	51.80	14.50		27.20	3.57
756A-1H-1, 130-135	1.30	4			36.0	50.80	16.40	562.00	27.00	3.10
756C-1H-1, 145-150	1.45	6			35.5	52.90	10.90	547.00	32.00	4.85
756D-1R-1, 148-150	1.48	1			36.0		15.30			
756D-1R-2, 148-150	2.98	14			36.0	51.80	15.20		28.00	3.41
756A-1H-3, 130-135	4.30	5			35.2	49.20	16.50	553.00	26.10	2.98
756C-1H-3, 145-150	4.45	4			35.5	53.20	11.60	559.00	30.40	4.59
756D-1R-3, 148-150	4.48	20	7.30	2.040	36.0	50.90	15.80		27.50	3.22
756B-1H-4, 145-150	5.95	30	7.40	2.130	35.5	50.10	16.30	562.00	28.70	3.07
756D-1R-4, 148-150	5.98	8			36.0	51.00	15.30		27.50	3.33
756C-1H-5, 145-150	7.45	23	7.60	2.380	35.5	53.40	11.70	549.00	29.80	4.56
756A-1H-5, 145-150	7.45	33	7.30	1.760	35.5	49.90	17.80	547.00	26.10	2.80
756D-1R-5, 145-150	7.45	20	7.50	2.010	36.0	50.70	15.50	554.00	27.80	3.27
756D-1R-6, 148-150	8.98	15			36.0	50.90	16.30		28.30	3.12
756A-1H-7, 44-49	9.44	3			36.2	49.30	17.30	559.00	25.00	2.85
756D-1R-7, 58-60	9.58	10			36.0	50.80	16.70		26.70	3.04
756B-2H-5, 37-41	14.87	5			34.8	48.20	18.30	547.00	24.70	2.63
756B-3H-5, 145-150	25.55	33	7.50	1.760	35.5	48.40	20.90	560.00	24.70	2.32
756B-4H-5, 99-103	34.69	3			35.8	46.40	23.60	563.00	24.40	1.97
756B-5H-6, 10-15	44.90	4			36.5	45.90	26.50	567.00	22.80	1.73
756B-6H-5, 145-150	54.35	48	7.50	1.700	35.5	43.90	29.80	562.00	23.60	1.47
756B-7H-4, 145-150	62.15	10			36.0	43.00	30.70	554.00	23.90	1.40
756B-8H-4, 145-150	71.55	5			35.5	43.40	31.20	564.00	23.00	1.39
756D-2R-1, 145-150	71.55	55			36.0	47.70	23.30		24.70	2.05
756D-2R-3, 145-150	74.55	50			36.0	47.10	23.50		24.20	2.00
756C-2H-5, 145-150	76.35	23	7.60	2.370	36.0	53.60	12.70	564.00	30.90	4.22
756C-3W-CC, 0-2	[a]78.60	4			36.0	54.00	12.50	551.00	32.00	4.32
756D-2R-6, 145-150	79.05	25	7.40	1.710	36.0	47.60	24.40	568.00	24.40	1.95
756D-3W-1, 120-125	[a]81.90	5			36.0	44.90	27.90	562.00	27.50	1.61
756B-9H-5, 145-150	82.65	30	7.50	1.340	35.8	43.20	31.00	566.00	22.50	1.39
756B-10H-5, 144-150	92.34	5			35.2	42.80	31.20	548.00	23.00	1.37
756B-11H-5, 144-150	102.04	6			35.0	41.30	32.80	558.00	21.90	1.26
756C-4X-5, 145-150	108.35	22	7.60	2.290	35.5	52.20	12.30	557.00	30.10	4.24
756C-5X-4, 40-44	113.42	20	7.60	2.290	36.2	52.40	12.30	567.00	31.20	4.26
756C-6X-3, 145-150	124.65	6			36.2	52.00	12.70	558.00	30.10	4.09
756C-7X-4, 145-150	135.75	33	7.60	2.720	35.5	51.70	12.30	561.00	31.20	4.20
756C-8X-1, 146-150	140.86	5			35.8	52.00	12.50	559.00	30.40	4.16

[a] Depth assignment uncertain for wash core.

same probe immersed in seawater (Table 12 and Fig. 29). The lowermost data were measured in an interflow ash layer with a thickness greater than 1 m.

The formation factor in the uppermost section (0–11 mbsf) has highly variable values of 2.16 to 1.30, indicating that it is the boundary layer between the water column and the underlying sediments. The sediments between 11 and 65 mbsf have a formation factor with a mean of 1.59 ± 0.07, and the sediments between 65 and 112 mbsf have a distinctly higher mean of 1.89 ± 0.08. Formation factor between 11 and 65 mbsf increases with depth with a gradient of 0.02/10 m. Higher values, to a maximum of 2.4, and more variation characterize the formation factor of the sediments between 112 and 139 mbsf. The only formation factor value measured in an ash layer in unit B was 2.11.

Compressional-Wave Velocity

Velocity data obtained from laboratory samples are listed in Table 13 and displayed in Figure 28 with the data obtained with the *P*-wave logger. The anisotropy of compressional-wave velocity was examined by measuring velocities in three directions of propagation. Only velocity A, corresponding to the vertical direction, is displayed in Figure 28. Acoustic impedance logs were computed from GRAPE and *P*-wave-logger data in unit A and from bulk density and compressional-wave velocity data (velocity A) in unit B (Fig. 28).

Velocities measured with the *P*-wave logger vary between 1500 and 1600 m/s. The mean velocity through the interval 0–123 mbsf is 1540 ± 30 m/s. *P*-wave-logger velocities between 0–46 and 68–99 mbsf are rather low, with a mean velocity of 1530 ± 30 m/s. Velocities between 46 and 68 mbsf are higher, with a mean value of 1560 ± 30 m/s.

Velocities are greater than 4000 m/s in unit B, where all of the samples are from basalts. The velocities in unit B fall into two groups of velocities, as clearly shown in Figure 30. The group of higher velocities has a mean value of 5350 ± 240 m/s, and the lower velocity group has a mean value of 4570 ± 150 m/s. The mean velocity of unit B is 5130 ± 420 m/s. The two velocity groups are a response to the vesicular to massive basalt flow structure. Vesicular flow tops and bases generally exhibit lower velocities, whereas the massive interiors have higher velocities. This variation is also apparent in the bulk-density and porosity values (Fig. 31). In addition to this variation, the interbedded volcaniclastic units would form an additional velocity/density contrast with the adjacent basalts. No systematic velocity anisotropy was observed (Fig. 30).

The acoustic impedance log matches the division of physical-properties units. Unit A has a much lower impedance than unit B (Fig. 28). The impedance contrast between units A and B is unequivocally a source for a basement acoustic reflector. The detailed correlation of acoustic impedance and seismic profile record is described in the "Seismic Stratigraphy" section.

Thermal Conductivity

Thermal conductivity was measured for both soft sediments and basaltic rocks (Table 14 and Fig. 32). Thermal conductivity

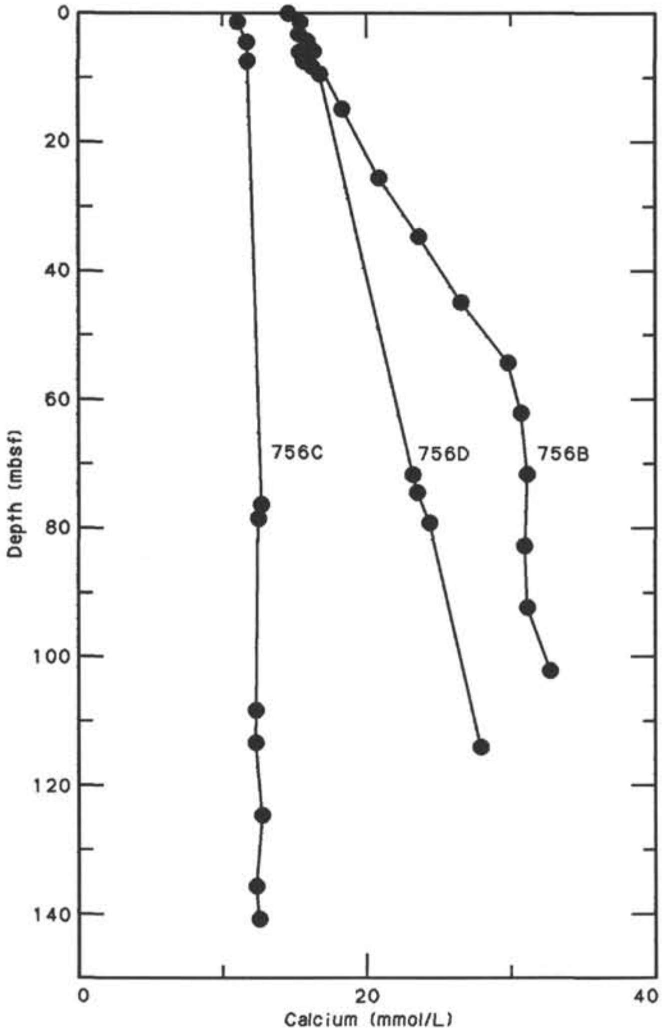

Figure 25. Pore-water calcium ion concentration profiles for Holes 756B, 756C, and 756D.

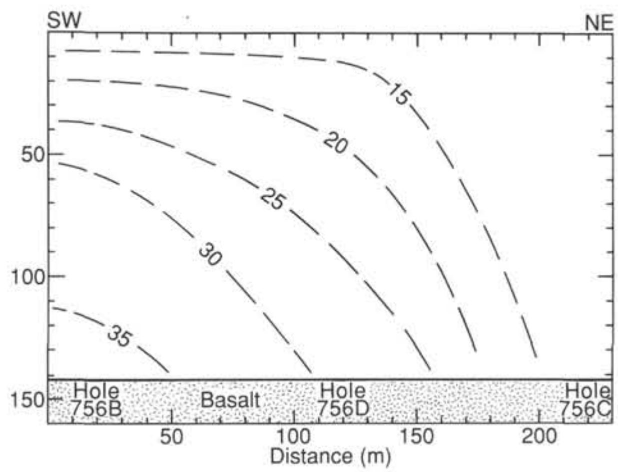

Figure 26. Cross section showing contours of pore-water calcium ion concentrations in the sediments (mmol/L) for the Site 756 area.

Table 9. Percentages of total carbon, inorganic carbon, organic carbon, and calcium carbonate in samples from Holes 756B and 756C.

Sample (interval in cm)	Depth (mbsf)	Total carbon (%)	Inorganic carbon (%)	Organic carbon (%)	Calcium carbonate (%)
756B-1H-2, 87-89	2.37	11.43	11.50	0.00	95.8
756C-1H-2, 90-92	2.40	11.47	11.54	0.00	96.1
756B-1H-4, 87-89	5.37		11.59		96.5
756C-1H-4, 90-92	5.40		11.49		95.7
756C-1H-6, 90-92	8.40		11.62		96.8
756B-2H-2, 90-92	10.90		11.66		97.1
756B-2H-4, 90-92	13.90	11.53	11.58	0.00	96.5
756B-2H-6, 90-92	16.90		11.63		96.9
756B-3H-2, 90-92	20.50		11.62		96.8
756B-3H-4, 90-92	23.50	11.52	11.58	0.00	96.5
756B-3H-6, 90-92	26.50		11.62		96.8
756B-4H-2, 90-92	30.10		11.59		96.5
756B-4H-4, 90-92	33.10	11.78	11.59	0.19	96.5
756B-4H-6, 90-92	36.10		11.63		96.9
756B-5H-2, 90-92	39.70		11.57		96.4
756B-5H-4, 90-92	42.70	11.55	11.49	0.06	95.7
756B-5H-6, 90-92	45.70		11.51		95.9
756B-6H-2, 90-92	49.30		11.47		95.6
756B-6H-3, 90-92	50.80		10.34		86.1
756B-6H-5, 90-92	53.80	9.97	9.92	0.05	82.6
756B-7H-2, 90-92	58.60		10.98		91.5
756B-7H-4, 90-92	61.60	11.01	11.01	0.00	91.7
756B-7H-6, 90-92	64.60		11.46		95.5
756B-8H-2, 90-92	68.00		11.41		95.1
756B-8H-4, 90-92	71.00	11.33	11.34	0.00	94.5
756C-2H-2, 90-92	71.30		11.43		95.2
756B-8H-6, 90-92	74.00		11.53		96.0
756B-9H-1, 90-92	76.10		11.45		95.4
756B-9H-3, 90-92	79.10	11.34	11.32	0.02	94.3
756B-9H-7, 60-62	84.80		11.38		94.8
756B-10H-1, 90-92	85.80		11.31		94.2
756B-10H-4, 90-92	90.30	11.27	11.33	0.00	94.4
756B-10H-7, 20-22	94.10		11.27		93.9
756B-11H-2, 90-92	97.00		11.23		93.6
756B-11H-4, 90-92	100.00	11.05	11.14	0.00	92.8
756B-11H-6, 90-92	103.00		11.44		95.3
756C-4X-2, 90-92	103.30		11.38		94.8
756C-4X-4, 90-92	106.30	11.42	11.46	0.00	95.5
756C-4X-6, 90-92	109.30		11.36		94.6
756C-5X-2, 20-22	111.02		11.40		95.0
756C-5X-4, 10-12	113.12	11.32	11.39	0.00	94.9
756C-5X-6, 90-92	115.18		11.22		93.5
756C-5X-8, 90-92	118.01		11.08		92.3
756C-6X-2, 90-92	122.60		11.28		94.0
756C-6X-4, 90-92	125.60	11.06	11.06	0.00	92.1
756C-7X-2, 85-87	132.15		11.03		91.9
756C-7X-4, 85-87	135.15	11.19	11.26	0.00	93.8
756C-7X-6, 85-87	138.15	10.57	10.60	0.00	88.3
756D-4R-1, 22-26	139.22		0.01		0.1
756C-8X-2, 90-92	141.80	11.04	10.89	0.15	90.7
756C-9X-CC, 7-9	144.63	11.35	11.34	0.01	94.5
756C-10N-3, 49-52	153.79		0.01		0.1
756C-11N-1, 90-92	155.40	0.14	0.04	0.10	0.3
756C-12N-1, 30-33	156.80		0.00		0.0
756D-6R-2, 49-52	160.29		0.01		0.1
756D-6R-3, 0-8	161.17		0.03		0.3
756D-7R-2, 38-40	169.86		0.00		0.0
756D-8R-1, 12-15	177.82		0.08		0.7
756D-9R-3, 137-140	191.44		0.09		0.8
756D-10R-2, 108-111	199.58		0.00		0.0
756D-11R-2, 123-130	209.33		0.03		0.3
756D-12R-2, 28-33	217.65		0.00		0.0
756D-12R-2, 90-92	218.27		0.01		0.1

shows a continuous increase with depth through units A and B. A linear regression of the data results in a following equation:

$$\text{thermal conductivity} = (1.40 \pm 0.0250) + (0.00154 \pm 0.000238) \times \text{depth},$$

where depth is in mbsf.

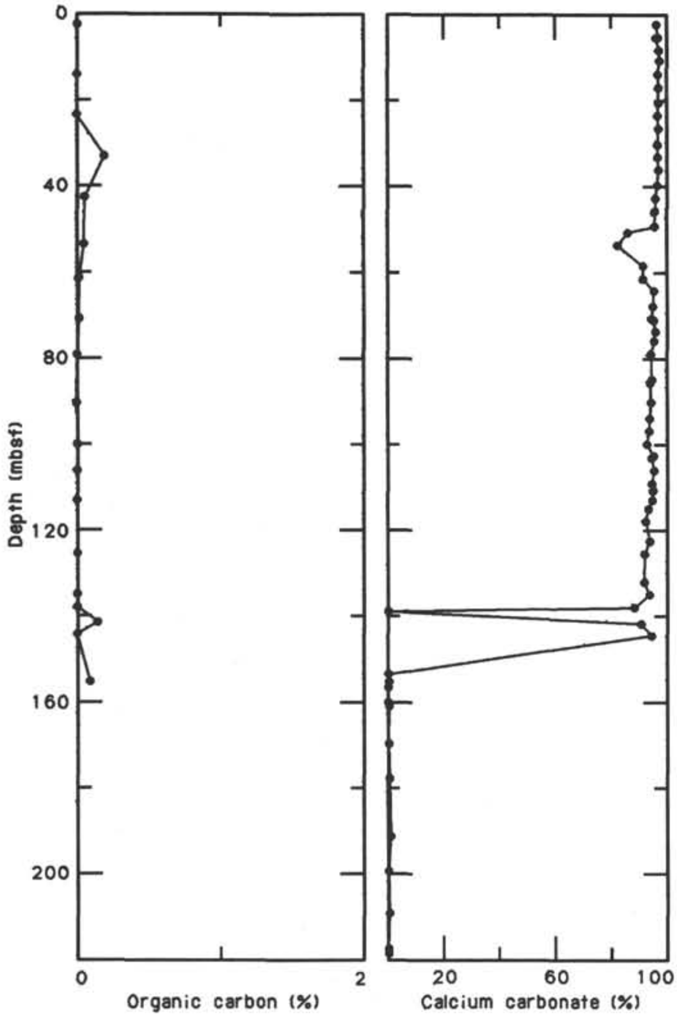

Figure 27. Organic carbon content and calcium carbonate content in samples from Holes 756B and 756C.

Summary

Two physical-properties units, A and B, are identified on the basis of differences in index properties and compressional-wave velocities. The boundary of units A and B is coincident with the boundary between lithologic Units I and II. The variations of vane shear strength, formation factor, and index properties in unit A correlate well to each other, making further subdivision possible. Subunits A1 (0–10 mbsf), A2 (10–50 mbsf), A3 (50–110 mbsf), and A4 (110–139 mbsf) can be roughly defined. Subunit A1 is a boundary layer between the water column and the underlying sediments in which there is a high variation of vane shear strength, formation factor, and thermal conductivity. Both vane shear strength and formation factor are lower in subunit A2 and higher in subunit A3. Subunit A4 is a boundary layer showing a high variation in shear strength and formation factor between the sedimentary column and underlying basement rocks.

Two groups of basalts, high-velocity basalt and low-velocity basalt, are distinguished on the basis of compressional-wave velocity. Basalts of both types account for the observed variation of index properties.

Table 10. Index properties of samples from Holes 756B, 756C, and 756D.

Sample (interval in cm)	Depth (mbsf)	Water content (%)	Porosity (%)	Density (g/cm³) Wet bulk	Dry bulk	Grain
756B-1H-2, 87	2.37	36.34	60.76	1.73	1.10	2.75
756C-1H-2, 90	2.40	37.09	61.29	1.71	1.07	2.72
756B-1H-4, 87	5.37	35.82	60.37	1.73	1.11	2.77
756C-1H-4, 90	5.40	38.05	61.99	1.70	1.05	2.69
756C-1H-6, 90	8.40	36.78	60.78	1.70	1.07	2.70
756B-2H-2, 90	10.90	34.72	58.95	1.75	1.14	2.74
756B-2H-4, 90	13.90	34.26	57.91	1.74	1.14	2.68
756B-2H-6, 90	16.90	35.69	59.91	1.73	1.11	2.73
756B-3H-2, 90	20.50	34.94	59.11	1.75	1.14	2.73
756B-3H-4, 90	23.50	35.08	59.23	1.73	1.13	2.72
756B-3H-6, 90	26.50	34.56	58.79	1.75	1.14	2.74
756B-4H-2, 90	30.10	36.12	59.95	1.71	1.09	2.68
756B-4H-4, 90	33.10	36.79	61.05	1.71	1.08	2.73
756B-4H-6, 90	36.10	36.03	60.05	1.72	1.10	2.70
756B-5H-2, 90	39.70	36.42	60.24	1.70	1.08	2.68
756B-5H-4, 90	42.70	34.73	58.78	1.75	1.14	2.72
756B-5H-6, 90	45.70	35.97	59.69	1.72	1.10	2.67
756B-6H-2, 90	49.30	35.97	60.00	1.71	1.10	2.70
756B-6H-3, 90	50.80	43.96	68.26	1.62	0.91	2.77
756B-6H-5, 90	53.80	43.13	67.54	1.64	0.93	2.78
756B-7H-2, 90	58.60	36.96	61.34	1.73	1.09	2.74
756B-7H-4, 90	61.60	38.45	62.70	1.68	1.04	2.73
756B-7H-6, 90	64.60	36.38	60.11	1.73	1.10	2.67
756B-8H-2, 90	68.00	34.84	59.27	1.75	1.14	2.76
756B-8H-4, 90	71.00	33.72	57.70	1.81	1.20	2.72
756C-2H-2, 90	71.30	39.65	64.16	1.69	1.02	2.76
756B-8H-6, 90	74.00	32.05	55.76	1.84	1.25	2.71
756B-9H-1, 90	76.10	33.49	57.56	1.79	1.19	2.73
756B-9H-3, 90	79.10	31.74	55.39	1.82	1.24	2.71
756B-9H-7, 60	84.80	29.99	53.75	1.86	1.30	2.75
756B-10H-1, 90	85.80	30.60	54.06	1.84	1.28	2.71
756B-10H-4, 90	90.30	30.20	53.90	1.87	1.30	2.74
756B-10H-7, 20	94.10	30.40	54.53	1.89	1.31	2.78
756B-11H-2, 90	97.00	31.74	55.05	1.82	1.24	2.67
756B-11H-4, 90	100.00	33.64	57.71	1.81	1.20	2.73
756B-11H-6, 90	103.00	30.55	54.91	1.86	1.29	2.81
756C-4X-2, 90	103.30	33.01	57.06	1.80	1.21	2.73
756C-4X-4, 90	106.30	31.58	54.78	1.80	1.23	2.66
756C-4X-6, 90	109.30	32.68	56.83	1.80	1.21	2.75
756C-5X-2, 20	111.02	31.40	55.22	1.81	1.24	2.73
756C-5X-4, 10	113.12	30.42	54.09	1.85	1.29	2.73
756C-5X-6, 90	115.18	31.63	54.84	1.80	1.23	2.66
756C-5X-8, 90	118.01	34.19	58.16	1.77	1.16	2.71
756C-6X-2, 90	122.60	31.81	55.70	1.81	1.23	2.73
756C-6X-4, 90	125.60	32.98	56.67	1.79	1.20	2.69
756C-7X-2, 85	132.15	35.23	59.45	1.76	1.14	2.73
756C-7X-4, 85	135.15	34.70	58.41	1.76	1.15	2.68
756C-7X-6, 85	138.15	35.96	60.17	1.72	1.10	2.72
756D-4R-1, 47	139.47	5.11	11.55	2.58	2.45	2.46
756C-8X-2, 90	141.80	33.84	57.51	1.77	1.17	2.68
756C-9X-C, 7	144.63	7.89	18.95	2.61	2.40	2.77
756D-5R-1, 46	149.06	2.32	6.02	2.78	2.72	2.74
756C-11N-1, 88	155.38	29.01	53.17	1.99	1.41	2.82
756D-6R-1, 73	159.03	1.66	4.39	2.76	2.71	2.76
756D-7R-1, 104	169.04	4.72	11.85	2.65	2.52	2.76
756D-7R-4, 66	173.02	2.38	6.22	2.77	2.71	2.77
756D-9R-3, 67	190.74	1.52	4.16	2.89	2.84	2.87
756D-10R-1, 124	198.24	2.01	5.46	2.77	2.71	2.86
756D-10R-2, 57	199.07	2.51	6.64	2.76	2.69	2.81
756D-10R-3, 46	200.46	0.96	2.75	2.91	2.88	2.96
756D-11R-1, 7	206.67	5.72	12.82	2.59	2.45	2.46
756D-11R-1, 97	207.57	2.25	5.90	2.75	2.69	2.78
756D-12R-2, 92	218.29	1.94	5.20	2.82	2.76	2.81

SEISMIC STRATIGRAPHY

General Setting

Site 756 is near the crest of southern Ninetyeast Ridge, midway between DSDP Sites 253 and 254. The site area was surveyed during the RC2708 cruise in September 1986. The survey was performed within a quadrangle bordered approximately by lines at 27°3′ and 27°30′S and 87°18′ and 87°42′E.

The bathymetry of the Site 756 operations area is rugged (Fig. 33). The sea bottom there is composed of rugged basement with small sedimentary ponds. The relief exceeds 1275 m in the survey area.

JOIDES Resolution approached the site on a heading of 301° along a dip line (Fig. 33). The line was continued about 13 km

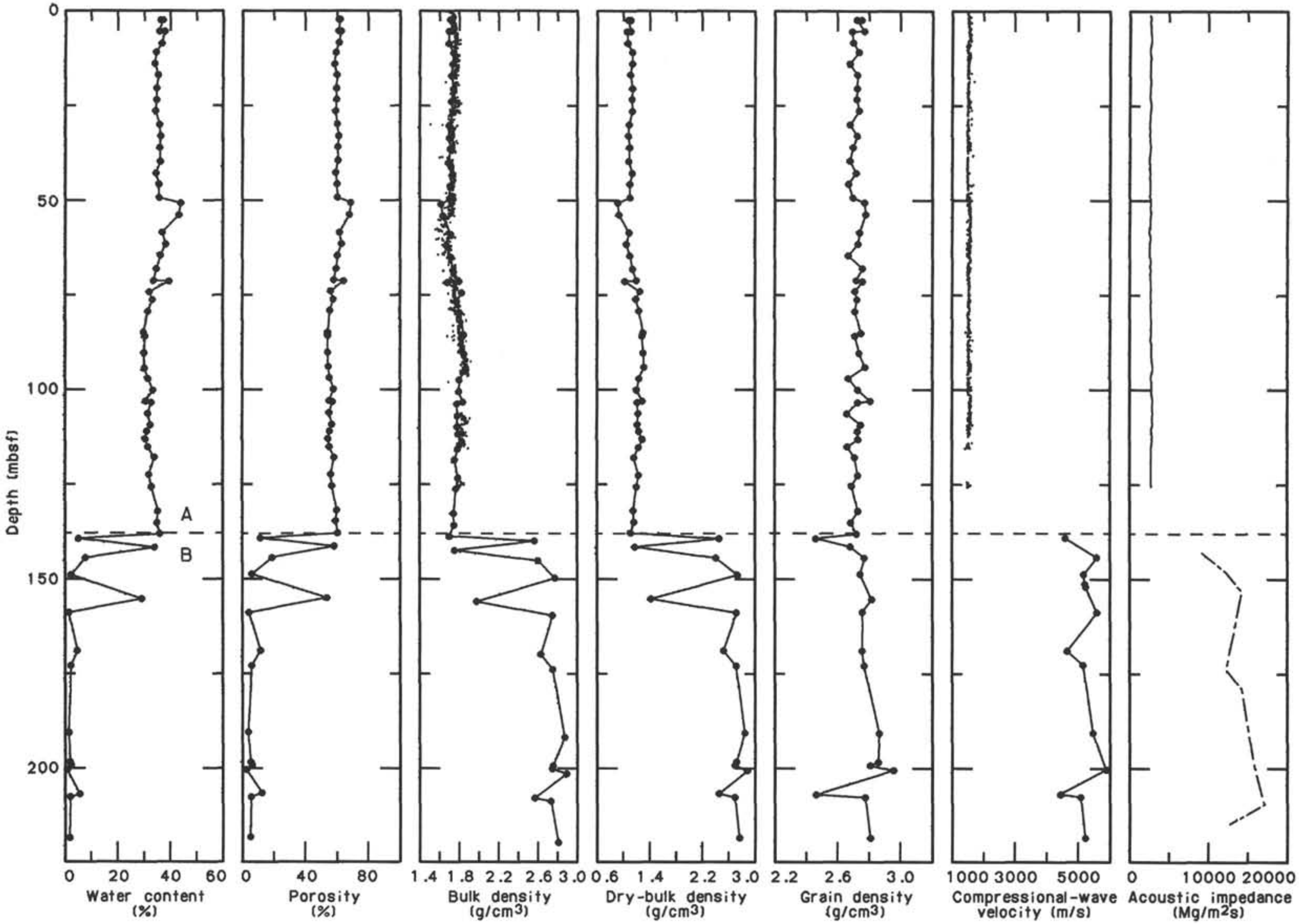

Figure 28. Water content, porosity, bulk density, dry-bulk density, grain density, compressional-wave velocity, and acoustic impedance profiles of sediments from Holes 756B, 756C, and 756D. Tightly clustered data are GRAPE densities and *P*-wave-logger velocities.

Table 11. Vane shear strength of samples from Holes 756B and 756C.

Sample (interval in cm)	Depth (mbsf)	Vane shear strength (kPa)
756B-1H-2, 90	2.40	5.1
756C-1H-2, 90	2.40	11.4
756C-1H-4, 90	5.40	11.9
756B-1H-4, 90	5.40	8.2
756C-1H-6, 90	8.40	6.1
756B-2H-2, 90	10.90	3.4
756B-2H-4, 90	13.90	4.2
756B-2H-6, 90	16.90	2.7
756B-3H-2, 90	20.50	5.4
756B-3H-4, 90	23.50	6.3
756B-3H-6, 90	26.50	4.1
756B-4H-2, 90	30.10	4.2
756B-4H-4, 90	33.10	2.7
756B-4H-6, 90	36.10	3.0
756B-5H-2, 101	39.81	5.8
756B-5H-4, 97	42.77	4.0
756B-5H-6, 90	45.70	3.7
756B-6H-2, 100	49.40	6.3
756B-6H-3, 90	50.80	15.4
756B-6H-5, 90	53.80	4.9
756B-7H-2, 90	58.60	13.7
756B-7H-4, 90	61.60	5.5
756B-7H-6, 90	64.60	4.5
756B-8H-2, 90	68.00	7.8
756B-8H-4, 90	71.00	3.7
756C-2H-2, 90	71.30	2.3
756B-8H-6, 90	74.00	4.4
756B-9H-1, 90	76.10	3.6
756B-9H-3, 94	79.14	14.2
756B-9H-7, 60	84.80	4.1
756B-10H-1, 96	85.86	10.2
756B-10H-4, 96	90.36	7.9
756B-10H-7, 26	94.16	11.6
756C-4X-2, 90	103.30	11.2
756C-4X-4, 90	106.30	3.3
756C-4X-6, 90	109.30	11.8
756C-5X-2, 20	111.02	5.6
756C-5X-4, 10	113.12	4.9
756C-5X-6, 90	115.18	4.9
756C-5X-8, 90	118.01	26.3
756C-6X-2, 90	122.60	4.1
756C-6X-4, 90	125.60	8.1
756C-7X-2, 85	132.15	18.6
756C-7X-4, 85	135.15	10.5
756C-7X-6, 85	138.15	42.6
756C-8X-2, 90	141.80	38.4

before the heading was changed to 106°, and the line then continued for approximately 16.5 km before turning to the southwest (heading 224°) in order to cross the site with a strike line. The direction of the strike line was chosen to be parallel to the predominant fault direction in the area, which appears to be about N50°E. The location of Site 756 is 27°21.29′S and 87°35.84′E (Fig. 33).

Site Survey

The site survey by the *JOIDES Resolution* was performed using a magnetometer, 3.5-kHz echo-sounder, and two 80-in.^{3} water guns as a seismic source of a digital, single-channel recording system. Two analog seismic records were filtered with 40–165-Hz and 65–165-Hz band-pass filters, respectively. The location of the drill site was moved about 500 m west-northwest of the proposed site (shotpoint 13920; Fig. 34) in order to avoid a minor intrasediment fault. Site 756 is on a sediment bench on the eastern side of Ninetyeast Ridge. The exact location of Site 756 is marked by arrows on the seismic profiles shown in Figures 35 and 36.

Correlation between Seismic Stratigraphy and Lithostratigraphy

Lithostratigraphy

Two lithologic units are recognized at Site 756. The first unit is a Pleistocene to upper Eocene nannofossil ooze with foraminifers from 0 to 150.3 mbsf in Hole 756C and from 0 to 148.6 mbsf in Hole 756D. This ooze gradually becomes more indurated downsection, which led to a failure of the piston coring device in Hole 756B. A minor chalk subunit immediately above the underlying basalt changes abruptly into limestone. The thickness of this subunit is uncertain because it was recovered only in the very bottom of Core 121-756C-8X and in Core 121-756C-9X, which had a poor recovery. The second major unit is composed of basalt flows with estimated thicknesses of 2–5 m which are intercalated with ash and soil layers (see "Lithostratigraphy and Sedimentology" section). The lithologic character of the drilled section largely agrees with that predicted at this location based on a seismic stratigraphic evaluation of the RC2708 site survey (Newman and Sclater, 1988).

Reflectors

Several reflections can be seen in the good echo-sounder record (Fig. 37) at 2.028 (water bottom), 2.036, 2.060, 2.072, 2.104, 2.114, 2.141, and 2.191 s two-way traveltime (TWT). Other reflectors can be seen in the seismic record (Figs. 35 and 36).

The water-bottom reflector was recognized at 2.025 s along a dip line and 2.028 s along a strike line on the seismic records. These times correspond to uncorrected water depths of 1519 and 1521 m, respectively, compared to the water bottom reached at 1518 m according to drill-pipe measurement. The next two strong reflectors at 2.04 and 2.06 s TWT along the dip line (2.043 and 2.065 s TWT along strike line) are sea-surface reflections (ghosts) of the outgoing pulse of the water gun. The continuous reflectors underneath can be recognized at 2.1 (2.1) and 2.143 (2.144) s TWT. We observed a zone of attenuated seismic signal of unknown origin between 2.09 and 2.19 s TWT in both strike and dip lines. The first "reverberant layer" reflector is at 2.195 (2.194) s TWT.

Velocities

Velocities measured by using sonobuoys during the site survey range from 1550 m/s in the shallower oozes to 1800 m/s in the deeper ones. The velocity of the acoustic basement measured near the proposed site (shotpoint 13960) is about 3800 m/s (Newman and Sclater, 1988). Actual sediment velocities measured aboard ship by the *P*-wave logger and on a Hamilton Frame (see "Physical Properties" section) are between 1500 and 1600 m/s in the ooze and approximately 5000 m/s in lava flows. The discrepancy between velocities measured on the discrete basalt samples (average 5000 m/s) and refraction survey velocities (3800 m/s) may be explained by the fact that the basalt sample velocities were measured in a solid basalt, whereas the refraction velocity averages velocities measured in basalts, altered basalts, ashes, or soils between flows. In addition, refraction velocities in an area of high relief such as this are subject to significant errors. We believe that the 5000 m/s velocity is the best estimate of velocity for the volcanic layer.

Impedance

Acoustic impedance was calculated throughout the section (see "Physical Properties" section). The acoustic impedance ranges from 2500 to about 3000 Mg/m^{2}s in the ooze and from 9000 to about 17,000 Mg/m^{2}s in the basalts (Fig. 38). The acoustic impedance does not show any great changes, except between the ooze and limestone layer at about 140 mbsf. There are sev-

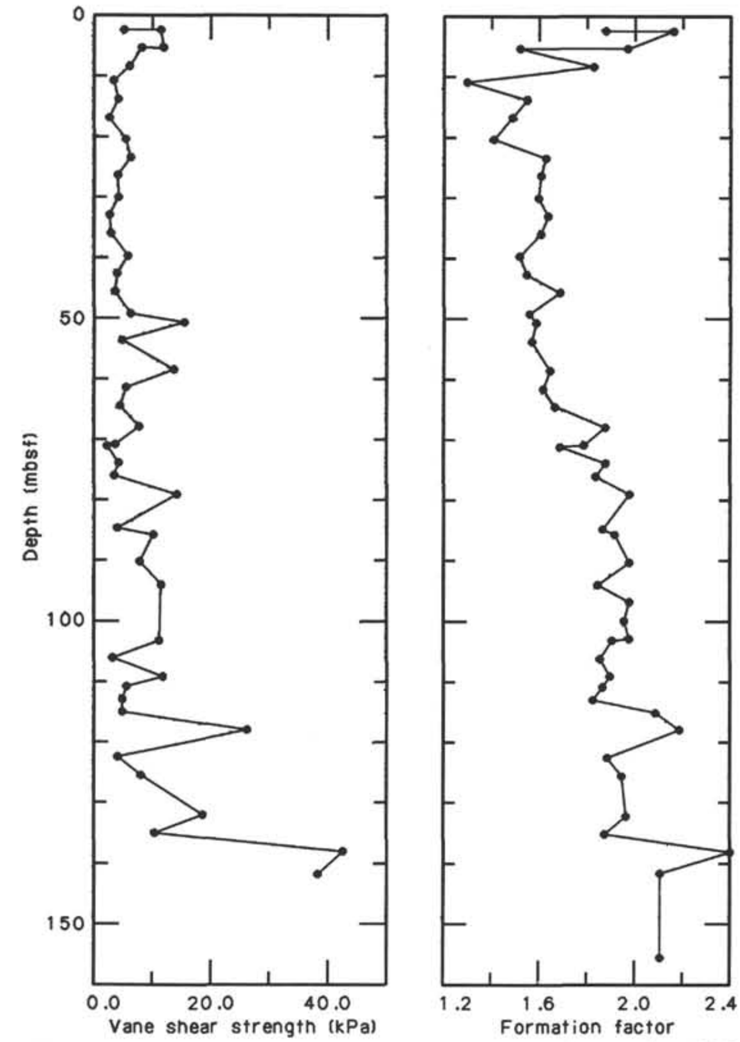

Figure 29. Vane shear strength and formation factor of sediments from Holes 756B and 756C.

eral small changes along the impedance profile in the oozes, and some of these may possibly correlate with seismic reflectors. The impedance changes of interest occur at following intervals: 24-25, 34-35, 55-60, 93-99, and 106-108 mbsf.

Grain Size

Grain size varies greatly throughout the sedimentary section. The grain size ranges from approximately 10 to 60 μm. Grain size (see "Lithostratigraphy and Sedimentology" section) is plotted as a three-value centered running average along the section in Figure 38. Peak values are at 25, 35, 57, 71, 100, 118, and just above 140 mbsf, where the lithology of the sedimentary column changes into limestone.

Correlation

Figure 38 shows the correlation of the seismic record reflections (dashed lines) with grain size, impedance, and lithology. A simple velocity structure was used in the interpretation: 1600 m/s to 60 mbsf, 1800 m/s from 60 mbsf to the top of the limestone at 143 mbsf, and 5000 m/s from 143 mbsf to the bottom of the hole. This velocity structure shows good results in matching reflectors to seismic stratigraphic units. The first reflector at 2.1 s TWT (58 mbsf) can be correlated with a large peak in the grain-size curve; with character changes in the impedance curve, vane shear strength, other physical properties, and magnetic susceptibility (see "Physical Properties" and "Paleomagnetics" sections); and also with a change in calcium ion concentration in the pore waters (see "Inorganic Chemistry" section). There is no lithology change associated with this reflector.

The next reflector is at 2.144 s TWT, which corresponds to a depth of 97 mbsf. There is a local impedance low between 93 and 99 mbsf, a peak in a grain size, and a peak in magnetic susceptibility between 94 and 103 mbsf. The depth of this reflector corresponds to the last piston core (Core 121-756B-11H) obtained in Hole 756B before the APC became stuck and could not be retrieved. This failure indicates that there may have been some changes in physical properties (strength) not recorded in the cores (except for a minor change in grain size), which possibly caused some reflection of seismic energy.

The lowermost reflector (the first of several "reverberant layers") that can be correlated with other physical or lithologic properties is at 143 mbsf. Whether this reflector can be correlated with the top of the limestone layer or the onset of the basaltic flows is not clear. Impedance was not measured immediately above this depth, but the last value measured in oozes at 124 mbsf is approximately 3000 Mg/m^2s, whereas the next value at 140 mbsf is about 9000 Mg/m^2s and rising.

Correlation of the echo-sounder reflections with grain size, impedance, and lithology is also shown in Figure 38 (dotted lines). The reflector times were converted to depths according to

Table 12. Formation factor of samples from Holes 756B and 756C.

Sample (interval in cm)	Depth (mbsf)	Formation factor
756B-1H-2, 90	2.40	1.88
756C-1H-2, 90	2.40	2.16
756C-1H-4, 90	5.40	1.97
756B-1H-4, 90	5.40	1.52
756C-1H-6, 90	8.40	1.83
756B-2H-2, 90	10.90	1.30
756B-2H-4, 90	13.90	1.55
756B-2H-6, 90	16.90	1.49
756B-3H-2, 90	20.50	1.41
756B-3H-4, 90	23.50	1.63
756B-3H-6, 90	26.50	1.61
756B-4H-2, 90	30.10	1.60
756B-4H-4, 90	33.10	1.64
756B-4H-6, 90	36.10	1.61
756B-5H-2, 92	39.72	1.52
756B-5H-4, 92	42.72	1.55
756B-5H-6, 92	45.72	1.69
756B-6H-2, 92	49.32	1.56
756B-6H-3, 95	50.85	1.59
756B-6H-5, 95	53.85	1.57
756B-7H-2, 90	58.60	1.65
756B-7H-4, 90	61.60	1.62
756B-7H-6, 90	64.60	1.67
756B-8H-2, 97	68.07	1.88
756B-8H-4, 95	71.05	1.79
756C-2H-2, 90	71.30	1.69
756B-8H-6, 91	74.01	1.88
756B-9H-1, 94	76.14	1.84
756B-9H-3, 92	79.12	1.98
756B-9H-7, 62	84.82	1.87
756B-10H-1, 95	85.85	1.92
756B-10H-4, 93	90.33	1.98
756B-10H-7, 22	94.12	1.85
756B-11H-2, 92	97.02	1.98
756B-11H-4, 92	100.02	1.96
756B-11H-6, 90	103.00	1.98
756C-4X-2, 90	103.30	1.91
756C-4X-4, 90	106.30	1.86
756C-4X-6, 90	109.30	1.90
756C-5X-2, 20	111.02	1.87
756C-5X-4, 10	113.12	1.83
756C-5X-6, 90	115.18	2.09
756C-5X-8, 90	118.01	2.19
756C-6X-2, 90	122.60	1.89
756C-6X-4, 90	125.60	1.95
756C-7X-2, 85	132.15	1.97
756C-7X-4, 85	135.15	1.88
756C-7X-6, 85	138.15	2.40
756C-8X-2, 90	141.80	2.11
756C-11X-1, 90	155.40	2.11

Table 13. Compressional-wave velocity of samples from Holes 756C and 756D.

Sample (interval in cm)	Depth (mbsf)	Direction[a]	Compressional-wave velocity (m/s)
756D-4R-1, 47	139.47	C	4512.7
756D-4R-1, 47	139.47	A	4577.5
756D-4R-1, 47	139.47	B	4654.4
756C-9X-CC, 7	144.63		5578.8
756D-5R-1, 46	149.06	A	5135.4
756D-5R-1, 46	149.06	B	5209.6
756D-5R-1, 46	149.06	C	5307.9
756C-10N-1, 124	151.54	B	5108.2
756C-10N-1, 124	151.54	C	5412.9
756C-10N-1, 124	151.54	A	5199.5
756C-10N-2, 57	152.37	A	5227.6
756C-10N-2, 57	152.37	C	5151.7
756C-10N-2, 57	152.37	B	5261.5
756C-11N-1, 88	155.38	C	4434.7
756D-6R-1, 73	159.03	A	5580.7
756D-6R-1, 73	159.03	B	5460.8
756D-6R-1, 73	159.03	C	5440.9
756D-7R-1, 104	169.04	A	4631.7
756D-7R-1, 104	169.04	B	4597.5
756D-7R-1, 104	169.04	C	4752.7
756D-7R-4, 66	173.02	C	5124.1
756D-7R-4, 66	173.02	A	5135.7
756D-7R-4, 66	173.02	B	5252.4
756D-9R-3, 67	190.74	B	5626.0
756D-9R-3, 67	190.74	C	5567.8
756D-9R-3, 67	190.74	A	5477.2
756D-10R-3, 46	200.46	B	5664.0
756D-10R-3, 46	200.46	C	5955.7
756D-10R-3, 46	200.46	A	5879.8
756D-11R-1, 7	206.67	A	4448.3
756D-11R-1, 7	206.67	B	4360.9
756D-11R-1, 7	206.67	C	4442.4
756D-11R-1, 97	207.57	A	5082.5
756D-11R-1, 97	207.57	C	4831.8
756D-11R-1, 97	207.57	B	5065.6
756D-12R-2, 92	218.29	A	5220.3
756D-12R-2, 92	218.29	C	5299.8
756D-12R-2, 92	218.29	B	5135.7

[a] A = vertical propagation; B = propagation perpendicular to the split-core face; C = propagation parallel to the split-core face.

the described velocity structure. The depths of the reflectors are as follows: 6, 26, 35, 61, 70, 94, and 137 mbsf. The reflectors at 61, 94, and 137 mbsf are presumably the same as the reflectors in the seismic survey (58, 97, and 143 mbsf), and their correlation with other sediment parameters was described previously. The reflector at 6 mbsf cannot be correlated to an impedance change or to a change in grain size, but correlates well with other physical properties, such as porosity, bulk density, water content, vane shear strength, and especially formation factor (see "Physical Properties" section). This reflector marks a boundary between very unconsolidated surface sediments and deeper, slightly more compacted sedimentary layers. The next reflector, at 26 mbsf, correlates with vane shear strength and electric resistivity (formation factor) increases and with a slight change in acoustic impedance. The reflector at 35 mbsf correlates with slightly increased impedance and decreased thermal conductivity; however, there is no lithology change. The reflector at 70 mbsf correlates with a local peak in porosity and a corresponding decrease in wet-bulk density, increased formation factor, and a local peak in grain size.

Conclusions

Site 756 can be divided by seismic stratigraphy into two major units and several subunits. An upper major unit (nannofossil ooze with foraminifers) has seismic velocities ranging from approximately 1600 to 1800 m/s and coincides with sedimentary sequence I (nannofossil ooze with foraminifers) at this site. The lower major unit is composed of successive basalt flows, with variable degrees of alteration, intercalated with ashes and soils. Seismic velocity in the basalts is about 5000 m/s, and is perhaps somewhat lower in the ash and soil horizons. The basaltic unit is separated from the upper unit by a thin limestone layer.

Subunit 1A of the upper seismic stratigraphic unit is an unconsolidated, water-saturated ooze that is separated from the next subunit by a seismic reflector at 6 mbsf. The velocity of this subunit is probably only slightly more than 1500 m/s. Subunit 1B continues from 6 to approximately 60 mbsf. This subunit consists of more consolidated ooze with a lower porosity and water content than Subunit 1A. The seismic velocity of Subunit 1B is approximately 1600 m/s. Subunit 1C seems to be still more consolidated, as evidenced by increased vane shear strength, decreased water content, and the measurement of formation factor (see "Physical Properties" section). Subunit 1C, which also has a seismic velocity of about 1600 m/s, is divided from the next subunit by a reflector at approximately 95 mbsf. Subunit

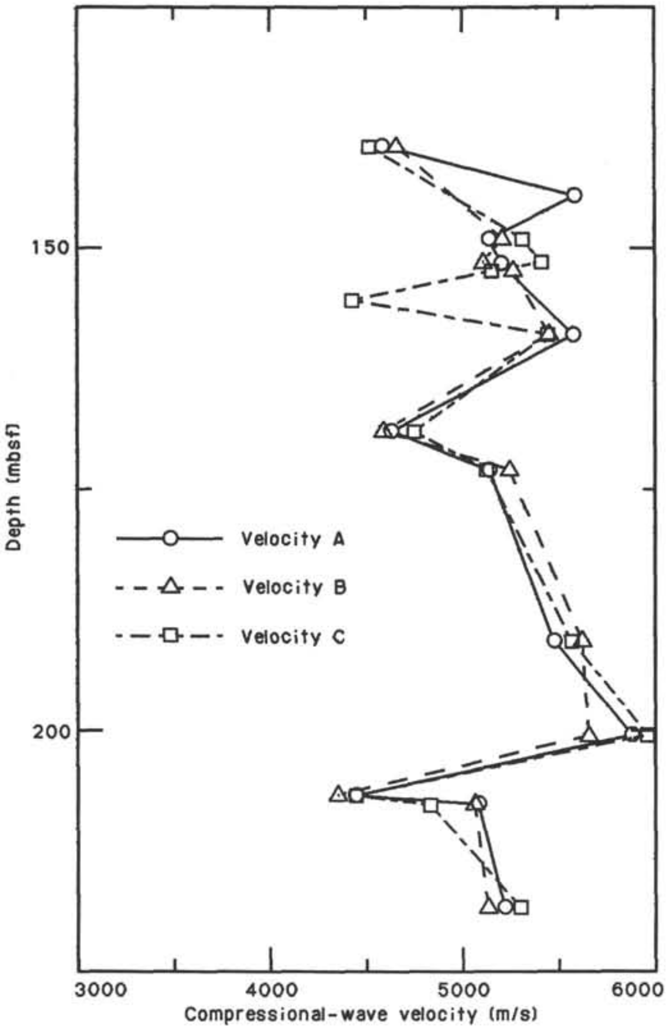

Figure 30. Compressional-wave velocity of samples from Holes 756C and 756D. Velocity A is a velocity of vertical propagation. Velocities B and C are velocities of horizontal propagation, where velocity B is perpendicular to the split-core surface and velocity C is parallel to it.

1D, from 95 to about 140 mbsf, is composed of well-consolidated ooze, which grades into chalk and a thin limestone layer. The velocity in this layer is estimated at 1800 m/s.

The volcanic unit is composed of separate flows intercalated with ash. There is no seismic stratigraphic evidence of intercalation other than the "ringing" character of the acoustic basement reflector. Based on our best estimate of velocity in this sequence, the total penetration of 221 mbsf is equivalent to 2.225 s TWT on the seismic records.

In general, the seismic stratigraphic division agrees with the lithologic division into two major units. Division of the sediment section into subunits is not supported by the lithologic evidence, except possibly by grain-size measurements. The division is instead based on the placement of seismic reflectors obtained from both the seismic and echo-sounder surveys and on changes of various physical properties in the sedimentary sequence.

REFERENCES

Banner, F. T., and Blow, W. H., 1965. Progress in the planktonic foraminiferal biostratigraphy of the Neogene. *Nature*, 208:1164–1166.

Berggren, W. A., Kent, D. V., Flynn, J. J., and Van Couvering, J. A., 1985. Cenozoic geochronology. *Geol. Soc. Am. Bull.*, 96:1407–1418.

Blow, W. H., 1969. Late middle Eocene to Recent planktonic biostratigraphy. *In* Bronnimann, P., and Renz, H. H. (Eds.), *Proc. Int. Conf. Planktonic Microfossils, 1st, Geneva, 1967*, 1:199–421.

Bolli, H. M., and Saunders, J. B., 1985. Oligocene to Holocene low latitude planktic foraminifera. *In* Bolli, H. M., Saunders, J. B., and Perch-Nielsen, K. (Eds.), *Plankton Stratigraphy*: Cambridge (Cambridge Univ. Press), 155–262.

Bolli, H. M., Saunders, J. B., and Perch-Nielsen, K. (Eds.), 1985. *Plankton Stratigraphy*: Cambridge (Cambridge Univ. Press).

Bougault, H., Treuil, M., and Joron, J.-L., 1979. Trace elements in basalts from 23°N and 36°N in the Atlantic Ocean: fractional crystallization, partial melting, and heterogeneity of the upper mantle. *In* Melson, W. G., Rabinowitz, P. D., et al., *Init. Repts. DSDP*, 45: Washington (U.S. Govt. Printing Office), 493–506.

Carmichael, I.S.E., 1964. The petrology of Thingmuli, a Tertiary volcano in eastern Iceland. *J. Petrol.*, 5:435–460.

Corliss, B. H., 1979. Recent deep-sea benthonic foraminiferal distributions in the southeast Indian Ocean: inferred bottom-water routes and ecological implications. *Mar. Geol.*, 31:115–138.

Davies, T. A., Luyendyk, B. P., et al., 1974. *Init. Repts. DSDP*, 26: Washington (U.S. Govt. Printing Office).

Duncan, R. A., 1978. Geochronology of basalts from the Ninetyeast Ridge and continental dispersion in the eastern Indian Ocean. *J. Volcanol. Geotherm. Res.*, 4:283–305.

Duncan, R. A., Backman, J., Macdonald, A., et al., in press. Réunion hotspot activity through Tertiary time: initial results from the Ocean Drilling Program, Leg 115. *J. Volcanol. Geotherm. Res.*

Frey, F. A., Dickey, J. S., Thompson, G., and Bryan, W. B., 1977. Eastern Indian Ocean DSDP Sites: correlations between petrography, geochemistry and tectonic setting. *In* Heirtzler, J. R., and Sclater, J. G. (Eds.), *A Synthesis of Deep Sea Drilling in the Indian Ocean*: Washington (Am. Geophys. Union), 189–257.

Gieskes, J. M., 1975. Chemistry of interstitial waters of marine sediments. *Annu. Rev. Earth Planet. Sci.*, 3:433–453.

———, 1983. The chemistry of interstitial waters of deep sea sediments: interpretation of Deep Sea Drilling data. *Chem. Ocean.*, 8: 221–269.

Haggerty, S. E., 1976. Opaque mineral oxides in terrestrial igneous rocks. *In* Rumble, D. (Ed.), *Oxide Minerals*: Short Course Notes Mineral. Soc. Am., 3:101–104.

Hekinian, R., 1974. Petrology of igneous rocks from Leg 22 in the Northeastern Indian Ocean. *In* von der Borch, C. C., Sclater, J. G., et al., *Init. Repts. DSDP*, 22: Washington (U.S. Govt. Printing Office), 413–447.

Kempe, D.R.C., 1974. The petrology of the basalts, Leg 26. *In* Davies, T. A., Luyendyk, B. P., et al., *Init. Repts. DSDP*, 26: Washington (U.S. Govt. Printing Office), 465–503.

Lawrence, J. R., and Gieskes, J. M., 1981. Constraints on water transport and alteration in the oceanic crust from the isotopic composition of pore water. *J. Geophys. Res.*, 86:7924–7934.

Ludden, J. L., Thompson, G., Bryan, W. B., and Frey, F. A., 1980. The origin of lavas from the Ninetyeast Ridge, eastern Indian Ocean: an evaluation of fractional models. *J. Geophys. Res.*, 85:4405–4420.

Luyendyk, B. P., 1977. The Ninetyeast Ridge. *In* Heirtzler, J. R., Bolli, H. M., Davies, T. A., Saunders, J. B., and Sclater, J. G. (Eds.), *Indian Ocean Geology and Biostratigraphy*: Washington (Am. Geophys. Union), 165–188.

Luyendyk, B. P., and Rennick, W., 1977. Tectonic history of aseismic ridges in the eastern Indian Ocean. *Geol. Soc. Am. Bull.*, 88:1347–1356.

Martini, E., 1971. Standard Tertiary and Quaternary calcareous nannoplankton zonation. *In* Haq, B. U. (Ed.), *Nannoplankton Biostratigraphy*: Stroudsburg, PA (Hutchinson Ross), 264–307.

Miyashiro, A., 1974. Volcanic rock series in island arcs and active continental margins. *Am. J. Sci.*, 274:321–355.

Molnar, P., and Tapponnier, P., 1975. Cenozoic tectonics of Asia: effects of a continental collision. *Science*, 198:419–426.

Mottl, M. J., Langseth, M. L., and the Scientific Party of Ocean Drilling Program Leg 111, 1987. Slow hydrothermal circulation through thick sediments confirmed by drilling on the south flank of the Costa Rica Rift. *EOS, Trans. Am. Geophys. Union*, 68:1326.

Mottl, M. J., Lawrence, J. R., and Keigwin, L. D., 1983. Elemental and stable-isotope composition of pore waters and carbonate sediments from Deep Sea Drilling Project Sites 501/504 and 505. *In* Cann,

J. R., Langseth, M. L., et al., *Init. Repts. DSDP*, 69: Washington (U.S. Govt. Printing Office), 461–486.

Newman, J. S., and Sclater, J. G., 1988. Site surveys of the central and southern Ninetyeast Ridge for the Ocean Drilling Program, Leg 121. *Tech. Rep. Univ. Tex. Austin Inst. Geophys.*, 74.

Okada, H., and Bukry, D., 1980. Supplementary modification and introduction of code numbers to the low latitude coccolith biostratigraphy (Bukry, 1973; 1975). *In* Haq, B. U. (Ed.), *Nannofossil Biostratigraphy*: Stroudsburg, PA (Hutchison Ross), 321–377.

O'Reilly, W., 1984. *Rock and Mineral Magnetism*: Glasgow (Blackie).

Patriat, P., and Achache, J., 1984. India-Eurasia collision chronology has implications for crustal shortening and driving mechanism of plates. *Nature*, 311:615–621.

Peirce, J. W., 1978. The northward motion of India since the Late Cretaceous. *Geophys. J. R. Astron. Soc.*, 52:277–312.

Peterson, L. C., 1984. Recent abyssal benthic foraminiferal biofacies of the eastern equatorial Indian Ocean. *Mar. Micropaleontol.*, 8:479–579.

Price, R. C., Kennedy, A. K., Riggs-Sneeringer, M., and Frey, F. A., 1986. Geochemistry of basalts from the Indian Ocean triple junction: implications for the generation and evolution of Indian Ocean Ridge basalts. *Earth Planet. Sci. Lett.*, 78:379–396.

Rea, D. K., Leinen, M., and Janecek, T. R., 1985. Geologic approach to the long-term history of atmospheric circulation. *Science*, 227: 721–725.

Royer, J.-Y., Sclater, J. G., and Sandwell, D. T., in press. A preliminary tectonic chart of the Indian Ocean. *Proc. Indian Acad. Sci., Earth Planet. Sci.*

Saunders, A. D., 1983. Geochemistry of basalts recovered from the Gulf of California during Leg 65 of the Deep Sea Drilling Project. *In* Lewis, B.T.R., Robinson, P., et al., *Init. Repts. DSDP*, 65: Washington (U.S. Govt. Printing Office), 591–622.

Storey, M., Saunders, A. D., Tarney, J., Leak, P., Thirwall, M. F., Thompson, R. N., Menzies, M. A., and Marriner, G. F., 1988. Geochemical evidence for plume-mantle interaction beneath Kerguelen and Heard Islands, Indian Ocean. *Nature*, 336:371–374.

von der Borch, C. C., Sclater, J. G., et al., 1974. *Init. Repts. DSDP*, 22: Washington (U.S. Govt. Printing Office).

Weis, D., Beaux, J. F., Gautier, I., Giret, A., and Vidal, P., 1988. Kerguelen Archipelago: geochemical evidence for recycled material. *In* Hart, S. R., and Gülen, L. (Eds.), *Crust/Mantle Recycling at Convergence Zones*: Nato ASI Workshop, Abst., May 25–29, Antalaya, Turkey, 122–125.

Ms 121A-110

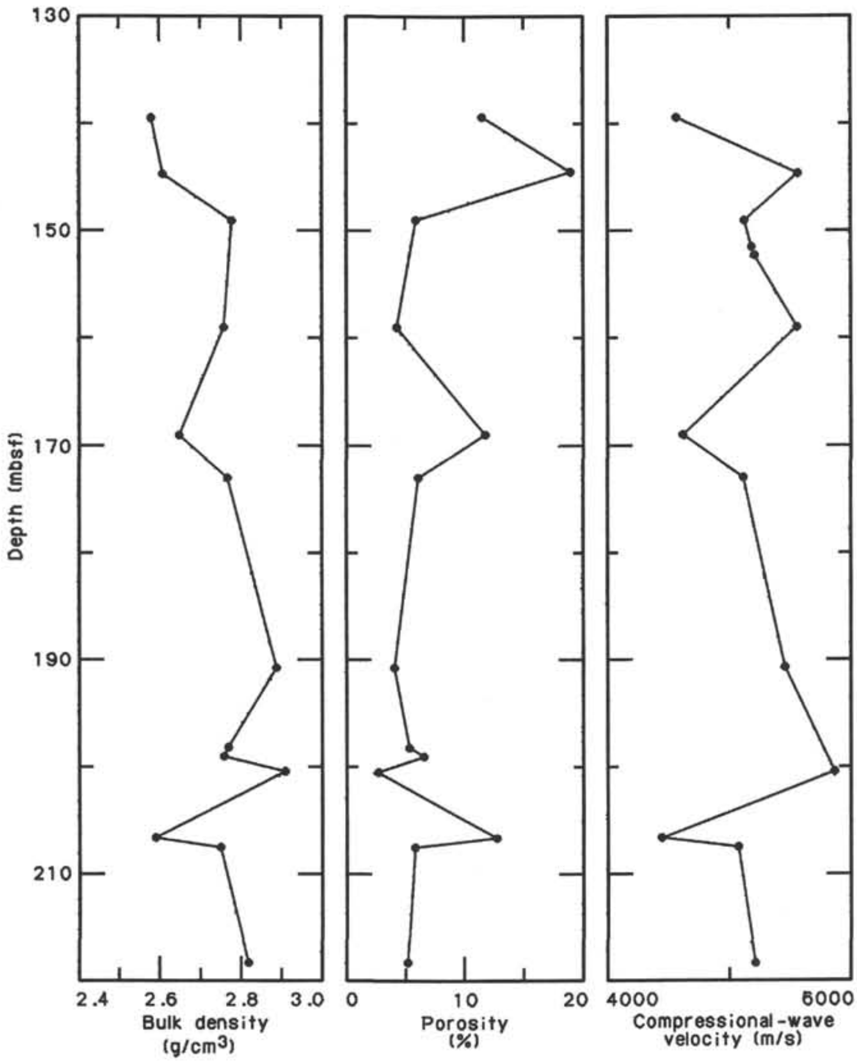

Figure 31. Bulk density, porosity, and compressional-wave velocity of basalts from Holes 756C and 756D.

Table 14. Thermal conductivity of samples from Holes 756B, 756C, and 756D.

Sample (interval in cm)	Depth (mbsf)	Thermal conductivity (W/m°C)
756B-1H-2, 70	2.20	1.391
756C-1H-2, 80	2.30	1.384
756B-1H-4, 70	5.20	1.432
756C-1H-4, 80	5.30	1.455
756B-1H-6, 70	8.20	1.480
756C-1H-6, 80	8.30	1.430
756B-2H-2, 70	10.70	1.457
756B-2H-4, 70	13.70	1.506
756B-2H-6, 70	16.70	1.526
756B-3H-2, 70	20.30	1.492
756B-3H-6, 70	26.30	1.519
756B-4H-2, 90	30.10	1.473
756B-4H-4, 90	33.10	1.376
756B-4H-6, 90	36.10	1.486
756B-5H-2, 90	39.70	1.510
756B-5H-4, 90	42.70	1.498
756B-5H-6, 90	45.70	1.547
756B-6H-2, 90	49.30	1.445
756B-6H-4, 90	52.30	1.297
756B-6H-6, 90	55.30	1.276
756B-7H-2, 70	58.40	1.436
756B-7H-4, 70	61.40	1.413
756B-7H-6, 70	64.40	1.472
756B-8H-2, 90	68.00	1.473
756B-8H-4, 90	71.00	1.463
756C-2H-2, 80	71.20	1.402
756B-8H-6, 90	74.00	1.610
756C-2H-4, 80	74.20	1.410
756C-2H-6, 80	77.20	1.416
756B-9H-2, 90	77.60	1.593
756B-9H-4, 90	80.60	1.481
756B-9H-6, 90	83.60	1.603
756B-10H-2, 80	87.20	1.570
756B-10H-4, 80	90.20	1.545
756B-10H-6, 80	93.20	1.596
756B-11H-2, 80	96.90	1.524
756B-11H-4, 80	99.90	1.431
756B-11H-6, 80	102.90	1.572
756C-4X-2, 80	103.20	1.612
756C-4X-4, 80	106.20	1.604
756C-4X-6, 80	109.20	1.709
756C-6X-2, 50	122.20	1.585
756C-6X-5, 50	126.70	1.581
756C-7X-2, 70	132.00	1.492
756C-7X-4, 70	135.00	1.586
756C-7X-6, 70	138.00	1.529
756D-4R-1, 40	139.40	1.530
756C-8X-1, 70	140.10	1.558
756C-8X-2, 70	141.60	1.494
756D-5R-1, 22	148.82	1.520
756C-10N-1, 115	151.45	1.780
756D-6R-1, 68	158.98	1.580
756D-7R-1, 98	168.98	1.530
756D-8R-1, 67	178.37	1.830
756D-9R-1, 95	188.35	1.990
756D-9R-3, 62	190.69	1.990
756D-10R-3, 43	200.43	1.900
756D-11R-1, 6	206.66	1.590
756D-12R-2, 91	218.28	1.520

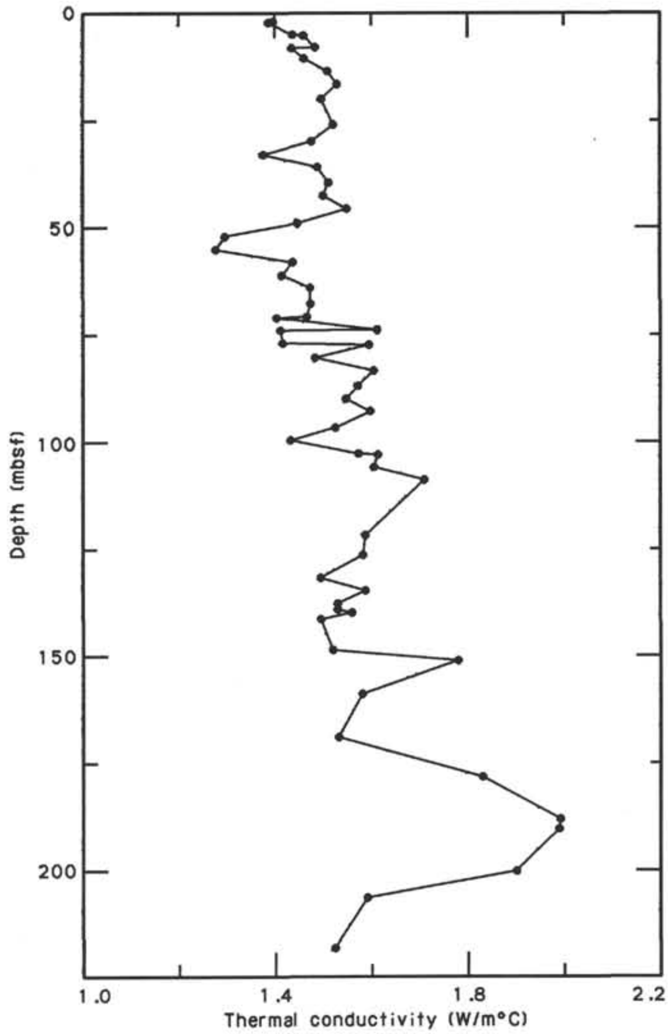

Figure 32. Thermal conductivity of samples from Holes 756B, 756C, and 756D.

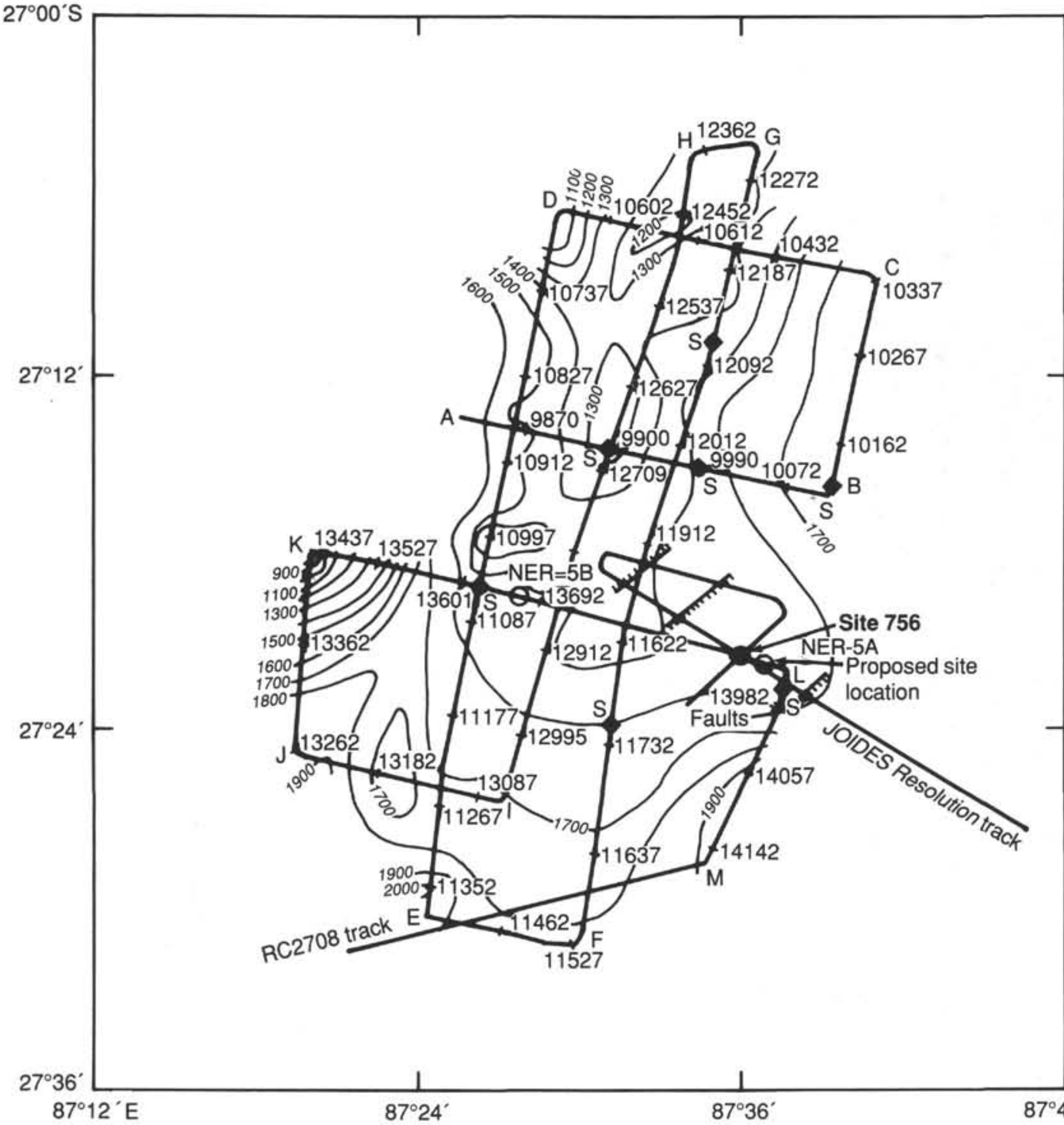

Figure 33. Southern Ninetyeast Ridge survey area. Solid lines delineate RC2708 and *Resolution* tracks, with shotpoints labeled on the RC2708 tracks. Bathymetry contour interval is 100 m. Diamonds labeled *S* show positions of the RC2708 sonobuoy refraction survey; circles are proposed drill sites. Site 756 was planned for proposed Site NER-5A, but was moved about 500 m west-northwest on the crossing of the *Resolution* track. The strike of faults crossing the *Resolution* track is approximately 50°.

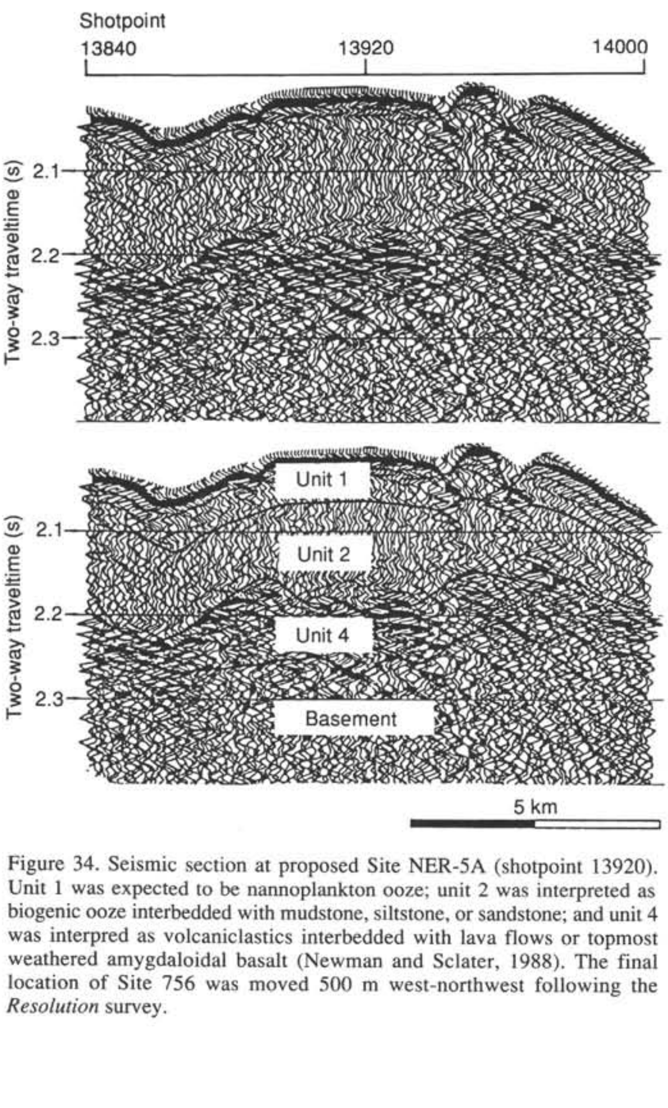

Figure 34. Seismic section at proposed Site NER-5A (shotpoint 13920). Unit 1 was expected to be nannoplankton ooze; unit 2 was interpreted as biogenic ooze interbedded with mudstone, siltstone, or sandstone; and unit 4 was interpred as volcaniclastics interbedded with lava flows or topmost weathered amygdaloidal basalt (Newman and Sclater, 1988). The final location of Site 756 was moved 500 m west-northwest following the *Resolution* survey.

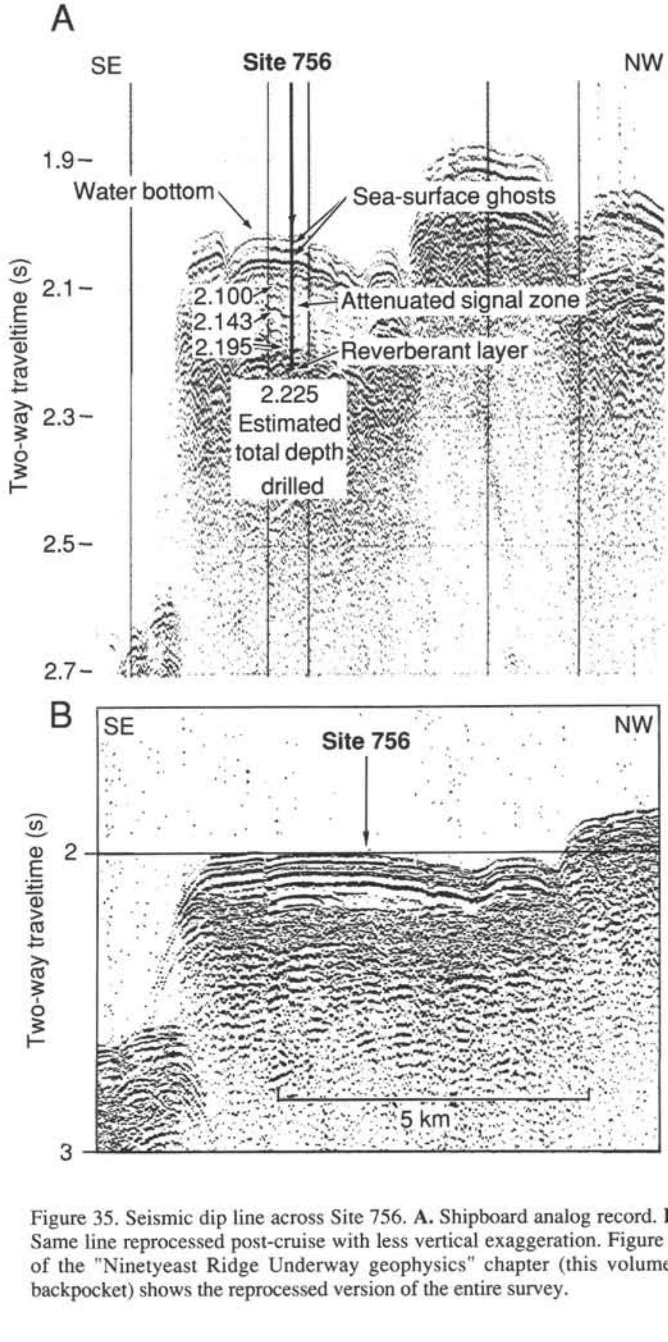

Figure 35. Seismic dip line across Site 756. **A.** Shipboard analog record. **B.** Same line reprocessed post-cruise with less vertical exaggeration. Figure 5 of the "Ninetyeast Ridge Underway geophysics" chapter (this volume, backpocket) shows the reprocessed version of the entire survey.

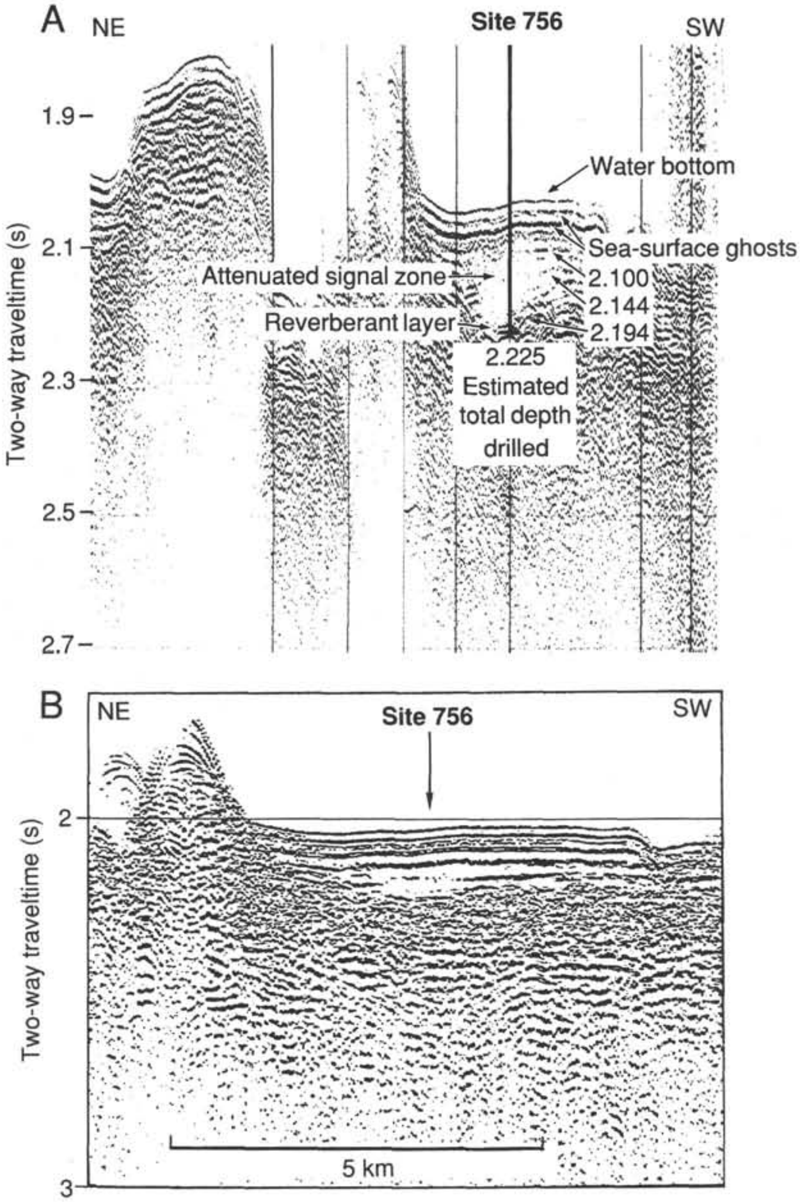

Figure 36. Seismic strike line across Site 756. **A.** Shipboard analog record. **B.** Same line reprocessed post-cruise with less vertical exaggeration.

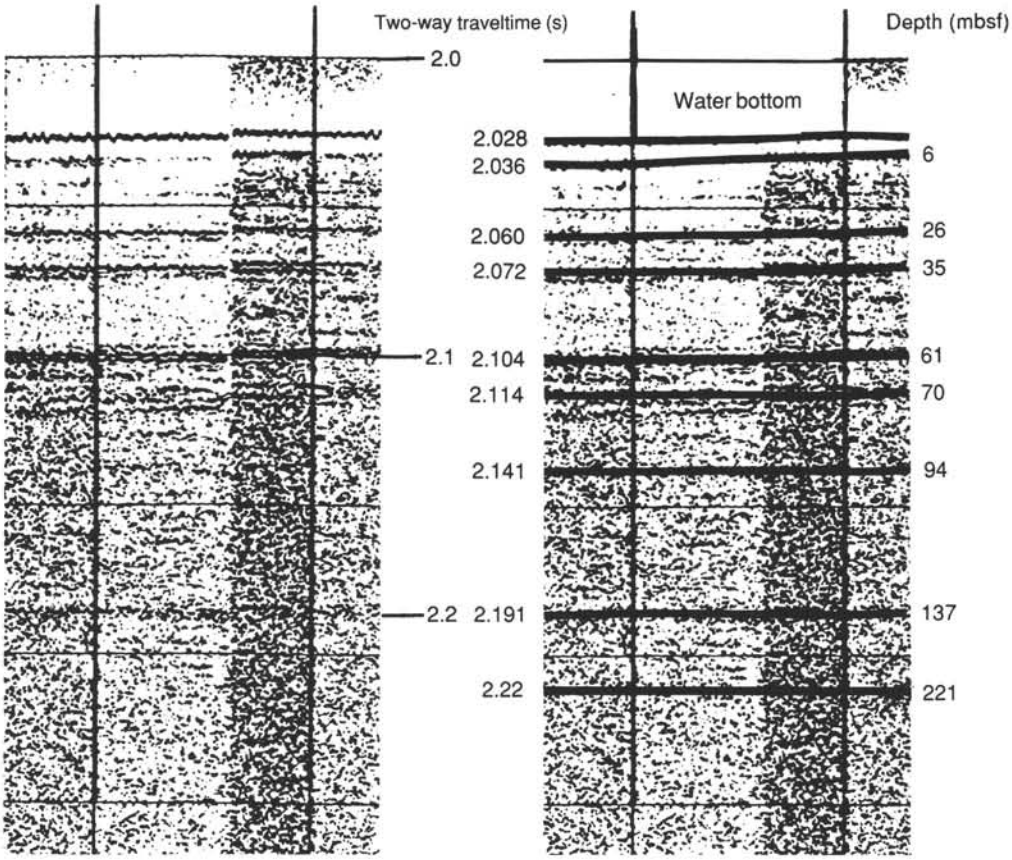

Figure 37. Uninterpreted and interpreted 3.5-kHz recording across Site 756. The line segment horizontal distance is less than 25 m at the location of Hole 756C. The major reflectors, their calculated depths, and the calculated time equivalent to total penetration are indicated.

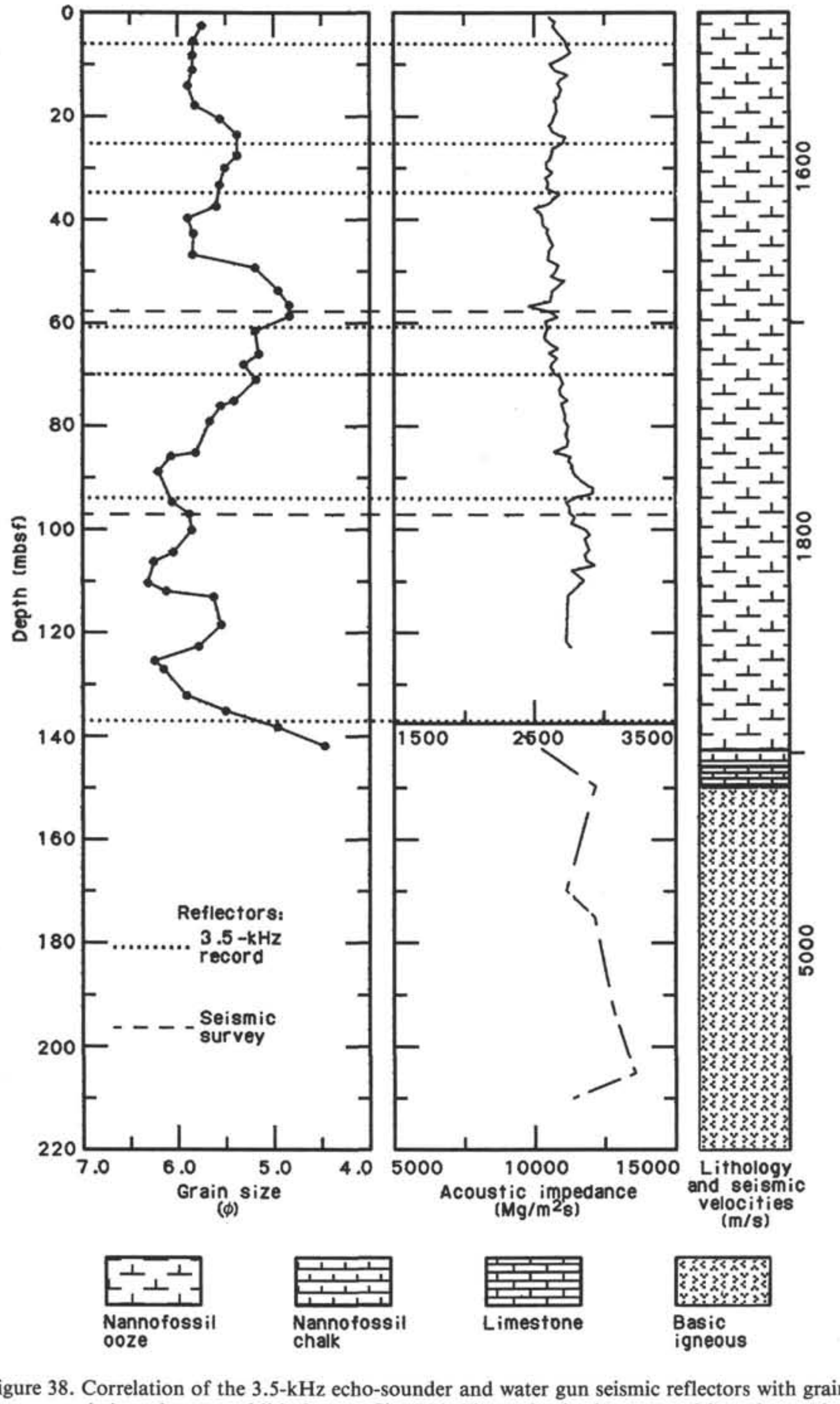

Figure 38. Correlation of the 3.5-kHz echo-sounder and water gun seismic reflectors with grain size, acoustic impedance, and lithology at Site 756. The grain size is expressed in a three-value running average. The graph of acoustic impedance uses two different scales, one for sediments and the other for basalt flows. The velocities to the right of the lithology column were used to calculate the depths of the reflectors.